3.04 Gravimetric Methods – Superconducting Gravity Meters

J. Hinderer, Institut de Physique du Globe, Strasbourg, France

D. Crossley, St. Louis University, St. Louis, MO, USA

R. J. Warburton, GWR Instruments, San Diego, CA, USA

3.04.1 The Superconducting Gravimeter

3.04.1.1 Historical

3.04.1.1.1 Early years at UCSD

The superconducting gravimeter (SG) was first introduced by Prothero and Goodkind (1968) as part of Prothero's (1967) thesis work on the design and development of the instrument at University of California at San Diego (UCSD). The SG broke new ground in geophysics instrumentation, and was an elegant realization of the principles of superconductivity. Although the basic sensor configuration has remained unchanged for nearly 40 years, continuous improvements in all other aspects of the original design have successfully converted the SG from a prototype laboratory instrument to a reliable research tool. (Note that in this article, the traditional gravity abbreviations are frequently used: 1 microgal $= 1\,\mu\text{Gal} = 10\,\text{mm}\,\text{s}^{-2}$, 1 nanogal $= 1\,\text{nGal} = 0.01\,\text{nm}\,\text{s}^{-2}$, and cpd = cycles per (solar) day.)

In 1970, Richard Warburton became a postdoctoral student with John Goodkind, and this collaboration was the foundation for the eventual line of commercial SGs. Richard Reineman, an undergraduate laboratory assistant working with William Prothero in 1969, was integral to the effort as a development technician with Goodkind and Warburton. Prothero and Goodkind (1972) published the first observations taken over a 4 month period and obtained precise tidal amplitude and phases, new information on ocean tide loading, and a recording of seismic normal modes following the 7.1-magnitude Kamchatka earthquake from 1969. Within a few years, the UCSD group generated significant papers using SG data on ocean tide loading (Warburton *et al.*, 1975) and the effects of barometric pressure on gravity (Warburton and Goodkind, 1977). This phase of the SG research culminated with a detailed tidal analysis of 18 months of data that included the first estimate of the effect of the nearly diurnal wobble on the resonant amplification of small diurnal tidal phases (Warburton

and Goodkind, 1978). These papers are still recommended reading for those interested in the basic issues concerning the treatment of gravity data.

3.04.1.1.2 Early commercial model TT instruments (1981–94)

The early publications as well as presentations at various conferences caught the attention of Paul Melchior (Royal Observatory of Brussels, Belgium, ROB) and Rudolf Brien and Bernd Richter (Institut für Angewandte Geodäsie, Germany, IfAG; now known as Bundesamt für Kartographie und Geodäsie, BKG), who contacted Goodkind about the possibility of using SGs to expand their previous work based on LaCoste Romberg (LCR) gravity meters. As a result, the commercial venture GWR Instruments (Goodkind, Warburton, and Reineman) was formed in 1979 to manufacture two SGs, one for ROB and one for IfAG. From this point on, two different design streams continued: Goodkind refined the original UCSD instruments and used them to develop new areas of geophysical research, and GWR began the manufacture of instruments for other scientific groups from their San Diego facilities. Eric Brinton joined GWR in 1986 to continue development of refrigeration, electronics, and data acquisition systems.

Melchior purchased a GWR Model TT30 dewar similar to those used at UCSD. The SG sensor was simply cooled by insertion through the 5 inch diameter neck of a dewar with the internal 200 l volume ('belly') filled with liquid helium. In a typical dewar, the belly is surrounded by a vacuum space, which contains two radiation shields with many thin layers of aluminized Mylar ('superinsulation') placed on the surface of the belly and shields. Hold time depends critically on efficiently using the cooling power of the gas (enthalpy) as it flows past the shields and neck before exhausting at room temperature. The dewar was suspended from a large concrete pier by 2 μm and a rear fixed point, which were used for leveling.

In 1981, the Model TT30 was installed in the basement vault at ROB. Visiting scientists who were familiar with modern SG installations would have been greeted by an eerie silence – there was no compressor noise, not even in an adjacent room. Silence had its disadvantage, however, as almost 200 l of liquid helium had to be replenished every 3 weeks or so, and each of these refills caused unpleasant disturbances to the data stream. Despite many problems that originated with a helium leak in the TT30 vacuum can lid (described in detail in De Meyer and Ducarme, 1989), this instrument was to continue without major interruptions for nearly 18 years until it was decommissioned in 2000. Early tidal results from the Brussels SG can be found in Ducarme (1983).

Helium was very expensive in Germany, so IFAG/BKG asked GWR to develop a refrigerated dewar system for their instrument. These systems use a cryogenic refrigerator (coldhead and compressor) to intercept and reduce the flow of heat via radiation and conduction from the outside of the dewar to its belly. This reduces the rate of boil-off so that the 'hold time' of the liquid helium is lengthened. Hold time depends on the cooling power of the refrigerator being used and how well it can be thermally coupled to the neck and radiation shields. On the first TT40 refrigerated dewar, the coldhead was bolted onto the top of the dewar wall and penetrated into the vacuum space through a special port sealed with an O-ring. The coldhead's two cooling stages (at 65 and 11 K) were connected directly to the outer and inner radiation shields using copper braid. The TT40 design was extremely successful with a holdtime of well over 400 days versus 50 days unrefrigerated. This project was beginning of a collaboration between GWR Instruments and Bernd Richter for developing new and improved SG models that has continued to the present day.

The provision of a commercial instrument proved to be a landmark opportunity for the geodetic and gravity community. In 1981, SG Model TT40 was installed in the basement of a castle at Bad Homburg, near Frankfurt Germany. At the International Union of Geodesy and Geophysics (IUGG) meeting in Hamburg, Richter (1983) presented a paper on data from the TT40 that showed the first gravitational determination of the 14 month Chandler component of polar motion, with amplitude of $\pm 5\,\mu$Gal ($1\,\mu\text{Gal} = 10\,\text{nm}\,\text{s}^{-2}$). To say the least, this took the audience by surprise and convincingly demonstrated the capabilities of the new gravimeter.

At the same time, Goodkind (1983) repeated his determination of the nearly diurnal wobble parameters from the tidal amplitudes using data from 1978, but the problem of accurately computing the ocean tidal loading of small waves still was a limiting factor. A few years later, Richter (1985) reported on the extension of his data set to 3 years of successful SG operation.

In 1985, Richter installed a second instrument – a new model TT60 – at Bad Homburg, and for over a year until the beginning of 1987 he obtained parallel recording with the original TT40. His thesis (Richter, 1987) contained many interesting insights into the operation of the instrument and its data, but being in German it was not widely read. A significant result

was that the gravity residuals from both instruments were highly correlated at the sub-μGal level (Richter, 1990), indicating that significant geophysical signals were still left in the data at this level. At the time, the cause was ascribed to the atmosphere, but this was before the environmental influence of hydrology on gravity became widely appreciated. Following the experimental work of Richter and the theoretical speculations of Melchior and Ducarme (1986), new refrigerated Model TT70's were installed in Wuhan, China, in 1986 (Hsu *et al.*, 1989), and in Strasbourg, France, in 1987 (Hinderer and Legros, 1989). The Model TT70 introduced the use of internal tiltmeters and thermal levelers to automatically keep the SG aligned with the plumbline at its tilt minimum.

As with the TT40 and TT60, the first two TT70's were manufactured with the coldhead bolted into the top of the dewar and penetrating the vacuum space. Although very efficient, this design made it difficult to service the coldhead without warming the dewar to room temperature. Later, TT70 models were manufactured with the coldhead supported by a separate frame and inserted through the neck of the dewar. Cooling power was coupled to the neck and radiation shields only via helium gas. In the new TT70 design, the coldhead could easily be removed for servicing or removal of any ice that may build up between the coldhead and the gravity sensor unit (Warburton and Brinton, 1995). New TT70's were soon installed at the National Astronomical Observatory in Mizusawa, Japan, in 1988, and two were located side by side at Kyoto University in the same year (Tsubokawa, 1991). Meanwhile, in 1989, Richter moved the TT60 from Bad Homburg to Wettzell, a fiducial station of the German geodetic network, and a TT70 was installed at Cantley, Canada in the same year (Bower *et al.*, 1991). Approximately 12 TT70 SGs were manufactured between 1986 and 1994, and many of these instruments are still operating as part of the Global Geodynamics Project (GGP) network (T007 Esashi, T009 Kyoto, T011 Kakioka, T012 Cantley, T015 Brasimone, T016 Kamioka, and T020 Metsahovi) – see Crossley (2004). TT70 dewars are 150 cm tall, have an 80 cm diameter, and weigh 150 kg. They require an annual transfer of 200 l of liquid helium and servicing the coldheads at 1–2 year intervals. In 1993, it was found that the TT70 SG was less susceptible to horizontal noise sources when the dewar was mounted from the bottom (Warburton and Brinton, 1995). **Figure 1** shows the TT70 operating at Cantley, Canada, after modification to the bottom-mounted configuration. The large concrete pier, previously used to support the dewar, now only supports the coldhead.

Figure 1 An example of the T T70 type instrument installed at Cantley, Canada, in 1989. The rack on the far left contains the chart recorders and noncritical electronics; the more sensitive components are in the enclosed temperature-controlled rack next to it. The 200 l dewar sits on three feet placed on small granite blocks. The front two feet with the X and Y thermal levelers attached to the dewar bottom are visible. The coldhead is supported from a frame resting on the top of a concrete pier. Normally, the entire SG is enclosed by thermal insulation.

3.04.1.1.3 The Compact SG (1994–2002)

In 1993, GWR produced a much smaller 125 l Compact Dewar designed to operate on a 1 m^2 pier or platform, so that it could be easily operated at many preexisting geodetic installations. The compact SG is 104 cm high, 66 cm wide, and weighs 90 kg. The SG sensor is built into the dewar belly, which allows the neck and radiation shields to be custom designed to mirror the dimensions of the coldhead. The Compact Dewar uses the same APD Cryogenics DE202 coldhead and HC-2 helium compressor as used in Models TT60 and TT70. However, the smaller neck diameter and volume dramatically reduces the heat load on the outer radiation shield, and the improved neck/coldhead interface allows much more efficient use of the coldhead cooling power. As a result, the dewar efficiency is doubled and less than 100 l of liquid helium is used annually.

Figure 2 shows Compact C023 operating in Medicina, Italy (Romagnoli *et al.*, 2003). The APD HC-2 compressor and its water chiller are on the left side (rear), with flexible stainless tubes connecting the compressed helium gas to the coldhead. The two thermal levelers and a third fixed point are attached to an aluminum band wrapped around the circumference of the dewar. These are supported by three feet that rest on small granite blocks placed upon the floor.

Figure 2 A compact instrument C023 installed at Medicina, Italy.

The coldhead is supported and centered in the neck using a metal tripod support frame. The neck–coldhead interface is sealed with a rubber gasket, which prevents air from entering, and provides vibration isolation between the coldhead and the SG sensor. The addition of stiff internal spokes placed between the inner belly and the outer dewar wall makes the compact SG less sensitive to horizontal noise. This structural change produces lower noise levels than observed in previous SGs (Boy *et al.*, 2000).

The first compact SG, C021, was tested next to T002 at the Royal Observatory Brussels before being moved in 1995 to a seismic station in Membach, Belgium, where it is still operating. The SG is installed in a separate room at the end of a 100-m-long tunnel, and because it is close to long-period seismometers, care was taken to minimize and measure vibrations produced by the cryogenic refrigeration system (Van Camp, 1995). Approximately 13 compact SGs were manufactured from 1994 to 2002 and are installed at over half the GGP stations.

3.04.1.2 Basic Principles of Operation

3.04.1.2.1 Superconducting components

Seismometers and relative gravimeters are based on a test mass suspended by a spring that is attached to the instrument support. A change in gravity or motion of the ground generates a voltage that becomes the output signal (velocity or acceleration). This system works well in many modified forms for seismometers and is still used successfully in the LCR and Scintrex models of field gravimeters. The major problem at periods longer than the seismic normal-mode range, for example, at 4 h and longer for the tides, is that (even in a thermally well-regulated environment) the mechanical aspects of a spring suspension cause erratic drift that is difficult to remove by postprocessing. Field gravimeters repeatedly occupy a reference station to monitor this drift, and observatory spring instruments have to be rezeroed when the signal exceeds the range of the voltmeter. Since the 1980s, spring gravimeters have incorporated electrostatic feedback that considerably improves their linearity and drift performance (e.g., Larson and Harrison, 1986).

The SG almost completely solves the drift problem by replacing the mechanical spring with the levitation of a test mass using a magnetic suspension. **Figure 3** shows a diagram of the GSU; the three major superconducting elements are the levitated mass (sphere), the field coils, and the magnetic shield. The displacement transducer is formed by a capacitance bridge that surrounds the sphere and is sealed with a partial pressure of helium gas in a separate cavity inside the coils. The field is generated by two niobium wire coils (superconducting below a temperature of 9.2 K) that carry, in principle, perfectly stable superconducting persistent currents to provide an extremely stable magnetic field. The stability depends on the zero-resistance property of superconductors – after the currents are 'trapped', no resistive (ohmic) losses are present to cause them to decay in time. The test mass is a small 2.54–cm-diameter sphere, also made of niobium, that weighs about 5 g. The coils are axially aligned; one just below the center of the sphere and one displaced about 2.5 cm below the sphere. When current flows in the coils, secondary currents are induced on the surface of the sphere, which by the Faraday induction law precisely cancel magnetic flux from entering the sphere. As with the currents in the coils, the induced currents are perfectly stable in the absence of any ohmic losses. The levitation force is produced by the interaction between the magnetic field from the coils and the currents induced on the surface of the superconducting sphere. **Figure 4** shows a schematic of the sphere, coils, capacitance bridge, and magnetic flux lines.

The use of two coils allows the operator to independently adjust both the levitation force and the magnetic gradient. The upward levitation force is mainly produced by the lower coil. Its current can be precisely adjusted to balance the time-averaged downward force of gravity on the sphere at the center of the displacement transducer. The upper coil is used to adjust the magnetic force gradient ('spring constant'), which can be made very weak. As a result, a very small change in gravity (acceleration) gives a large displacement of the test mass, generating an instrument of very high sensitivity.

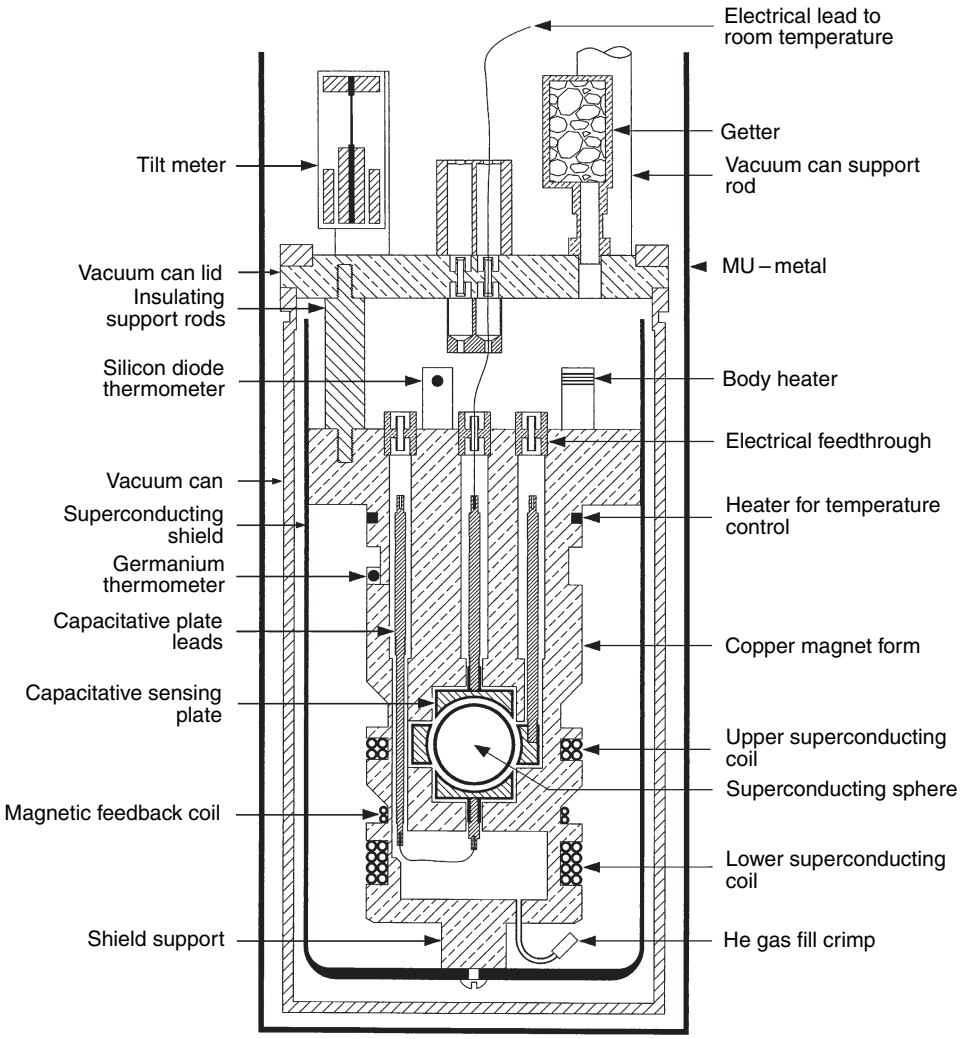

Figure 3 Schematic of SG sensor showing arrangement of the sphere, coils, vacuum can, and shielding.

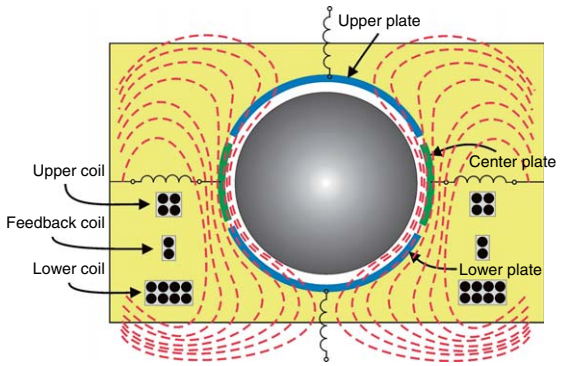

Figure 4 Schematic diagram of the Nb sphere, coils, plates, and general pattern of magnetic flux lines. Flux is excluded from the sphere and is confined externally by the Nb shield.

Because the levitation is magnetic, changes in the Earth's magnetic field would seriously degrade the stability of an unshielded SG. A superconducting cylinder with a hemispherical closure on one end surrounds the sphere and levitation coils and is attached to the bottom of the copper magnet form. This provides the primary magnetic shielding from changes in the Earth's magnetic fields, which in its absence would seriously degrade the stability of the magnetic levitation force. When the magnetic coils are turned on, persistent currents also are induced in the inside surface of the shield, which prevents the levitation magnetic field from penetrating the shield. An additional μ-metal shield is placed on the outside of the vacuum can. During the initialization process, this shield reduces the Earth's magnetic field by a factor of

about 100 before the superconducting components cool through their transition temperature. This process minimizes any trapped flux in the sphere, coils, or shield that could produce instability in the sensor.

3.04.1.2.2 Displacement transducer and feedback system

Relative motion between the ground (to which the coil assembly is attached) and the sphere, or any other perturbation of the gravity potential, moves the sphere from its equilibrium position. The position of the sphere is detected by using a phase-sensitive lock-in amplifier in conjunction with a capacitance bridge. Three capacitor plates surround the sphere with 1 mm clearance (**Figure 3**). The upper and lower plates are hemispherical caps that surround the upper and lower portions of the sphere. The center plate is a spherical ring around the equator of the sphere (**Figure 4**). A 10 kHz reference signal from the lock-in amplifier drives the primary of a carefully shielded transformer. The two balanced secondary windings of the transformer apply equal and opposite voltages to the upper and lower capacitor plates. The AC signal from the center ring plate is proportional to the displacement of the sphere from the center of the bridge. The sensor is operated in feedback to take advantage of the increased linear dynamic range and rapid response compared to open-loop operation. The AC signal is amplified, demodulated, filtered, and applied to an integrator network. The DC output is connected to a precision resistor in series with a five-turn coil wound on the copper magnetic form below the sphere. The resulting feedback force is proportional to the product of the feedback current and the current on the surface of the sphere. This force is given by $F = CI_F(I_{IC} + I_{IF})$, where I_F is the feedback current, I_{IC} is the current induced on the surface of the sphere by the levitation field, I_{IF} is the current induced on the surface of the sphere by the feedback field, and C is a constant. Because I_{IC} is proportional to g and I_{IC} is atmost the maximum amplitude of the tides, the maximum nonlinearity is $(I_{IF}/I_{IC})_{MAX} \sim 10^{-7}$. Therefore, the sensor is extremely linear. The gain (scale factor) of the sensor is determined by the geometry, the resistor size, the number of turns on the coils, and the mass of the sphere.

3.04.1.2.3 Temperature control

The sensor and superconducting shield are located inside a vacuum can surrounded by the liquid helium bath at about 4.2 K. In response to atmospheric pressure, the boiling point varies by about $1\,\mathrm{mK\,mb^{-1}}$, and during storms may change as much as 100 mK. Therefore, the sensor must be temperature regulated (Goodkind, 1999). A germanium thermometer measures temperature and forms one arm of a Wheatstone bridge that has its null point preset to 4.5 K. The bridge output supplies feedback power of a few milliwatts, which is applied to a heater attached to the copper magnetic form. Variations in control power almost perfectly follow the inverse of atmospheric pressure. With small bath-temperature variations, high vacuum isolation, and high thermal conductivity of materials, it is relatively easy to regulate to a few microkelvins at cryogenic temperatures. As a result, the SG is almost completely isolated from environmental effects caused by changes in external temperature, humidity, and barometric pressure. This is a major advantage over mechanical gravimeters that operate near room temperature.

3.04.1.2.4 Tilt compensation system

To measure the magnitude of the gravitational acceleration $\boldsymbol{g}$, the gravimeter must be aligned with a plumbline along $\boldsymbol{g}$. For most types of gravimeter, the test mass is constrained to move only along its axis of measurement. Therefore, when its axis is tilted with respect to the vertical plumbline, it measures only the component of $\boldsymbol{g}$ along its axis of measurement. The measured magnitude is $g\cos\theta$, where θ is the angle between the vertical and axis of the instrument. For small angles, the apparent decrease in gravity produced by tilts is $\delta(\theta) = (g\cos\theta - g) \approx g(\theta^2/2)$. The LCR is aligned along $\boldsymbol{g}$ by tilting it systematically along two orthogonal directions and setting it at the maximum value of g.

When an SG is tilted, the component of gravity along its axis of measurement decreases as $g\cos\theta$. The magnetic force gradient perpendicular to its axis of measurement is relatively weak, however, so the sphere moves off axis in response to the force component $g\sin\theta$. Because the magnetic levitation force supporting the sphere decreases off axis, the sphere position moves downward. This apparent increase in gravity has the same angular dependence as the equation above but its magnitude is about 2 times larger. As a result, the SG tilt dependence becomes $\delta(\theta)_{SG} \approx -g_{SG}(\theta^2/2)$, where the magnitude of $|g_{SG}| \approx |g|$. Therefore, the SG is aligned along $\boldsymbol{g}$ by tilting systematically along two orthogonal directions and setting it at the minimum value of g (not at the maximum, as for other gravimeters). This phenomenon explains why cultural noise such as nearby trains or automobiles will cause downward spikes on the SG signal. The horizontal accelerations move the sphere off axis where the magnetic support force is

weaker. This effect was first observed in 1981 when the TT30 was installed in the cellar vault in the ROB. In contrast, trains did not affect operation of the LCR gravity meter operating in a nearby vault.

The SG is supplied with an automatic leveling system consisting of two tiltmeters mounted orthogonally on top of the gravimeter vacuum can and two thermally activated levelers that are placed under two of the dewar support points. After tilt-minimizing the SG sensor, the tiltmeters are 'aligned' to the same null by electronically setting their output voltages to zero. In feedback, the tiltmeters continuously adjust the power controlling the expansion of the levelers to keep alignment better than 1 μrad. This leveling precision is essential in gravity studies where apparent tilt-induced gravity changes must be kept less than 1 nGal ($1\,\text{nGal} = 0.01\,\text{nm}\,\text{s}^{-2}$). The tilt minimum adjustment is made on initial installation and checked every year or so by the operator. A recent study (Iwano and Fukuda, 2004) on SG data from the Syowa station shows the clear advantage of the tilt compensation system in reducing the noise in gravity, especially in the tidal range.

3.04.1.2.5 Sphere and sphere resonance

The sphere is a hollow superconducting shell that is manufactured with a slight mass asymmetry so that it has a preferred orientation when levitated. Various manufacturing processes are discussed in Warburton and Brinton (1995). A small hole is drilled on the top of the sphere to allow the helium gas to enter and to prevent a differential pressure from developing when it is cooled to 4 K. Just as important, the volume of the shell displaces 15 times less helium gas than the volume of the sphere; so the hole reduces buoyancy forces that result from changes in the surrounding helium gas pressure.

When the gravimeter is tilted, particularly impulsively, the horizontal displacement of the sphere turns into an orbital motion (precession) with an associated vertical component in the feedback output. This mode appears as a sphere 'resonance' that has a period of 60–120 s depending on the particular instrument. In the absence of trapped magnetic fields and helium gas in the chamber, the Q of this mode is several thousand, so it is always excited making the instrument not usable. Slow damping of the mode is provided by adding helium gas to the chamber, but the resonance remains underdamped and is clearly visible in some of the instruments' data. By comparison, the vertical resonance of the sphere is heavily damped with a period close to 1 s. Further technical details on the instrument design can be found in Goodkind (1991, 1999).

3.04.1.3 Development of the Dual-Sphere Design

In the early commercial SGs manufactured up to 1990, offsets (or 'tares') occurred in the SG gravity records that affected both long-term stability and measurement of tidal factors (Seama *et al.*, 1993; Harnisch and Harnisch, 1995; Hinderer *et al.*, 1994). The offsets could be quite large (up to 100 μGal) if caused by mechanical shock from transferring liquid helium, power failures, or earthquakes. Small instrumental offsets less than 5 μGal could occur at random intervals that were not associated with outside disturbances. Rapid offsets larger than 0.2 μGal and occurring in less than 1 min could be easily detected and corrected (Merriam *et al.*, 2001). However, there was a concern that the residual data would depend arbitrarily on the threshold value chosen in automatic offset detection programs (Harnisch and Harnisch, 1997). When two SGs were operated side by side, the difference in recordings provided a much clearer determination of the occurrence of offsets (Klopping *et al.*, 1995).

On the basis that random offsets will seldom occur in two sensors simultaneously, a dual-sphere SG was manufactured to solve the instrument offset problem (Richter and Warburton, 1998). The two spheres are mounted one above the other and separated by about 20 cm. The lower sensor is manufactured exactly like previous single-sphere sensors, and the temperature and tilt control remain the same. Small differences in the sphere masses, superconducting shield, coil windings, and machining tolerances produce magnetic asymmetries that are not identical in the two sensors. These asymmetries produce slightly different tilt minima and require more complicated electronics to align the tilt minimum of the upper sensor with the lower sensor.

The complications of a dual-sphere system are justified by providing a built-in instrumental offset detector. Because the outputs are treated as signals from two different gravimeters, the user can combine the processed data sets, select the least disturbed sphere output for any one time period, or convert the two signals into a gravity gradient by using the known vertical separation. CD029 was the first dual-sphere SG produced and it was tested at Bad Homburg beginning July 1998 before being moved

permanently to Wettzell in November 1998 (Harnisch *et al.*, 2000). Results at Bad Homburg showed that careful calibration of both amplitude and phase was required to minimize the difference signal and that indeed offsets of a few tenths of a μGal could easily be detected. Surprisingly, after moving to Wettzell, no spontaneous random offset exceeding about 0.1 μGal was observed. Larger offsets that occurred were due to other causes, that is, failures in the cooling system or during extensive maintenance procedures (coldhead maintenance, He refills, or removal of ice from the neck).

More recent data from all four dual-sphere SGs support the early observations with CD029 (Kroner *et al.*, 2004, 2005). No offsets have occurred in CD029 at Wettzell or D034 at Moxa, and only one or two offsets per year are observed in CD028 at Bad Homburg and in CD037 in Sutherland. From these data, GWR concludes that the changes in its manufacturing process, in particular improvements to the Nb spheres and shields, have greatly reduced the incidence of random offsets. With this success, one might argue that the dual-sphere SG is no longer needed. However, as gravity changes are examined with higher and higher resolution, they may still be used to discriminate sub-μGal observations of instrumental origin (see figure 3 of Meurers, 2004), or illuminate more subtle instrumental effects that need improvement (Kroner *et al.*, 2005). More importantly, the gradient signal itself may yet prove useful in modeling environmental gravity variations.

3.04.1.4 Instrument Performance

3.04.1.4.1 Instrument drift

One SG design goal was to produce an instrument that is stable to a few μGal per year. Meeting this goal with a commercial instrument took approximately a decade. Drift in the early model TT70s could be more than 100 μGal yr^{-1} during the first year of operation but decreased steadily with time to less than 10–20 μGal yr^{-1} after 5 years of operation. Drifts were modeled as the sum of one or two exponentials, a low-degree polynomial, or a combination of both (Boy *et al.*, 2000; Seama *et al.*, 1993), but uncertainty in the exact functional form decreased the precision with which long-period tides and polar motion could be determined from the data.

A dramatic decrease in drift was made in the early 1990s owing to a variety of design changes described in Warburton and Brinton (1995). At present, drifts are characterized by a small initial exponential followed by a small linear term. The exponential component decays in 4–6 months, after which it is negligible. For example, the initial drift for C023 manufactured in 1995 is $d(t) = -16.0\exp(-t/31)$ μGal, where t is in days (Schwahn *et al.*, 2000). Long-term linear drift rates (including real secular changes) reported for the nine SGs operating in Europe vary from 1.6 to 4.9 μGal yr^{-1} (Crossley *et al.*, 2004). An 8-year comparison of an FG5 absolute gravimeter (AG) next to SG C023 in Membach confirmed that, after removal of the linear term (4.2 μGal yr^{-1}), the SG has an identical spectra to the AG for frequencies less than 1 cpd (cycles per (solar) day) (Van Camp *et al.*, 2005). This confirms that the SG drift is restricted to DC (very low frequency), and that it provides a continuous low noise record of all gravity variations.

The only reliable method to determine instrumental drift is to compare the SG with collocated measurements made with an AG at regular intervals. The SG provides a complete time history of gravity at the site, which is invaluable for correlating with other geophysical variables, whereas the AG provides an absolute reference from which the drift and secular changes can be inferred. Precise drift measurement is complicated by real gravity variations due to hydrology, crustal uplift, annual terms, seasonal terms, or signals of unknown origin (e.g., Zerbini *et al.*, 2002).

3.04.1.4.2 Calibration stability

The question of calibration will be covered in more detail later in this report, but it is worth noting here that recalibration of single sensor instrument using AGs over time periods of 5 years or more have rarely shown differences that exceed the calibration error (between 0.1% and 0.01%). For dual-sphere sensors, the constancy of calibration is verified to 10^{-3}% by least-squares fitting the time series of the upper sphere to the lower sphere (Kroner *et al.*, 2005). This constancy means that the analysis of very long records by tidal analysis, for example, can be done without fear of any evolution in the calibration constants.

3.04.1.4.3 Instrumental noise and precision

Most of the GGP data acquisition systems record and digitize the full output of the SG electronics board. A voltmeter with 7.5 digits of resolution has the equivalent of 22 bits; when applied to a signal that includes the full range of tides (300 μGal), this translates into a smallest significant change of about

0.1 nGal. This is in effect the quantization noise of the SG + data acquisition system, but not necessarily its precision. There is no reference gravity more accurate than the SG itself, so the precision of the SG can only be obtained by inference. In the frequency domain for studies of tides or normal modes, it is common for the SG to measure small periodic tidal signals and long-period seismic signals with a sensitivity of 1 nGal and better. Therefore, 1 nGal is generally referred to as the nominal precision, or sensitivity, of the SG.

The determination of the instrumental noise of the SG is complicated by the fact that sources of the Earth noise (signals from the atmosphere, oceans, and hydrology) are generally much larger than instrumental noise for frequencies ranging from 3×10^{-8} Hz (1 cycle per year) to 1 Hz. The SG noise is higher than Earth noise only in the small subseismic band between 1 and 20 mHz where the noise level is typically from 1 to $3\,\mathrm{nm\,s^{-2}\ Hz^{-1/2}}$ (0.1–0.3 μGal $\mathrm{Hz^{-1/2}}$) for most SG stations (Rosat *et al.*, 2004). This is more than 2 orders of magnitude lower than the noise level of the AG as reported by Crossley *et al.* (2001) and Van Camp *et al.* (2005).

It is common practice to filter and decimate data to 1 min samples to look at small temporal gravity variations; assuming white noise, the above noise level translates into a precision of 0.01–0.03 μGal. This level is consistent with common experience. For example, Meurers (2000) easily observed gravity signals of magnitude 0.1–0.3 μGal over 10–30 min intervals and Imanishi *et al.* (2004) identified reliable coseismic offsets of a similar magnitude.

The best way to determine real-world accuracy in the temporal domain is to compare different instruments operating side by side. Two comparisons have been done – one in Miami (Richter, 1990; Klopping *et al.*, 1995, Harnisch and Harnisch, 1995) and one in Boulder (Harnisch *et al.*, 1998), with the result that different pairs of instruments agree to 0.1 μGal, or better. For a dual-sphere instrument, the data streams from the two spheres are largely independent, and the difference signals between two sensors of the four dual-sphere SGs are typically 1 μGal over record lengths of years. Additionally, the residual curves from the dual SG in Moxa agree within a few tenths of a μGal to the polar motion modeled using data provided by the International Earth Rotation Service (IERS). These results suggest that 0.1 μGal is the time-domain accuracy of the SG for long periods.

3.04.1.5 Recent Developments

3.04.1.5.1 Ultralong hold time dewar

Although Compact Dewars were extremely successful, the goal remained to further decrease helium consumption and annual disturbances from helium transfers. By 1997, the first commercial (and somewhat) practical 4 K refrigeration systems became available. The Leybold Vacuum Products KelKool 4.2 GM coldhead produced cooling power of 50 W at 50 K at its upper stage and 0.5 W at 4 K at its lower stage. It cooled well below the 4.2 K liquefaction temperature of helium and produced more than 5 times the cooling power of the APD DE202. Soon afterward, GWR produced an ultralong hold time dewar (ULHD) based on the 125 l Compact Dewar design with its neck modified to accommodate the much larger 4.2 GM coldhead. This is a closed-cycle system, because the helium gas condenses in the neck on the lower stage and drips back into the storage volume of the dewar (Richter and Warburton, 1998). This success pointed to the future in which SGs could operate indefinitely without transferring liquid helium or consumption of liquid helium. The first ULHD system is shown in **Figure 5**.

Figure 5 One of the first dual-sphere instruments (CD029, now at Wettzell, Germany) with a ULHD using a Leybold KelKool 4.2 K GM coldhead. The support cranes used to insert and remove the coldhead are shown in the background.

Two dual SGs using the KelKool 4.2 GM coldhead (CD029 and CD030) have been operating continuously since June 1999 at Wettzell and at Bad Homburg, Germany. The coldheads are extremely reliable and require maintenance only at approximately 3 year intervals. However, the coldhead is too heavy for one person to handle and requires a support crane for insertion and removal. Also, the combination of compressor and water chiller requires 7 kW of power versus 2 kW power for the DE202 system.

Two more ULHD systems were manufactured, R038 operating in Concepción, Chile, since December 2002, and C043, which replaced T016 at Syowa station, Antarctica, in March 2003. Neither of these stations could supply 7 kW, so these ULHDs were designed to use a Leybold 4.2 Lab coldhead, which with water cooling reduced the power load to 3.5 kW (Warburton *et al.*, 2000).

3.04.1.5.2 Observatory dewar

Within a year of shipping C043, Leybold stopped manufacturing the 4.2 Lab coldhead and the 5 year effort to develop a closed-cycle system was threatened. Fortunately, in the same year, Sumitomo Heavy Industries, who had extensive experience with large 4 K cryocoolers, entered the market with a new smaller refrigeration system – the SHI RDK-101 coldhead and CAN-11 compressor. Physically, the RDK-101 coldhead is about the same size as the APD 202, but it uses small 16–mm-diameter flex hoses and is easy for one person to handle. The CAN-11 compressor uses only 1.3 kW power and is air cooled. As a result of the smaller size and power, the RDK-101 has less than half the cooling and liquefaction power of the Leybold 4.2 Lab, but it has excellent prospects for continued future production in Japan.

Over the next 2 years, GWR re-engineered and tested several coldhead/dewar interfaces to fully utilize all the cooling power of the RDK-101. Small dewars have several attractive features: they are visually appealing, lighter and easier to move and install, and, most importantly, the input heat load decreases with surface area. Larger dewars provide longer hold times in the event of coldhead failure. After experimenting with dewar volumes as small as 10 l, GWR chose a 35 l capacity for its Observatory Dewar design. This compromise allows 20 days operation in failure mode: either with the power off, or the coldhead inoperative, and enough excess cooling capacity to liquefy helium gas at a rate greater than 1 l per day.

Figure 6 The newest Observatory Model SG and SHI RDK-101 coldhead. All of the control and data acquisition electronics are contained inside one temperature-regulated electronics enclosure. During installation, the front panel is removed and all the controls are accessed by the local keyboard and computer screen normally stored inside the enclosure. After installation, all functions and data retrieval are remotely accessed through an Internet connection. The dewar is 42 cm in diameter and the combined height of the dewar and coldhead is 130 cm.

The first OSG O040 was installed in Walferdange in December 2003, the second in South Korea in March 2005, with two more installed in Taiwan in March 2006. **Figure 6** shows OSG O049 SG dewar system, with all its control electronics and data acquisition system.

3.04.1.5.3 Data acquisition system and remote control

In the early years, GWR supplied analog electronics (Gravimeter Electronics Package – GEP) for controlling the gravity, temperature, and tilt functions; and a current supply (Dual Power Supply and Heater Pulser – DPS) for sphere levitation. Analog filters were copies of those used for the International Deployment of Accelerometers (IDA) network of LCR gravity meters and took the approach of dividing the signal between a low-passed tidal gravity output that was the main system output, and a short-period high-passed output that displayed signals such as earthquakes and disturbances. The high-frequency signal was initially recorded only on a strip chart recorder, and atmospheric pressure was also sampled at the station. Each user provided their own data acquisition system.

As more users began to acquire SGs for a variety of purposes, it became standard practice to sample at high rate (1–10 s) the full signal (tides + seismic frequencies). Nevertheless, it took some time for the gravimeter community to achieve the goal of a common set of standards for the acquisition and exchange of SG data. As part of this goal, GWR provided a replacement gravity card (GGP gravity card) with a filter designed for 1 s sampling and additional circuitry for measuring the phase response of the gravimeter system (GGP newsletters #2 and #3).

The first GWR data acquisition system manufactured in 1995 used CSGI software running on a PC with a QNX operating system. Soon, however, uncertainty in the future of the QNX operating system and software maintenance convinced GWR to develop a Windows-based system. In 1999, GWR and BKG reported on an ambitious project to control the SG remotely (Warburton *et al.*, 2000). The prototype Remote SG R038 has been operating at Concepción, Chile, since December 2002, and almost all goals for remote operation have since been implemented. In 2004, GWR decided that all new observatory SGs should be provided with a GWR data acquisition system with remote control capabilities. This is required not only to further standardize GGP data but also to enable GWR to remotely diagnose problems as they arise and to solve them without requiring travel to the site of operation.

3.04.1.6 User Requirements

3.04.1.6.1 Operation and maintenance

The SG sensing unit contains only one moving mechanical part, the niobium sphere. It is therefore virtually free of any maintenance requirements, and this has been verified by field installations of 15 years. SG support equipment, however, does need periodic maintenance to assure proper operation and can fail unexpectedly as the result of a lightning strike or other natural catastrophes. Many of the major gaps in SG data have been caused by power supply failure during major storms, or failure of the data acquisition systems. Planning for failure of either electronics or refrigeration is necessary to minimize interruptions in long (decadal) gravity records. It is most important to keep the dewar at least partially filled with liquid helium so that the sensor and superconductors remain below 4.5 K. Upon complete helium loss, the sensor will start warming up to room temperature. Although no damage occurs to the sensor, it requires that the sphere be relevitated, which reactivates the initial drift discussed in Section 3.04.1.4.1 In practice, therefore, operators are very careful to make sure the liquid helium volume is kept above a minimum level, so that in the case of a power or coldhead failure there is enough time to either transfer more liquid helium or to fix the source of the failure. With the coldhead off, the maximum hold time for a Compact Dewar is about 60 days. Prudently, most operators do not let the liquid He fall below about one-third full. Therefore, even under severe interruptions, such as the fire at Mt. Stromlo, Australia, in January 2003, the operator has at least 20 days to solve the resulting problems without warming the sensor up. It is also important to follow the manufacturers' and GWR's instructions for maintenance of the coldhead, compressor, and water chiller to prevent equipment failure. Many operators keep a backup refrigeration system available for immediate replacement.

At most of the GGP stations, operators check weekly that the refrigeration system and data acquisition system are functioning properly and ensure general site integrity. When problems develop, they will be observed either in the support status variables that monitor operation of the support equipment (temperature control, tilt-leveling control, and the refrigeration system), or will cause an increase in the instrumental gravity noise. For example, refrigeration problems cause immediate increase in helium boil-off rate and warming of dewar neck thermometers. Ice buildup around the coldhead that touches the inside of the dewar neck will cause an immediate increase in noise observed through the mode filter and on the gravity residual. Problems with the leveling system will be observed on the tilt X and Y balance signals and as gravity noise on the mode filter and gravity residual.

The new GWR data acquisition system (DDAS) allows the operator to monitor about 30 status variables remotely. In addition, alarm levels can be set to automatically generate warnings and alert the operator by e-mail to initiate investigation and repair. After collection and analysis of 1 month data, the operator can enter a calibration factor, tidal parameters, and barometric pressure admittance, and the DDAS will automatically generate a theoretical tide and display the gravity residual signal in real time. This allows visual examination of the gravity noise at the sub-μGal scale. Changes in noise level are immediately observable and with some experience can be identified as those of geophysical origin (atmosphere, ocean, or earthquakes) or due to possible equipment problems. In the latter case,

GWR can consult online with the operator to analyze the problem and provide a rapid solution. Remote access should reduce the frequency of data gaps and ensure higher quality of overall long-term data.

3.04.1.6.2 Site location

The SG measures an extremely wide bandwidth of signals from periods of seconds to years and the origin of signal sources ranges from local to global. The scientific objective is to determine the signals of most importance and site selection is paramount to achieving these goals. In practice, a site may be chosen to maximize gravity signals of interest and to minimize signals that are of less interest that will be considered as 'noise'. For example, a site must be near a volcano if one wishes to measure signals from magma intrusion, or it must be close to the ocean to measure nonlinear ocean tides or sea-level changes. In contrast, if the goal is to measure short-period signals, such as seismic waves, normal modes, or tides, the site needs to be as quiet as possible (see below).

Site selection may be restricted to the country providing the research funds and by the goals of the funding agency; however, some sites are cooperative efforts chosen to expand the geographic distribution of the GGP network. Examples of the latter include Ny-Alesund, Norway (Sato *et al.*, 2006a), Sutherland, South Africa (Neumeyer and Stobie, 2000), and Concepción, Chile (Wilmes *et al.*, 2006). Neumeyer and Stobie (2000) discuss both geographic and practical criteria used for choosing the Sutherland site. The SG has been used in a wide variety of field situations including harsh conditions such as a salt mine in Asse, Germany (Jentzsch *et al.*, 1995), and on the edge of the Antarctic continent at Syowa station (Sato *et al.*, 1991). Most of the sites, however, are more instrument friendly and have been chosen to use existing facilities where other geophysical instrumentation is already operating and to share infrastructure (such as power, telephone, or satellite communications) and staff.

3.04.1.6.3 Site noise

The SG is an extremely low-noise instrument and requires a quiet site for optimum operation. A quiet site is one that is removed, by distances of at least several kilometers, from nearby cultural environments such as a city, town, railroad, or major highway. These are strong noise-generating environments that not only increase short-period disturbances but also introduce ground tilts and loadings that will be seen in the residual gravity. If at all possible, it is highly recommended that potential sites be pretested for ambient Earth noise using a STS-1 VBB long-period seismometer. To detect low-noise signals, the site noise must approach the new low-noise model of Peterson (1993) and the best IRIS Global Seismographic Network (GSN) stations (Widmer-Schnidrig, 2003; Berger *et al.*, 2004).

Note that a site may be isolated from cultural influences, but may still be part of a scientific research station containing large (and massive) instruments such as a VLBI antenna. These fiducial stations are of great interest from geodetic and geophysical points of view because of the advantages of combining gravity and geodetic measurements. If, however, an SG is housed within a busy scientific building that is visited constantly or is running other machinery, the quality of the data will clearly suffer. Ideally, the SG should be housed by itself some distance (100 m or more) from other instruments or heavy traffic areas and should pass the seismometer test proposed above.

3.04.1.6.4 Site stability

Monitoring of long-term crustal deformation using gravity and space techniques requires careful integration of GPS, AG, SG, environmental sensors, and ocean gauges (Zerbini *et al.*, 2001; Zerbini *et al.*, 2002; Richter *et al.*, 2004). All piers must be constructed carefully, since differences in pier construction and separation of piers (non-collocation) may cause subtle and spurious signals of non-geophysical origin. The deformation characteristics of the ground immediately below and around the instrument are obviously important. Ideally, if an instrument can be placed on a concrete pad that is anchored directly to nearby nonfractured bedrock, deformations at the SG will reflect those over a much larger surrounding area. Frequently, SGs are located in an underground setting together with other instrumentation (seismometers and tiltmeters) that is normally on bedrock. There is no problem in siting an SG within such a complex, provided an environment is created around the instrument to protect it and the associated electronics from excessive humidity and temperature changes. The coldhead and compressor may be too noisy to be placed near other instruments and these need to be sited with some care.

For above-ground situations, it may not be possible to find bedrock and the gravimeter will have to sit on a concrete pad secured to unconsolidated material. The

type of material (clay, gravel, sand, etc.) will play an important factor in the interpretation of meteorological and other seasonal effects. For example, it has been found that porous material can compress and deform under loading and thus generate an unwanted signal. Whatever the height of the SG with respect to the local ground level, an important factor effect is the soil moisture content of the local and regional area from 1 to 100 m around the gravimeter. Soil moisture resides largely in a layer no more than 1 or 2 m thick, but the effect on an SG can be significant. Installation of groundwater sensors, soil moisture probes, rainfall gauge, and other meteorological sensors are required for developing advanced hydrological models at the sub-μGal level.

The requirements of location, site noise, and site preparation need to be assessed very carefully by potential new users. Considerable experience lies both with the manufacturer (GWR) and with many experienced SG owners, who have maintained their stations for a decade or longer. Although there is no central funding source for establishing new SG sites, potential new users are encouraged to contact existing SG groups for advice, particularly through the GGP website, GGP workshops, and by visiting operating GGP sites.

3.04.2 SG Data Analysis

As with all modern geodetic techniques, data from SGs require specialized processing before it can be used to its fullest advantage. There is a large amount of GGP data available from GGP-ISDC (Information System Data Center) online, hosted by International Center for Earth Tides (ICET), but it may be of limited use to scientists unfamiliar with these kinds of data. The purpose of this section is to review the common procedures in analyzing the data for different end uses. A summary of the GGP project is given in Crossley *et al.* (1999), and station names and details can be found in Crossley (2004).

3.04.2.1 Preprocessing

3.04.2.1.1 Second data sampled from an SG

SG data acquisition systems usually record two types of signals: the gravity feedback signal at high accuracy (0.1 nGal) and at precise times, and many auxiliary channels such as environmental data (e.g., atmospheric pressure, room temperature) and instrument parameters (e.g., tilts). The gravity is typically recorded at 1, 2, or 5 s intervals, whereas the auxiliary signals are often sampled at lower rates, for example, 1 min.

Examples of raw SG data are shown in **Figure 7**. **Figure 7(a)** shows data from the Cantley and Boulder instruments at 1 and 5 s sampling, respectively. There is a noticeable difference in high-frequency noise between the recordings due to the different sampling rates and antialiasing filters. Most of the noise is microseismic, that is, the incessant propagation of surface waves generated by wind and ocean turbulence, between 1 and 10 s, in the period range where most SG data are sampled. **Figure 7(b)** shows data from the Strasbourg instrument for the day after the Sumatra–Andaman earthquake (26 December 2004). The earthquake clearly dominates the tides, but SGs are not gain-ranging instruments, so the surface waves from large events are frequently clipped.

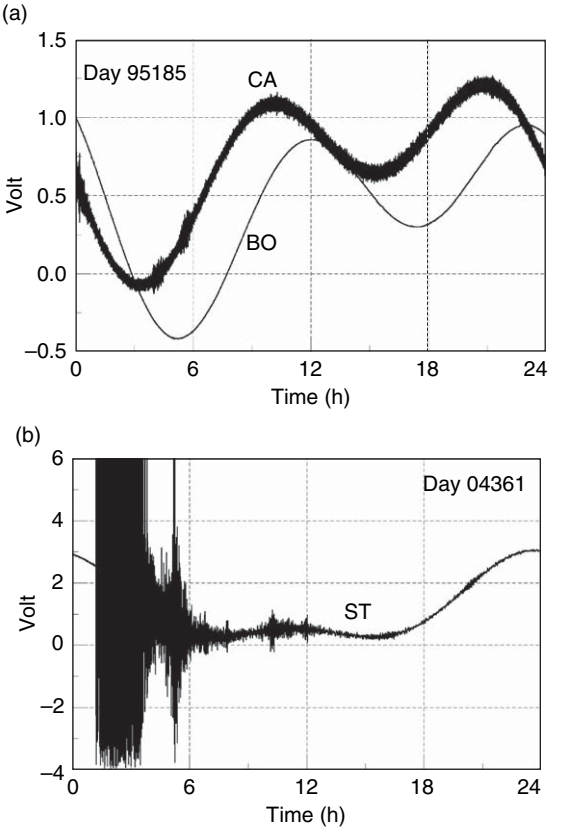

Figure 7 Examples of 1 day of raw SG data (a) from stations CA (Cantley, Canada) (1 s sampling) and BO (Boulder, USA) 5 s sampling) and (b) from station ST (Strasbourg, France) (2 s sampling) that includes the $M_w = 9.3$ Sumatra–Andaman earthquake.

The 1 or 2 s data are usually not sent to ICET, although there is a mechanism for receiving it. Initially, the issue was one of file size, but also the high rate data are not generally interesting from a geodetic point of view. Some of the raw data are transferred to the Incorporated Research Institutions for Seismology (IRIS) database, where it is of interest in the study of seismic normal modes of the Earth (Widmer-Schnidrig, 2003).

3.04.2.1.2 Minute data from the GGP database (ICET)

Most of the data available at ICET/GFZ are 1 min data sent by each station on a regular basis (one file per month). The requirements of GGP are that operators must apply a digital decimation filter to their raw data and resample it at 1 min using a zero-phase digital filter. The local air pressure is also decimated to 1 min, and the two series are combined in a simple ASCII file; each sample is date and time stamped and the file has appropriate header information. A sample of data from the Strasbourg station is shown in **Table 1** in the PRETERNA format that is part of the ETERNA Earth tide analysis program (Wenzel, 1996b). This data is uncorrected, that is, data disturbances such as spikes, offsets, and other problems still remain, inevitably smoothed by the decimation filter.

A display of minute data from ICET is shown in **Figure 8**; this is from station Boulder for the month of September 1997. The month is chosen for illustration purposes because it has data gaps, spikes, and (not visible at this resolution) signals that seem to be offsets. Generally, the data at ICET vary from bad months like this to completely trouble-free data; a typical file may contain one or two problems to be fixed. Each monthly file is about 1.5 MB uncompressed.

Two different philosophies have been used to solve problems in the data: either leave gaps (i.e., simply ignore bad segments), or remove disturbances and offsets and fill the gaps with a synthetic signal from a model. The former (leave gaps) requires that all processing steps have to maintain the integrity of the gaps and this reduces the flexibility of using most time series analysis algorithms in their standard form. The latter (fix gaps) requires further choices about what level of disturbances to treat and what to leave alone, but it is the preferred approach within the gravity community. The main reason is the convenience of dealing with continuously sampled data rather than data in sequences of blocks and gaps. Computer algorithms are also easier to implement for continuous data than data organized into blocks, but this is not the only reason to repair bad data.

Some geophysicists would argue, with justification, that one should not 'invent' data for the convenience of processing. Pagiatakis (2000) proposed the treatment of SG data using a least-squares inversion for all possible constituents at once, as is commonly done for other complex data sets, for example, very long baseline interferometry (VLBI). In passing over 'bad' data, the amplitudes of offsets are included as variables in the inversion; so they are removed simultaneously with tides, pressure, drift, and other modeled effects. This obviously requires a large computational effort,

Table 1 Sample GGP 1-min data file

```
Filename                                    :  ST041200.GGP
Station                                     :  Strasbourg, France
Instrument                                  :  GWR C026
Phase Lag (sec)                             :  17.1800   0.0100    measured
N Latitude (deg)                            :  48.6217   0.0001    measured
E Longitude (deg)                           :  7.6838    0.0001    measured
Height (m)                                  :  180.0000  1.0000    estimated
Gravity Cal (nm.s-2/V)                      :  -792.0000 1.0000    measured
Pressure Cal (hPa/V)                        :  22.2222   0.1000    estimated
Author                                      :  jhinderer@eost.u-strasbg.fr
yyyymmdd  hhmmss  gravity (V)  pressure (V)
C*******************************************************************************
77777777
20041201  000000  2.448085  4.914420
20041201  000100  2.452300  4.912670
20041201  000200  2.456466  4.910337
20041201  000300  2.460378  4.908314
20041201  000400  2.464132  4.906599
```

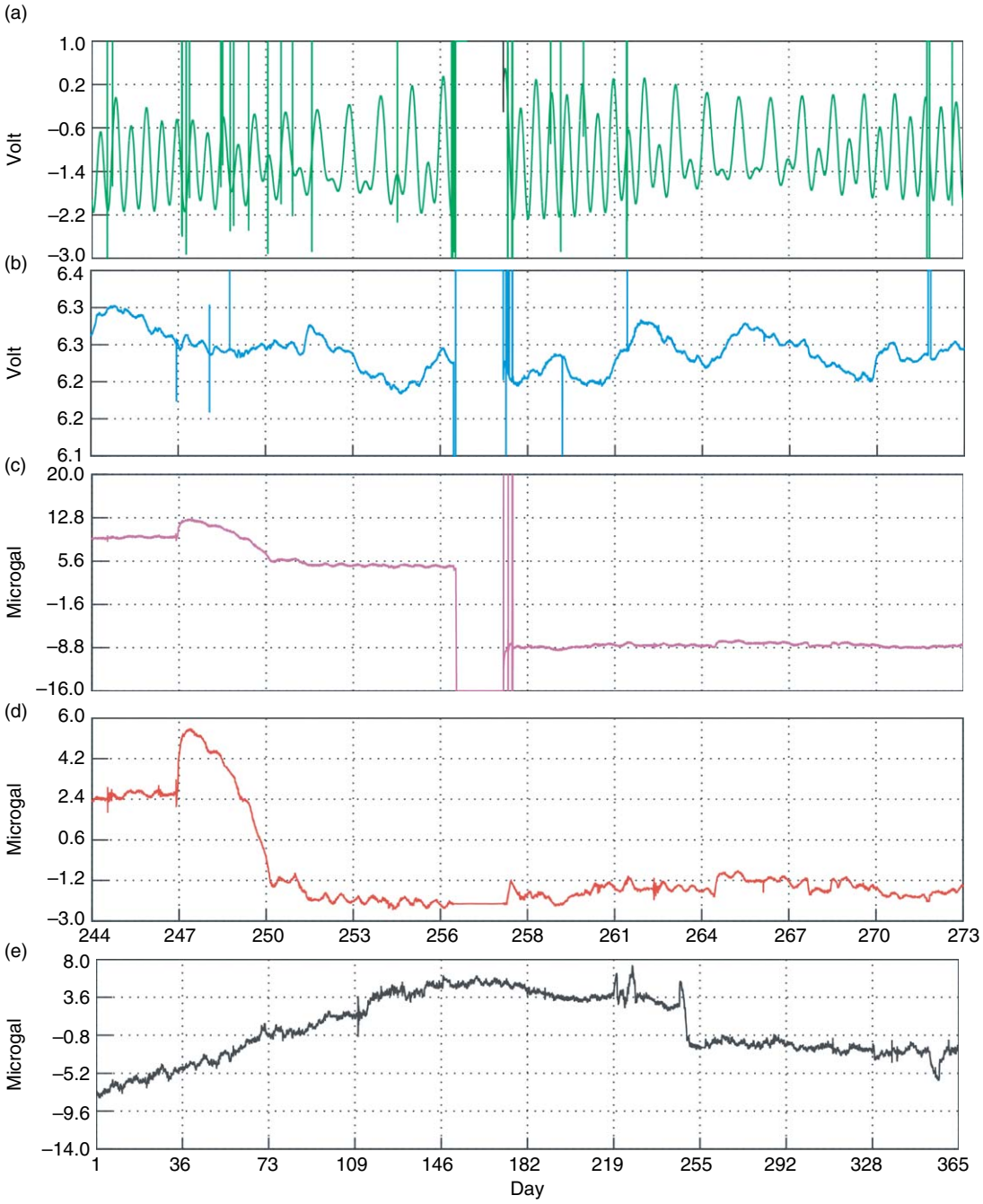

Figure 8 Preprocessing of 1 min data for station BO (Sep. 1997): (a) original gravity; (b) original pressure; (c) after small gaps (<10 s) are filled and removal of tides and nominal pressure; (d) after a large gap with offset is corrected; and (e) the residual gravity for the whole of 1997 after gaps and offsets are removed.

particularly when using 1 s data (as opposed to 1 min data) and when the data spans many years or even decades. The inversion also requires interpretation of the resulting parameter covariance matrix to see what tradeoffs exist in the model. This approach does not give an intuitive feel for the effects of various processing steps and there are many different corrections to be included. For the rest of the article, we turn to the gap-filling approach and assume that the goal is to produce and analyze a uniformly sampled residual gravity series.

A simple model will suffice for most of the following discussion.

$$\begin{aligned} g\ (\text{observed}) = {} & g\ (\text{disturbances}) \\ & \quad (\text{of instrument and station origin}) \\ & + g\ (\text{tides}) \\ & \quad (\text{solid Earth, ocean}) \\ & + g\ (\text{nontidal loading}) \\ & \quad (\text{atmosphere, ocean currents}) \\ & + g\ (\text{polar}) \\ & \quad (\text{annual and Chandler polar motion}) \\ & + g\ (\text{drift}) \\ & \quad (\text{instrument drift function}) \\ & + g\ (\text{hydro}) \\ & \quad (\text{rainfall, soil moisture, groundwater}) \\ & + g\ (\text{residual}) \\ & \quad (\text{ocean currents, other signals,} \\ & \quad \text{deformation, tectonics,} \\ & \quad \text{slow eartquakes, etc.}) \end{aligned} \qquad [1]$$

The purpose of data processing and analysis is to remove the effects that are not the subject of investigation and model the effects that remain. We note at this point that the instrument amplitude calibration factors are required in the next step in order to convert the observed data (g, p) in volts to their equivalent gravity and pressure values:

$$g\,(\mu\text{Gal}) = g\,(\text{volt})^{*}\text{GCAL}$$

$$p\,(\text{hPa}) = p\,(\text{volt})^{*}\text{PCAL}$$

Calibration issues are discussed in detail later in this chapter.

3.04.2.1.3 Remove–restore technique

The most widely used approach is to first make nominal corrections for some of the largest influences such as tides and pressure (remove), then fix the problems in the residual signal and put back the removed signals (restore). The data can then be used for whatever processing and analysis is desired. Before any corrections are made to gravity, the first step is therefore to deal with problems in the atmospheric pressure, because this will be used in the remove–restore phase. **Figures 8(a)** and **8(b)** show the residual gravity and pressure for 1 month; clearly, the pressure has disturbances and gaps at the same time as in the gravity channel, indicating problems in the data acquisition system.

With pressure data, it is difficult to generate data within gaps, short of running computationally intensive weather forecasting codes or interpolating data from meteorological stations surrounding the gravimeter. Meteorological services give hourly pressure data that is available by request or through the Internet. For simplicity, a linear extrapolation between the beginning and end points of the gap, even for gaps extending for days or more, may be sufficient. Pressure variations have only a small seasonal signal, and no significant daily variation, so this interpolation is at least reasonable, if not ideal. For longer gaps of several days or more, an auxiliary source of data as mentioned above should be considered, especially where the pressure channel has failed but the gravity data are still good.

Pressure sensors are usually factory calibrated (PCAL), but this calibration factor needs to be monitored by the user. From time to time, the sensors need recalibration for drift or other problems, or even replacement, and this can introduce a dilemma in the processing. Having detected a problem, should one allow for instrument drift over a previous period of time, or simply assume an offset? No one solution is ideal in all cases. We assume that the pressure record has been made continuous through gaps, and been cleaned of spikes and other disturbances. Depending on the circumstances, this might have required ancillary data, or perhaps linear interpolation.

The gravity signal is not so easily dealt with. The data in **Figure 8(a)** are dominated by the tidal signal that varies usually between 100 and 300 μGal in amplitude, depending mainly on station latitude and the phase of the lunisolar cycle. For very short gaps or spikes (10 s or less), linear interpolation will work without much problem even without removing the tides. This is especially effective if applied to the original raw data (at second sampling), because spikes or gaps are then not smeared into the record by the second-to-minute decimation filter. For longer gaps, we need a version of the remove–restore philosophy.

3.04.2.1.4 Treatment of gaps in gravity data

To repair gravity data, we normally construct a preliminary model based on the tides and nominal atmospheric pressure. For longer gaps, it may be appropriate to add instrument drift and perhaps polar motion. The tides are usually modeled by summing wave groups with specific gravimetric factors (δ, κ) determined in some prior tidal analysis at the station (see below). The preliminary model is then subtracted from the observed data to reveal

hidden problems that need to be fixed. We call the residual gravity g (temp):

$$g\,(\text{temp}) \;=\; g\,(\text{observed}) - g\,(\text{removed}) \qquad [2a]$$

where

$$g\,(\text{removed}) \;=\; g\,(\text{tides}) + g\,(\text{nominal pressure}) + g\,(\text{drift}) + g\,(\text{polar motion}) \qquad [2b]$$

The instrument calibration factor already enters eqn [2]. Note that a linear function is normally used to fill in a residual gap, so we are interested only in modeling signals that are not linear during a gap. Polar motion is very well defined by IERS data, but at a level of 5 μGal yr^{-1} (or 0.01 μGal day^{-1}) it is not important for gaps of less than a week or so. Instrument drift over the time period of most gaps can usually be taken as a simple linear function of time. Other components of the signal such as hydrology or nontidal ocean loading are, however, too complex to be included as part of the removed function, even though they can have an effect of several μGal over time spans of days.

Figure 8(c) shows g (temp) for the case when g (removed) consists of a local tide model and a nominal pressure correction. All the short spikes were previously replaced by a simple linear interpolation on the original data, as discussed above. Because the pressure is included in the g (removed) model, it is corrected before the gravity in order to avoid introducing spurious signals in the gravity. The gravity series still has a major problem between days 256–258, but otherwise looks 'better'.

At ICET/GFZ, the basic files for all stations have uncorrected minute data of the form of **Figures 8(a)** and **8(b)**, that is, raw data decimated to 1 min but with no data repair prior to decimation. ICET produces corrected minute data in which data repair has been done on this already-decimated minute data. Some users also send data that have been repaired at the second sampling rate prior to decimation.

3.04.2.1.5 Disturbances and offsets

To make further progress, we now work with the residual series g (temp), as in **Figure 8(c)**. The major disturbance at day 256 contains an offset and there is a suspicious signal at day 247 that requires consideration. Repairing (fixing) the offsets in **Figure 8(c)** is one of the most critical processing steps, requiring choices as to which problems to leave alone, and which to fix. We consider an offset (or tare) to be any apparent change in the instrument base level. This could be a small offset (0.5 μGal) that takes place within one time step (e.g., 1 s) due to an instrumental or electronic event. Alternatively, an offset may occur during helium refilling (maybe 10–20 μGal) or a major electrical strike that causes level changes of 100 μGal or more.

Here we choose to fill the gap between days 256 and 258 with a straight line and to absorb the apparent level change into an offset that is 13.816 μGal. We have no means of knowing the actual offset during this time (the gap), so we simply join the good data before and after with a straight line and compute the offset needed to minimize the residual signal. This is a large offset that is clearly associated with something that happened to the instrument, involving also the pressure; the instrument base level was changed by a non-geophysical event. Unfortunately, the data log is unavailable for this time period at Boulder, but at most stations there should be a written explanation of such events (stored in the GGP database as 'log' files). Some disturbances will not cause an obvious offset in the data, but clear offsets should be removed.

The 'fixed' residual is shown in **Figure 8(d)** (that interpolates the gap), but there is still an anomaly at day 247 with a jump of 2 μGal followed by a gradual decrease of 4 μGal. We know that rapid changes of gravity can be caused by physical processes such as heavy rainfall (Crossley and Xu, 1998; Klopping *et al.*, 1995), but there is no reason at this point to adjust the data, even though the disturbance causes an apparent offset. Even though a log file helps to indicate a non-geophysical cause for an offset, it usually cannot help to decide what the size of a particular offset may be.

After going through the whole year 1997, we find a total of 29 problems that need to be fixed, three of which were readily apparent offsets. The residual curve for the whole year is shown in **Figure 8(e)**. Day 247 still shows up as a possible nonphysical anomaly, as there is no apparent subsequent recovery from the level jump. Without the 'offset', the data would show a smooth annual variation that arises predominantly from polar motion. Although it might be tempting to treat more aggressively the level change as an offset, doing so will affect all the subsequent data, and it is clearly risky to do so without good reason.

3.04.2.1.6 Automatic procedures

Ideally, each day's raw data record should be scanned visually for potential disturbances. Where this is not possible, simple numerical algorithms can scan the data for the rapid detection of anomalies. One

Table 2 Maximum slew rates for some geophysical signals

	(μGal min^{-1})
Solid earth tides	0.95
Atmospheric pressure	0.20
Groundwater variations	0.02

method uses the slew rate (Crossley *et al.*, 1993) that computes the simple forward data derivative and flags data points that exceed a certain threshold. We indicate from typical records the maximum slew rates in **Table 2**, although these may be exceeded in some situations. With the solid tides in the gravity signal, slew rates can reach up to 1 μGal min^{-1}, and this rate is important when trying to determine the phase calibration of the instrument, as discussed later. The next largest slew is from the atmosphere, and this is an order of magnitude larger than the slews from groundwater, rainfall, and soil moisture. Disturbances and offsets can have much larger slew rates, but sometimes they are small slews that cannot be distinguished from the real signals above. Most users would use slew rate as a diagnostic but not as a corrective procedure. Another approach is to compare each data point with a predicted value based on the accumulated statistics of previous data.

Two widely used software packages, TSOFT (Van Camp and Vauterin, 2005) and PREGRED (part of the ETERNA package; Wenzel, 1996b), deal especially with the preprocessing of gravity data, provide some automation of data analysis, and incorporate many other processing options. TSOFT is probably the most widely used package for GGP data.

To give further insight into the effect of processing choices, we show some examples from Hinderer *et al.* (2002a). In each case, the same 6 months of data (March–December 1997) were given to different scientists to repair, and the results were compared. **Figure 9(a)** shows how four different operators approached the problem of a moderate-sized earthquake that was removed. The results ranged from removal of just the large surface waves (SR) to removal of most of the disturbed record (JPB). For a transient disturbance without offset, four different choices were made about which parts of the signal to repair (**Figure 9(b)**); depending on the choice, the final and starting levels of the different options obviously diverge. Finally, a highly disturbed portion of the record due to a helium refill (**Figure 9(c)**) was an opportunity for two operators (JPB, DC2) to remove an apparent offset, and two others chose to leave it in. Some of this processing was done using TSOFT and some using other algorithms and procedures.

3.04.2.1.7 Processing for different purposes

For several end purposes, the long-term trends in the data are unimportant. This is the case for tidal processing, that is, for finding gravimetric tidal factors, ocean loading, and related signals such as the resonance effect of the free core nutation (FCN). Other possibilities are signals in the 1–24 h range (e.g., the possible Slichter triplet) and, of course, high-frequency seismic modes. In these cases, a more aggressive treatment of disturbances and offsets might be beneficial. **Figure 10(a)** shows the effect of the different processing options from **Figure 9** in the frequency domain, that is, the power spectral density (PSD) function. There are five different options ranging from a very minimal treatment (DC1 – not shown in **Figure 9**) to a comprehensive removal of problems (JPB). The latter has effectively reduced the noise floor in the long-period seismic band (up to about 5×10^{-5} Hz or 5.5 h) by more than an order of magnitude. This is mainly due to the removal of offsets and disturbances that contain high frequencies.

When the goal is to preserve the long-term evolution of the gravity residual rather than search for short-period signals, offsets must be examined carefully. If offsets occurred randomly in time and with random amplitudes, their accumulated impact is similar to a brown noise or random walk type of process. The mean value drifts from the true gravity, and this would be detectable only by comparison with absolute gravity measurements. Large offsets (5–10 μGal or more) need to be corrected, especially when they are logged as due to specific causes. Sometimes, smaller offsets happen without apparent cause, but if not corrected a bias can easily accumulate. Even with appropriate software this can be a time-consuming process, as already discussed.

We show in **Figure 10(b)** the effect of different options in the time domain, over the 6 month test period referred to earlier. All the traces coincide at the beginning but diverge by up to 1.5 μGal after 6 months, the largest part of this difference being due to the different treatments of the disturbance in **Figure 9(c)**. As indicated above, the use of the AG measurements can be very useful in identifying offsets at the level of a few μGal. Note that in **Figure 10(b)** instrument drift plays no role in the processing differences.

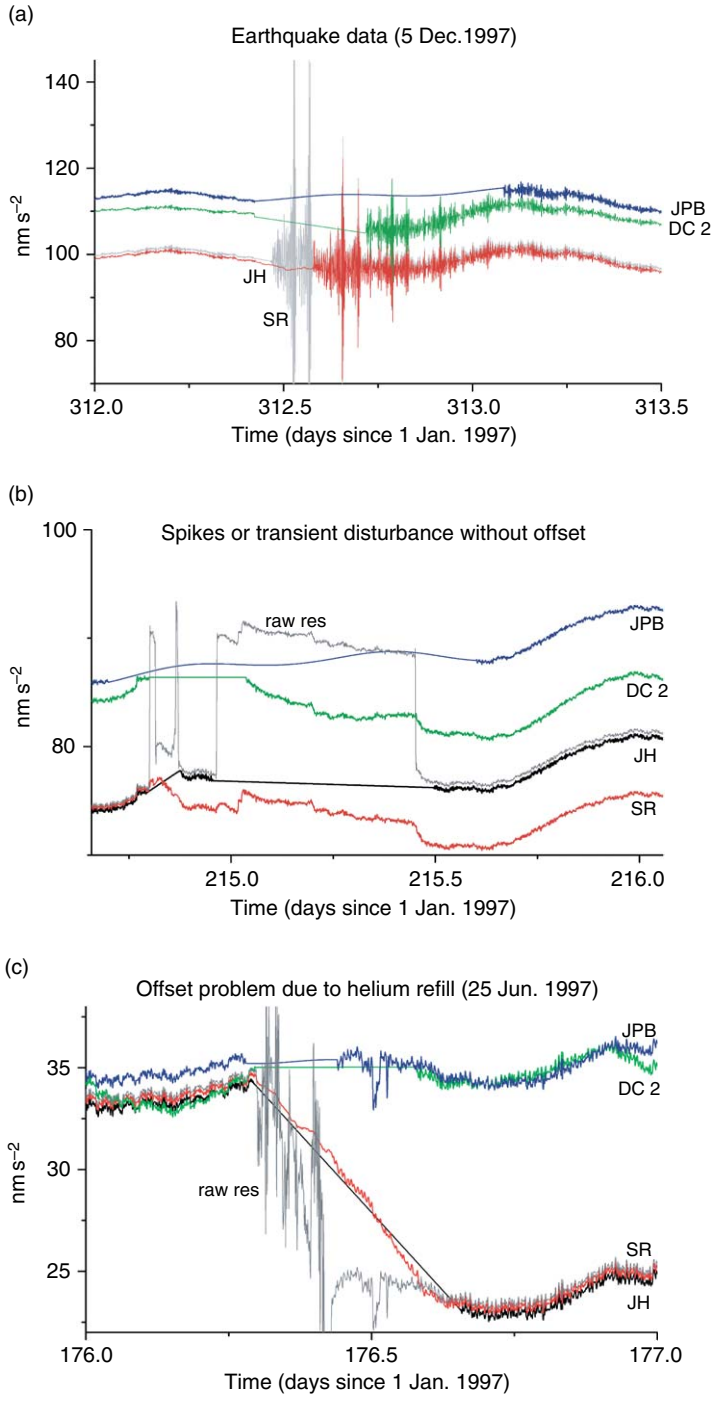

Figure 9 Examples of the data corrections done independently by different operators (identified by initials) for the removal/interpolation of (a) an earthquake, (b) disturbances without offsets, and (c) an offset caused by a helium refill. From Hinderer J, Rosat S, Crossley D, Amalvict M, Boy J-P, and Gegout P (2002a) Influence of different processing methods on the retrieval of gravity signals from GGP data. *Bulletin d'Informations des Marées Terrestres* 123: 9278–9301.

Long gaps in a record make determination of offsets difficult, if not impossible. There are two saving strategies – either to rely on the co-location of AG measurement to anchor the SG record at the ends of a long gap, or possibly use a fit to the polar motion when there is a suspected large offset within the

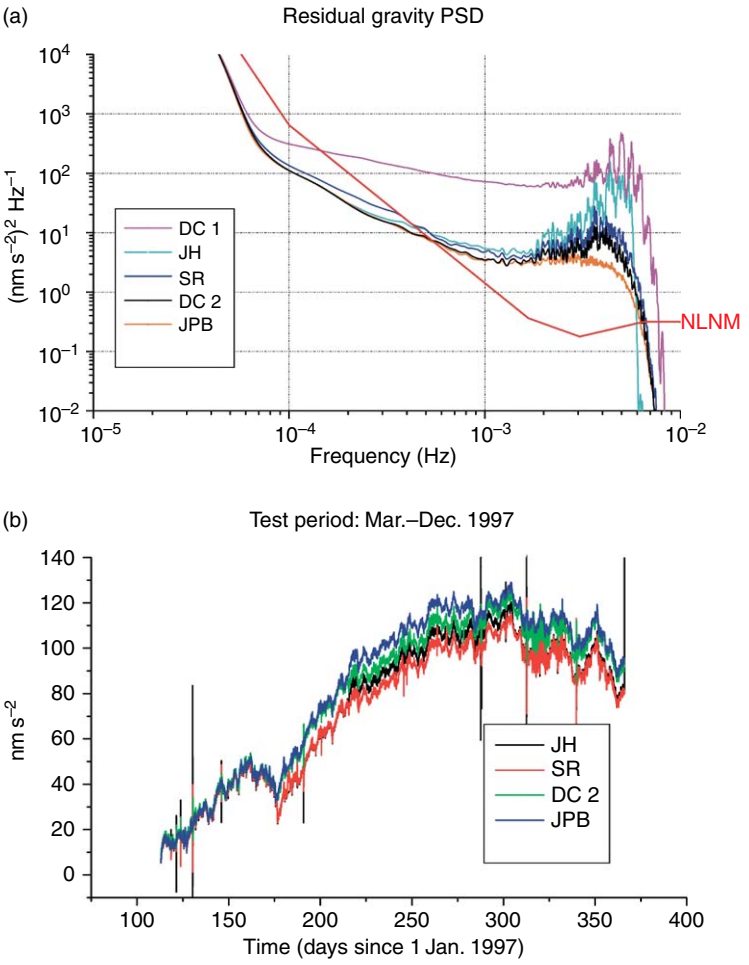

Figure 10 The cumulative effect of data corrections for a test period of 6 months of data from different treatments (a) in the time domain, showing a 1.5 μGal offset between treatments and (b) in the frequency domain – NLNM is the new low noise model of Hinderer *et al.* (2002a).

downtime of the gravimeter. Long gaps in the record are generally due to serious problems in the instrument or data acquisition system, so an offset is certainly possible. Unfortunately, other instruments (e.g., spring gravimeters), even when available, have too much drift to provide a good interpolation signal to fill in an SG record for more than a few hours.

3.04.2.1.8 *Restoring the signal*

When all problems have been removed from g (temp), it is easy to recover the observed gravity from [2], so that

$$g\,(\text{fixed}) = g\,(\text{temp}) + g\,(\text{removed}) \qquad [3]$$

is now the observed gravity with the problem segments repaired. Referring to eqn [1], we note that the fixed data have a signal in the gaps that do not contain the more complex effects such as hydrology. In all other respects, however, the data in the good portions are identical to the observations, and the fixed gravity can now be analyzed for the components in eqn [1]. By subtracting g (fixed) from g (observed), it is always possible to see exactly what has been removed during this stage of the processing.

3.04.2.2 Solid Earth and Ocean Tides

3.04.2.2.1 *Tide-generating potential*

The basis for computing a theoretical gravity tide is the tide-generating potential (TGP). Using the orbital and rotational data for the Earth as forced by the Sun and Moon, this potential was first given as a catalog by Doodson (1921), who included only terms of degree 1–3 (i.e., 24, 12, and 8 h periods). The tides occur in the

rotating frame of the Earth's mantle, but they also lead to forced nutations of the Earth in the space-based (nonrotating) coordinate system (e.g., Melchior and Georis, 1968). There is one tidal wave associated with each component of the Earth's nutation. The most extensive tidal developments now include the perturbation effects of all the major planets and terms up to degree 6 for the moon (period 4 h) as well as terms allowing for the nonspherical shape of the major bodies. The most recent references on the tidal potential for gravity work are Hartmann and Wenzel (1995a, 1995b), Roosbeek (1996), and Wenzel (1996a).

There are two approaches to cataloging the TGP. First, the ephemeris – a catalog of apparent positions of the bodies in the solar system as seen from a position and time on the Earth; each body is defined by a longitude, latitude, right ascension, and obliquity. In this method, an ephemeris tide program (e.g., Merriam, 1992a) generates a time series from the TGP on the surface of a rigid Earth. The accuracy of this TGP is directly related both to the accuracy of the ephemeris itself and the analytic theory used to describe the motions of the planetary bodies. Merriam estimated for GTIDE an rms time-domain accuracy of 0.25 nGal, with a maximum error of 0.8 nGal.

Wenzel (1996a) compared three tidal ephemeris programs: GTIDE as updated in Merriam (1993a), and two JPL programs DE200T and DE403T that he used to generate six benchmark gravity tides series. These series were gravity at 1 h spacing for two example epochs (1987–93; 2017–23) at the Black Forest Observatory (BFO) in Germany (chosen because of the availability of gravimeter data at BFO). The internal time-domain accuracy of the benchmark series derived from the JPL ephemerides is better than 0.1 nGal, and in the frequency domain the rms errors are about 100 times smaller.

The second approach, which is a more widely used method for the TGP, is to sum together a number of harmonic terms, each of which represents a partial tide. The frequencies and amplitudes of these waves can be derived from the ephemerides by constructing a time series and then filtering it, as in the CTE potential (Cartwright and Taylor, 1971; Cartwright and Edden, 1973), or using analytic means as for the Xi89 potential (Xi, 1987, 1989), and the potential RATGP95 (Roosbeek, 1996). Alternatively, the waves can be found by fitting coefficients to a series based on an ephemeris – the spectral method – as used in the Tamura87 and Tamura93 potentials (Tamura, 1987, 1993) and in HW95 (Hartmann and Wenzel, 1995a, 1995b). These TGPs (except for CTE that has now been superseded) shown in **Table 3**, are those most commonly used in high-precision gravity work. They include tables (catalogs) specifying the frequencies and amplitudes of the waves (actually wave groups) that must be summed. By selecting different subsets of waves, the speed of computation can be adjusted according to the accuracy required.

Merriam (1993a) compared the catalogs of Tamura (1987) and Xi (1989) with GTIDE and concluded that although their differences should be detectable using SGs, in practice either of the catalogs could be used for SG analysis. Wenzel (1996a) compared all the above series and catalogs and concluded that the HW95 was the most accurate for high-precision work. Roosbeek (1996) notes this is expected because HW95 is derived from one of the benchmark series itself and its only error should be computational. Tamura93 is widely used as a compromise between speed and accuracy.

3.04.2.2.2 Elastic response of the Earth

Once the tidal forcing series has been accurately computed for a precise latitude and longitude, it is necessary to allow for the deformation of the Earth to compute an approximation to the observed solid tide.

Table 3 Tide-generating potential used in SG data reduction

Catalog	# waves	# coeffs.	Degree	Time (ngal)	Frequency (ngal)
CTE	505	1010	3	38.44	0.565
Tamura87	1200	1326	4	8.34	0.118
Xi89	2934	2934	4	6.42	0.090
Tamura93	2060	3046	4	3.08	0.046
RATGP95	6499	7202	6	2.00	0.026
HW95	12935	19271	6	0.14	0.002

The last two columns refer to rms accuracies in the time and frequency domains respectively.
Modified from Wenzel H-G (1996a) Accuracy assessment for tidal potential catalogues. *Bulletin d'Informations des Marées Terrestres* 124: 9394–9416.

This is usually done within the tide program through the use of elastic load Love numbers (h_n, k_n, l_n) for each of the harmonics (denoted by n) in the TGP. The Love numbers are computed by solving the gravitoelastic equations of motion for the Earth and finding the surface displacement $\mathbf{u}$ and potential Ψ for any kind of forced deformation (e.g., tides or loading) (e.g., Wang, 1997):

$$\begin{aligned} \mathbf{u} &= h_n \boldsymbol{\psi}^1 / e_r + \ell_n \nabla_1 \boldsymbol{\psi}^1 / g_0 \\ \boldsymbol{\psi} &= k_n \boldsymbol{\psi}^1 \\ \delta_n &= 1 + 2h_n - (n+1)k_n/n \end{aligned} \quad [4]$$

Here, $\boldsymbol{\psi}^1$ is the perturbation in the gravity potential, $\mathbf{e}_r$ is the radial vector, ∇_1 is the surface gradient operator, and g_0 the surface gravity. The Love numbers completely describe any kind of deformation, elastic or inelastic, and therefore contain all the complexity of the actual Earth, that is, resonances for all the Earth's normal modes, anelasticity and frequency dependency (e.g., Dickman, 2005). Love numbers have been frequently computed for seismic Earth models such as PREM (Dziewonski and Anderson, 1981) and given in a number of different forms; they are in principle complex numbers because of the Earth's anelasticity (e.g., Mathews, 2001). Of interest here are the real gravimetric tidal factors (δ_n, κ_n), where κ_n defines the phase of the tidal wave as observed (or computed, note it is 0 for an elastic model) with respect to the TGP and δ_n is found from a combination involving h_n and k_n, as above (ℓ_n is not used in gravity). Typical elastic values are $h_n = 0.602$, 0.291, and 0.175, and $k_n = 0.298$, 0.093, and 0.043, yielding $\delta = 1.155$, 1.167, and 1.121 for $n = 2$, 3, and 4, respectively. A nominal pair of values is taken as ($\delta = 1.16$, $\kappa = 0$).

Gravimetric factors can be used to construct the synthetic tide at a station and are thus the simplest way to 'de-tide' a gravity record (especially a short one where tidal fitting would be problematic), and of course are perfectly suited to constructing the 'removal' signal discussed above. They can be found empirically from a tidal analysis at a station, noting that there should be no phase lag entered into the program (e.g., Crossley and Xu, 1998). When the synthetic tide is reconstructed from the empirical gravimetric factors, both the ocean loading, considered in the next subsection, and the system phase lag will be automatically included along with the solid tide.

3.04.2.2.3 Ocean tides and loading

Ocean tides have the same frequencies as solid-Earth tides, but they derive from the vertical and (small) horizontal components of the TGP that generates water movement in shallow areas such as the continental shelves. This variable water depth loads the crust and modifies the amplitudes of the bodily tides as seen on land stations. One problem in computing ocean tides is their variability, due primarily to oceanic weather systems. A further difficulty is the need to define the coastal topography and bathymetry, particularly in remote and icebound locations such as Antarctica.

Ocean tidal loading is almost an invisible effect when doing tidal analysis, because the gravimetric factors are adjusted to the total tide signal that includes ocean loading. There are several problems for which ocean tides and their loading effects need to be studied in detail, and in these cases the ocean loading must be computed separately. Depending on the location, ocean tide loading varies between 1% and 10% of the body tide.

As in atmospheric loading (see Section 3.04.2.3), the ocean load function is generally expressed as the convolution of a Green's function with a suitable data set representing ocean heights. Most ocean loading programs consider the tide heights to be given, for each wave, within cells that follow the coastlines, but the height variability due to weather systems is ignored. Ocean tide heights are now determined almost exclusively by satellite altimetry (TOPEX/POSEIDON), but this still leads to a large number of ocean tide models constructed with differing assumptions and constraints.

Ocean tide loading is an essential element of the complex problem that includes mean sea levels and global warming. It is therefore an important topic in gravimetry that has greatly benefited from the availability of high-quality SG data. Baker and Bos (2003) and Boy *et al.* (2003) have discussed the issue of whether SG data can discriminate between competing ocean tide models, and they emphasize the need for accurate SG calibration. Several computer programs can do the appropriate calculations. Three of the most widely used are SPOTL (Agnew, 1997), OLFG by Scherneck (1991), and GOTIC2 by Matsumoto *et al.* (2001). Boy *et al.* (2003) showed significant differences between these programs and tide models that left the role of calibration unclear. On the other hand, Bos and Baker (2005) concluded that with care the computational errors can be resolved and the programs show almost identical results for all programs and for all tide models. This suggests that there are still calibration issues for SGs. They offer a new program CARGA that incorporates most of the features of the other programs.

Ocean loading corrections are frequently geared to the need for precise geodetic information in particular areas such as Antarctica (Bos *et al.*, 2000) or the Pacific Northwest (Lambert *et al.*, 2003).

3.04.2.2.4 Tidal analysis

Tidal analysis consists of determining the amplitudes and phases of tidal waves of specific frequencies from observational data. How many waves can be determined and to what accuracy depends on the length of the record used and on the noise characteristics of the site. In most approaches, the ocean tides are grouped in with the solid tides of the same frequency, and they cannot be separated by a simple fit of data to known tidal frequencies. Ocean tide variability is reflected in the time dependence of the gravimetric tidal factors at a particular site.

Three programs are used within the SG community for tidal analysis. The most widespread program is ETERNA, developed over many years by Wenzel (1996b) and now in its final form (version 3.3). It consists of a suite of several programs that deal with all the common aspects of processing gravimeter data and it can be adapted to a variety of different data sets; it can also be used for analysis of strain and tilt data as well as gravity. ETERNA is a harmonic method that does a direct least-squares fitting of the (δ, κ) factors for various wave groups to gravity data sampled at fixed intervals, for example, 1 min or 1 h. The program can handle different sub-blocks of data if there are gaps. The user has the choice of simultaneously fitting an admittance function to pressure or other auxiliary data. It includes polar motion and different assumptions regarding the instrument drift function. The program is well documented and available through ICET.

The second approach is a program called BAYTAP-G that was developed by Japanese geophysicists during the 1980s (Tamura *et al.*, 1991). The approach is a hybrid method using a combination of harmonic series and the response method (Lambert, 1974) to estimate the various components of a gravity record (i.e., the tidal parameters, a pressure perturbation effect, a 'drift' function, and irregular noise). One of the distinguishing aspects of the program is a focus on a statistical description of the 'drift', which in this context means the entire long-term gravity signal and not just the instrument drift, and of the random noise Using Bayesian estimates, the procedure involves the nonlinear estimation of a tradeoff parameter between the tidal harmonic series and the residual gravity.

A third program is available, called VAV, which was described most recently by Venedikov and Viera (2004). The origins of this approach go back 50 years or more when gravimeter records were processed by the application of suitable filters of various lengths to account for the tides. Comparisons exist between VAV and ETERNA but the former has not been as widely adopted by the SG community as the other programs. Dierks and Neumeyer (2002) compared all three programs using both synthetic data and a 1 year observed SG data set from station Sutherland (SA). They found the performance of the three programs to be similar, but with different treatments of the statistics between signals (tides, pressure, and drift) and residual gravity. The spectra of the final residuals were noticeably different between the programs, and the reader should consult their paper for details (also for valuable tips on how to set some of the parameters in the program inputs).

A few words should be said about the response method in SG tidal analysis, as discussed by Merriam (2000). Rather than allocating for all waves within a group the same gravimetric factor, the response method selectively interpolates the gravimetric factors using only waves that seem unperturbed by noise (i.e., that are close to their theoretical expectations). Waves that seem anomalous are thus treated independently, requiring a more hands-on treatment, but one that has some practical advantages. The additional flexibility allows a greater reduction in tidal residuals, because it can accommodate the more variable ocean loading.

3.04.2.3 Atmospheric Pressure Effects

The atmosphere provides a significant gravity effect (up to 10% of the tidal signal) with a transfer function (or admittance factor) that approximates $-0.3\ \mu\text{Gal hPa}^{-1}$ for a typical continental station. The effect is a combination of gravitational attraction by atmospheric density anomalies with a loading that vertically deforms the crust and mantle. For a positive atmospheric density anomaly, simple theory gives about $-0.4\ \mu\text{Gal hPa}^{-1}$ for the upward attraction and $+0.1\ \mu\text{Gal hPa}^{-1}$ for the loading. A number of well-studied empirical and physical methods exist for making a pressure correction to the gravity data, but even with the most sophisticated treatments it is not possible to completely remove the atmospheric pressure effect.

3.04.2.3.1 Single admittance factors

Atmospheric effects on gravity became an important consideration with the higher precision and lower noise of the SG compared to previous instruments. Warburton and Goodkind (1977; henceforth called WG77) anticipated most of the issues that were revisited in many subsequent papers (e.g. Spratt, 1982; Müller and Zürn, 1983; Rabbell and Zschau, 1985; and van Dam and Wahr, 1987). A useful review of the role of local, regional, and global effects was given by Merriam (1992b), from which we restate the following conclusions:

1. Approximately 90% of the atmospheric effect comes from the local zone, defined as within 0.5° (or 50 km) of the station, and 90% of this effect is from the direct Newtonian attraction of the atmosphere; the remaining 10% is from loading and deformation of the crust.
2. The regional zone extends from 0.5° to ~3°, or from 50 to 100–500 km (depending on the topography surrounding the station), and in this zone the atmospheric correction is small (a few percent) and primarily comes from loading.
3. The rest of the atmosphere, at distances >3°, is the global effect and contributes only a few percentage of the total atmospheric gravity.

Merriam found a local admittance factor of –0.356 μGal hPa^{-1}, and with a variable regional correction, a combined admittance that varied between –0.27 and -0.43 μGal hPa^{-1}. This is consistent with the factor of -0.30 found by WG77 for frequencies <1 cpd, a factor that is widely applied for the quick 'correction' of gravity due to atmospheric pressure. Note that this factor applies to relative changes in pressure and gravity that have to be propagated from one data sample to the next by maintaining appropriate reference levels.

3.04.2.3.2 Frequency-dependent admittance

WG77 first recognized that a single admittance factor was not appropriate at all frequencies, partly because of the separate effect of atmospheric tides at harmonics of a solar day (e.g., Elstner and Schwahn, 1997). In addition, however, the atmosphere shows more coherency toward higher frequencies (2–8 cpd) and the admittance factor from data at a single station is larger than at lower frequencies (<1 cpd) when regional scales become important. WG77 also introduced the cross spectrum between gravity and pressure to find an admittance function in the frequency domain, and this was extended by Crossley *et al.* (1995) and Neumeyer (1995), who showed the advantages that could be realized under certain conditions. Frequency dependence is equivalent to allowing the admittance function to vary in time, as would arise in the passage of weather systems (e.g., Müller and Zürn, 1983).

To give some insight into these points, we show in **Table 4** a comparison of different processing methods, from Crossley *et al.* (1995). Four different corrections are given with the notation TD = time domain; FD = frequency domain; δg = gravity correction in the TD; Δg = Fourier transform of δg; and $p(t)$ = pressure.

Note that fitted values of the admittance α (cases 2 and 3) are smaller than the nominal correction (case 1), because they respond to the lower coherence in the atmospheric signal at long periods and at frequencies that are harmonics of 1 cpd. This is clear in **Figure 11** that shows the amplitude component of the admittance from 2 years of gravity and pressure data from Cantley (CA). The smooth background obtained by binning segments of the spectra uses an averaging window of 1.5 cpd and represents the increasing coherence with frequency of the atmosphere as sampled from a single location. Note that the asymptotic value is consistent with the values of 0.356 μGal hPa^{-1} quoted by Merriam. The sharp negative lines are computed separately from a narrow window of 0.01 cpd centered on the harmonics of a day and reflects the low coherence between gravity at a single location and the global atmospheric tides. There are issues with using such a function, however, because the choice of averaging window has a large effect on how much signal is removed from the gravity residuals.

Table 4 Comparison of atmospheric pressure corrections

Case	Type	Formula	α-value	rms
1	Nominal admittance in the TD	$\delta g(t) = -0.3\, p(t)$	0.30	
2	Fitted admittance in the TD	$\delta g(t) = -\alpha\, p(t)$	0.257	1.147
3	Fitted admittance in the FD	$\Delta g(\omega) = -\alpha\, P(\omega)$	0.255	1.142
4	General FD admittance	$\Delta g(\omega) = -\alpha(\omega)\, P(\omega)$	Fig. 11	0.672

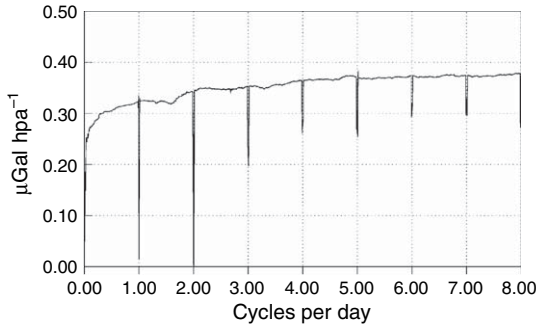

Figure 11 Amplitude of frequency-dependent barometric admittance in **Table 4**, case 4. Reproduced from Crossley D, Jensen O, and Hinderer J (1995) Effective barometric admittance and gravity residuals. *Physics of the Earth and Planetary Interiors* 90: 221–241, with permission from Elsevier.

In the time domain, we compare the signals in **Figure 12**. The upper trace is the uncorrected gravity, the middle trace is corrected with a single admittance (case 3), and the lower trace is for a frequency-dependent correction (case 4). As noted by Kroner and Jentzsch (1999), one should not assume that a smaller residual necessarily means a 'better' correction because the atmosphere is not the only source of gravity variations. In the period range 1–8 cpd, it is known that rainfall and hydrology also contribute significantly to gravity and this extra 'noise' considerably complicates the determination of an accurate admittance. Except for specialized studies, a frequency-dependent admittance is rarely done as part of regular processing. Aside from ease of use, a nominal value of $-0.30\ \mu\text{Gal hPa}^{-1}$ has the advantage that such a correction can be quickly 'restored' to gravity residuals if required.

We note that the atmospheric admittance effects in coastal areas depart from continental areas (discussed above) because water responds to surface pressure as a fluid rather than elastically as for the solid Earth. This inverted-barometer effect permits the water column to adjust isostatically to ocean surface pressure, and the ocean bottom pressure does not contribute to atmospheric loading. The local admittance for near-coastal stations may therefore depart from that represented in **Figure 11**.

3.04.2.3.3 Green's functions and nonlocal pressure corrections

The admittance approach is suited to single pressure series taken at the station but it can approximate only the local part of the atmospheric effect. For regional and global corrections, it is necessary to compute gravity directly from spatial meteorological data. All discussions on loading start with Farrell (1972), who showed how to convolve an observed distribution of surface pressure (data) with a Green's function (or kernel) that represents the effect of a point load for a given source–station separation. The method is quite general and can be used for any kind of surface load as well as local and nonlocal corrections for any kind of atmospheric model.

Two-dimensional loading calculations can take one of two forms: either the surface pressure alone is used or the surface temperature is included which allows the incorporation of thermal changes in the air column using a simple gas law (Merriam, 1992b). The former option is easier to implement because pressure data are widely available from meteorological

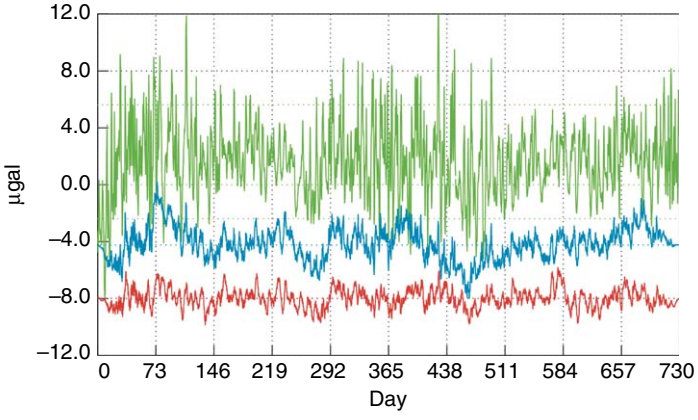

Figure 12 Pressure corrections using an empirical scalar admittance function. The upper trace (green) shows uncorrected gravity residuals (tides, polar motion, and drift removed), the middle trace is after correction using a single admittance (blue), and the lower trace the correction using an empirical frequency dependent admittance. Reproduced from Crossley D, Jensen O, and Hinderer J (1995) Effective barometric admittance and gravity residuals. *Physics of the Earth and Planetary Interiors* 90: 221–241, with permission from Elsevier.

centers, though sampled usually only at 6 h intervals. The thermal admittance given by Merriam is $\delta g = +0.013\ (T_c - 15°)\,\mu\text{Gal}\,°\text{C}^{-1}$ which combines the effects from local and regional zones. In the passage of a cold front, for example, with pressure and temperature changes of 3 hPa and 10°C, respectively (Müller and Zürn, 1983), the gravity effect from temperature is only 10% (i.e., 0.1 μGal) of the pressure effect and may be reasonably ignored.

Numerical computations using global surface meteorological data need to be done for a spherical Earth (Merriam, 1992b), so the computational task becomes nontrivial, especially when using the high-resolution pressure data. Some notable results were found by Mukai *et al.* (1995) and Sun (1995). Boy *et al.* (2002) considered the improvement to be expected at low frequencies when the regional and global loading is done explicitly using various assumptions for the vertical structure of the atmosphere and different meteorological data sets (ECMWF at 1.125° vs NCEP at 2.5°). In addition, they demonstrated that the inverted-barometer assumption is appropriate for periods longer than 1 week. We show in **Figures 13(a)** and **13(b)** their results for two different corrections in zone 2 (the region >0.5°) that provide a reduced gravity residual compared to the local admittance. Note that the use of a simple gas law model of the atmosphere (pseudostratified loading) reduces the size of the nonlocal effect compared to the loading that uses only the surface pressure. As in Merriam (1992b), the atmospheric correction due to temperature and water vapor has been assumed to be small.

Finally, we mention the importance of including topography when making atmospheric corrections in hilly or mountainous terrain (Boy *et al.*, 2002).

3.04.2.3.4 3-D atmospheric corrections

In recent years, and of particular importance to the correction of atmospheric effects in the *GRACE* satellite data (Boy and Chao, 2005), it has been recognized that seasonal mass changes within the atmosphere are not reflected in surface pressure data. This means that an additional 3-D Newtonian attraction needs to be modeled when high-quality atmospheric corrections are required. This has been known for some time, and a correction for this effect can take the form of a simple annual sinusoidal term of amplitude about 0.8 μGal, as reported in Zerbini *et al.* (2001, 2002). A more complete treatment of the effect and the computations required can be found in Neumeyer *et al.* (2004a). Here we show in **Figure 13(c)** sample calculations from this study for four stations in central

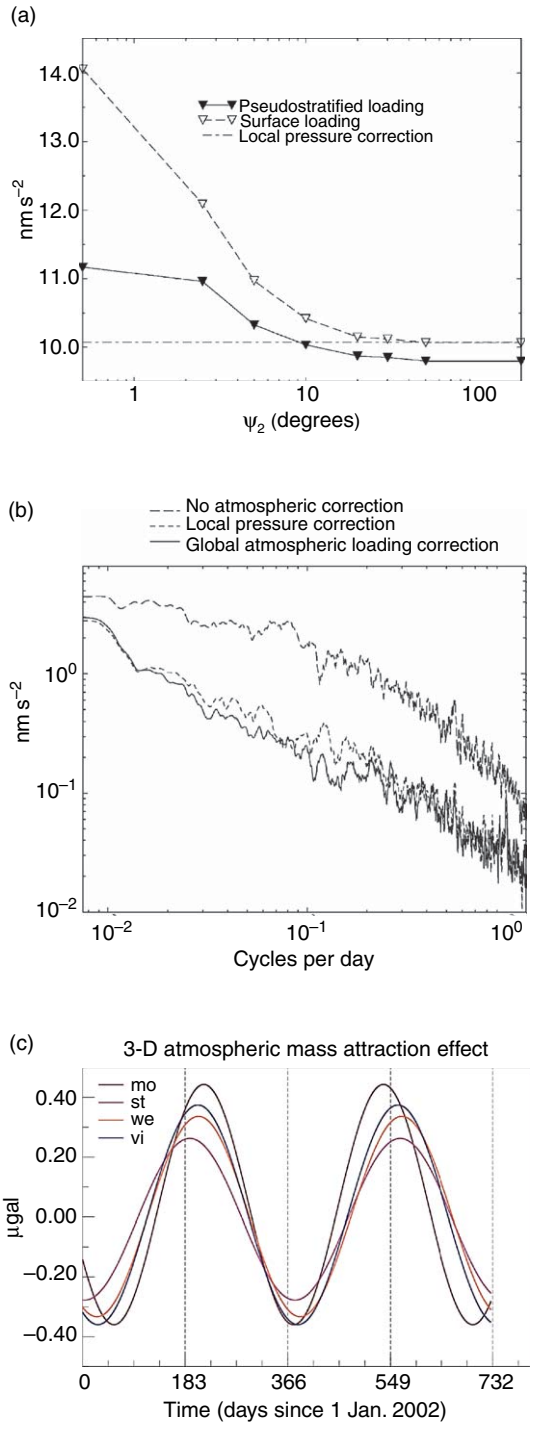

Figure 13 Atmospheric pressure corrections (a) from 0.5° to 180° using 2-D Green's functions compared to a local scalar admittance, (b) the reduction of noise in the frequency domain, and (c) seasonal air mass effect for atmospheric attraction at four GGP stations. (a) and (b) Reproduced from Boy J-P, Gegout P, and Hinderer J (2001) Gravity variations and global pressure loading. *Journal of Geodetic Society of Japan* 47: 1, 267–272, with permission from Geodetic society of Japan.

Europe over a 2 year period (only the annual fitted function is shown). In the summer months, the air masses within the atmosphere rise and the gravitational attraction effect decreases (upward); this causes a net positive gravity effect at the ground that is about 1 μGal larger than that in winter months. Neumeyer *et al.* (2004a) showed that the effect is not the smooth function shown in **Figure 13(c)**, but there are sudden changes that occur over periods of days. The computational effort to include this term is not trivial and it is being done routinely only at a few SG stations; one limitation is the need to interpolate the meteorological data that is available only at 6 h sampling and 0.5° (50 km) spacing. This is also a factor for the data reduction in *GRACE* because the atmospheric pressure corrections are done on the inter-satellite distance timescales that are aliased by 6 h sampling.

3.04.2.4 Calibration Issues

3.04.2.4.1 Basics

SGs are relative instruments and no 'factory calibration' is provided by the manufacturer. The instrument must be calibrated to convert its output feedback voltage, as recorded by a digitizing voltmeter, to units of acceleration. The amplitude calibration factor (GCAL) is frequently called the scale factor of the instrument and is expressed in $\mu Gal\,V^{-1}$ or $nm\,s^{-2}\,V^{-1}$, with a typical value of about $-80\,\mu Gal\,V^{-1}$ (**Table 5**). In addition, the system transfer function of the complete system (sensor and electronics) must be measured to determine the frequency dependence of both the amplitude and phase. Although it is easy to find the approximate calibration (to a few % in amplitude or phase), it is nontrivial to improve the calibration to be better than 0.1%. There are three applications for which accurate calibration is most important: (1) ocean tide loading or solid Earth tidal deformation including the FCN resonance, (2) the subtraction of a synthetic model for tides and the atmosphere whenever residuals are required to high accuracy, and (3) for determining precise spectral amplitudes in normal-mode studies.

The SG output has a very large bandwidth, from ~1 s (the raw sampling) to periods as long as the data length (years to decades). It is common to refer to the long period limit as 'DC' (vaguely meaning beyond

Table 5 Representative SG calibration experiments using an absolute gravimeter

Station	Instrument	AG or method	#drops	Time	SF ($\mu Gal\,V^{-1}$)	(%)
BH[a]	CD030_L	FG5 #101	18 000	2 yr	-73.690 ± 0.088	0.12
		platform			-73.971 ± 0.023	0.03
	CD030_U	FG5 #101			-67.626 ± 0.084	0.12
		platform			-67.922 ± 0.041	0.06
BO[b]	C024	FG5 #205	20 800	9 d	-80.281 ± 0.063	0.08
		platform			-80.341 ± 0.009	0.01
CA[c]	T012	JILA-2	NA	3 yr	-78.3 ± 0.1	0.13
CB[d]	C031	FG5 #206	15 778	6 d	-76.098 ± 0.169	0.22
			46 560	12 d	-75.920 ± 0.061	0.08
MA[e]	T011	FG5 #210	100 000	27 d	-92.801 ± 0.034	0.04
					-92.851 ± 0.049A	0.06
					-92.879 ± 0.036B	0.04
MB[f]	C021	FG5 #202	275 468	47 d	-78.457 ± 0.001	0.06
MC[g]	C023	FG5 #101, 103, 206	18 000	4 yr	-74.822 ± 0.137	0.18
		platform			-74.824 ± 0.013	0.02
ST[h]	TT05	JILA-5	5600	1 d	-76.05 ± 0.55	0.72
ST[i]	C026	FG5 #206	412 244	3 yr	-79.19 ± 0.05	0.06
ST[j]	C026	FG5 #206	450 000	4 yr	-79.40 ± 0.03	0.04
SY[k]	T016	FG5 #203	55 743	15 d	-58.168 ± 0.061	0.10

[a]Falk *et al*. (2001);
[b]Francis *et al*. (1998);
[c]Merriam *et al*. (2001);
[d]Amalvict *et al*. (2001b);
[e]Imanishi *et al*. (2002);
[f]Francis (1997);
[g]Hinderer *et al*. (1991);
[h]Amalvict *et al*. (2001a);
[i]Amalvict *et al*. (2002);
[j]Iwano *et al*. (2003).
Scale factors (SF) are by direct regression except (a) tidal analysis, (b) modified least squares. Station codes, etc., are given in Crossley (2004).

tidal periods), and some of the calibration methods effectively measure this DC amplitude calibration constant, whereas other techniques attempt to find other parts of the transfer function. Even in well-controlled laboratory experiments, it is difficult to provide a suitable acceleration at periods beyond a few hours. This is not an issue for seismometers because they are not designed to measure periods longer than 1 h. For gravimeters at tidal periods, however, one has to either extrapolate the results from shorter periods or extract the calibration from the data under normal operating conditions.

As noted by Richter (1991), some of the methods used to calibrate other types of gravimeters are inappropriate for SGs. One of these is the use of calibration 'lines' where an instrument is repeatedly moved to precise locations arranged in a horizontal or vertical line; due to the instrument size this is impractical for the SG. The application of electromagnetic or electrostatic forces is also difficult due to the need for a precise knowledge of the reference force.

For a relative calibration, an SG is compared over a period of time with another instrument whose calibration is known (including calibration by an AG). In this case, the two sets of measurements can be compared indirectly, for example, by comparing the elastic gravimetric factors from a tidal analysis, or by a direct regression of the data from one instrument to the other. For absolute calibration, two methods have been used – either a test mass is moved with respect to the gravimeter and the Newtonian attraction is measured directly, or the instrument itself is subject to a known acceleration provided by an acceleration platform.

3.04.2.4.2 Amplitude calibration, relative methods

3.04.2.4.2.(i) Calibration using a theoretical tide

The best theoretical solid Earth tidal models are accurate to about 1 nGal in frequency-domain amplitude. This is about 10^{-5} of the full tidal amplitude (300 μGal), so it would seem a straightforward task to calibrate an instrument using the tidal signal. In practice, however, the observed tidal amplitudes are a combination of theoretical amplitudes, elastic response of the Earth, and ocean tidal loading. Variability in ocean crustal loading of about 1 μGal limits the accuracy of tidal calibration to about 0.3% accuracy.

Several authors have argued that the tidal analysis of an SG record is a useful calibration tool (e.g., Goodkind, 1996). Of equal importance is the relative stability of the amplitude calibration, and Merriam (1993b) has inferred this for the model TT70 at Cantley using the tidal admittances of the M2, O1, and K1 waves from 3 years of data. He concluded that the amplitude calibration was stable at the 0.013% level and the phase calibration to within 0.01° for M2. The use of a theoretical tide (solid tide + elastic yielding + ocean tide loading) for calibration is still, however, model-based, and therefore of a different character to the other methods listed below.

3.04.2.4.2.(ii) Calibration using spring gravimeters

Many early SG calibrations came from the side-by-side comparison of data from spring gravimeters that had already been calibrated either in the laboratory or on calibration lines. Due to limitations in the original calibrations, it is unlikely that the amplitude factors can be trusted below about the 0.5% level (Richter, 1991).

3.04.2.4.2.(iii) Calibration using AGs

For several reasons, the use of an AG has become the most widely used method in recent years. First, the SG is not disturbed during the calibration because the AG measurements are done on a nearby pier or adjoining room. The instrument separation needs to be kept small, however, to prevent horizontal gradients due to local gravity variations (e.g., hydrology), from affecting the instruments differently. Second, even though the AG has a repeatability of 1–2 μGal over a typical measurement campaign, with care a precision of about 0.05% can be achieved (**Table 5**).

Another advantage is that the processing of the data from the two instruments is straightforward and no complicated physical effects have to be accounted for because the instruments measure the same temporal changes whatever their origin. Finally, the co-location of the two instruments also enables the long-term drift of the SG to be estimated and this provides obvious advantages in cross-checking the AG measurements.

Hinderer *et al.* (1991) reported an early calibration of a model TT70 SG using a JILA-5 AG in Strasbourg. They introduced the direct regression technique whereby all SGs and AGs are used without correction, save for allowing different linear drifts between the two lasers of the JILA instrument. When tested against theoretical tides for O_1 (a common method for European stations because the solid tide O_1 is large and the ocean tide loading is small), agreement was found at about the 0.1% level. The full-size T012 at Cantley was calibrated a number of times using AGs. Bower *et al.* (1991) obtained 0.4% from tidal gravimetric factors using a JILA-2, and

Merriam *et al.* (2001) reported on a series of nine calibrations to achieve a precision of 0.13%.

Several authors have engaged in extensive campaigns to intercompare the instruments. Francis (1997) reported on 47 days of recording involving a large number of AG drops. A precision of about 0.1% was achieved both by linear regression and by comparing tidal amplitude factors. A significant finding of this study was that the precision of calibration was not significantly improved for times longer than 5 days, suggesting that this is an optimum period for such a comparison. Similar results were found for the C024 instrument in Boulder (Francis *et al.*, 1998) that agreed very well at a level of 0.08% with the absolute calibration using an acceleration platform.

Okubo *et al.* (1997) performed tests using FG5 #107 at two of the Japanese SG sites, T007 in Esashi and T011 in Matsushiro. Their results pointed out that the internal consistency of the SG was 0.3 and 0.62 μGal for Esashi and Matsushiro, respectively, even better than the error in the AG residuals at the two sites (1.55 and 1.52 μGal); the overall precision was 0.2%.

A sampling of other results of AG calibrations is given in **Table 5**. Amalvict *et al.* (2001a, 2002) showed a series of 28 different calibration (totaling almost half a million drops) runs over a 4 year period for ST, with an average length of 5 days each. The regression method gave an overall precision of 0.04% with a repeatability of 0.1%. Imanishi *et al.* (2002) presented a study of the various ways to cross-calibrate the AG and SG using a simple regression, tidal factors, and a combined method (**Table 5**). They found that the SG is not the only instrument subject to 'drift', and the AG showed a bias of several μGal over the 1 month of the experiment. Nevertheless, they were able to extract a very precise calibration of about 0.04%, which approaches the best calibrations by an acceleration platform method. Finally, Falk *et al.* (2001) and Harnisch *et al.* (2002) have given useful results on a number of SGs and AGs, together with some acceleration platform calibration results.

Note that for BH the two spheres have different calibration factors – this is true of all dual-sphere instruments. Also, MC is one of many stations that have been visited by several different AGs. The 'errors' are generally the precision of a least-squares fit, and are known to underestimate uncertainties obtained from differing sets of measurements. Thus, some SGs have been DC-calibrated to better than 0.05%, but others are probably closer to 0.15%.

Francis and Hendrickx (2001) turned the calibration issue around and used an SG as the reference signal in the calibration of a spring gravimeter. This is possible due to the extremely low drift and high precision of the SGs and produces good results, especially when the variable drift of the spring gravimeter is modeled along with the calibration, as in Meurers (2002).

3.04.2.4.3 Amplitude calibration, absolute methods

3.04.2.4.3.(i) Calibration using a moving mass Warburton *et al.* (1975) first described the use of a heavy mass calibration experiment. They rolled a 321 kg hollow steel sphere filled with mercury to a fixed position under the SG, thus generating a 10 μGal test signal. Within the accuracy of the various parameters, the most critical being the exact distance between the center of the test sphere and the niobium sphere, they found a precision of 0.2%. In such an experiment, other factors limiting accuracy are the homogeneity of the sphere, the exact geometry of the position of the sphere with respect to the niobium sphere, as well as loading and tilting effects that are induced by the heavy mass itself.

A similar calibration was done by Goodkind *et al.* (1993), who used a moving mass system to test the inverse square law of Newtonian gravity. A spherical mass was moved vertically under the SG in a specially designed chamber; an accuracy of 0.09% was achieved for two different types of sphere materials. The ultimate limit in this type of calibration is the uncertainty in the gravitational constant, though at 0.01% it is below the precision of the above calibrations.

Achilli *et al.* (1995) implemented a unique moving mass system for the full-sized T015 SG in Brasimone as part of a test for constancy of the gravitational constant. Their ring, weighing 272 kg, is raised and lowered around the SG from strong supports in the roof, but a limited range of about 1 m reduced the mass effect to 6.7 μGal. During two calibrations, they found a precision of 0.2% and a repeatability of 0.3%.

3.04.2.4.3.(ii) Calibration using a moving platform The idea of using an acceleration platform for the calibration of spring gravimeters was used successfully for LCR gravimeters by Van Ruymbeke (1989). The idea was applied to SGs by Richter (1991), who pioneered the development of what is now known as 'The Frankfurt Calibration Platform'. The SG instrument design, in which the dewar and coldhead are mounted separately, limits the maximum vertical range through which the gravimeter can be lifted. For a

Table 6 Maximum accelerations available from a moving platform, amplitude ±5 mm

Period (s)	Acceleration (μGal)	Output (V)
300	219.30	3.96042
480	85.60	1.50698
600	54.81	0.95092
900	24.36	0.43222
1200	13.70	0.25497
2400	3.42	0.07782
3600	1.52	0.02585
7200	0.38	0.00065

Modified from Richter (1991).

sinusoidal signal of amplitude 5 mm, **Table 6** shows the maximum accelerations that are possible. Note that for periods longer than 2 h, the amplitude is smaller than atmospheric and hydrological effects. Other limitation to this technique arises from the gravity gradient effect, mechanical stresses deforming the support systems, and the need to avoid tilting the gravimeter, which causes the horizontal resonance of the sphere to be excited.

This type of calibration also allows the phase response to be measured through the phase offset between the instrument response and the acceleration function (Richter *et al.*, 1995a). A calibration precision of better than 0.02% in amplitude and 0.1 s in time delay has been achieved using this system (**Table 6**).

3.04.2.4.4 Phase calibration

3.04.2.4.4.(i) Response of the analog filter

The ideal amplitude gain of the electronic analog antialiasing filter should be constant from DC up to the corner frequency of the antialiasing filter and the ideal phase response should be linear with frequency. These aspects are generally met in most SG recordings, but depart from the ideal at high frequencies, which for gravity data analysis means periods shorter than about 1 h. The GGP filter, used on the GWR gravity card, is an eight-pole Bessel filter designed to achieve the desired linearity.

The phase response at longer periods can be well represented by $\phi(\omega) = -\alpha\omega$, where α is a constant, ϕ is measured in degrees, and ω is in cpd. Given $\phi(\omega)$, it is simple to find the group delay $\tau(\omega) = -\mathrm{d}\phi/\mathrm{d}\omega$, usually measured in seconds. For a linear phase filter, one has (with α in degress per cpd)

$$\tau(\omega) = 240\,\alpha = \text{constant} \qquad [5]$$

For example, for the IDA filter, $\alpha = 0.15°\text{cpd}^{-1}$ so $\tau = 36.0$ s. For the GGP filter board at 1 s sampling, $\alpha = 0.035°\text{cpd}^{-1}$ so $\tau = 8.4$ s. In order to usefully measure the nonelastic response of the Earth to tidal waves, accuracies of 0.002° are required in the tidal wave phases (Wenzel, 1994). The phase lag of the recording system therefore has to be known at least to the same accuracy, that is, 0.5 s. An electronic calibration method is necessary to achieve this precision.

3.04.2.4.4.(ii) System response

The antialiasing filter is not the only component in the data acquisition system that causes time delays and phase shifts. They can occur throughout the electronics, including the feedback sensor, the digitizing voltmeter, and the time stamping of the signal onto the hard disk. Therefore, the overall phase response is best determined *in situ*, and not assumed from the design characteristics of only the antialiasing filter.

3.04.2.4.4.(iii) The step response method

The amplitude and phase response (the transfer function) of the complete system can be measured by injecting a known voltage to the feedback coil and recording the output voltage of the feedback network. The transfer function completely describes the electronic response of the system, but is not a substitute for determining the instrument calibration, that is, the conversion from voltage to acceleration. The injected voltage can be either a step function, which gives both amplitude and time responses but is sensitive to noise, or a series of sine waves that suppresses noise but requires a longer measurement time (Van Camp *et al.*, 2000). A third possibility is to inject a randomized input signal to the instrument and find the transfer function by cross-spectral analysis, but Richter and Wenzel (1991) conclude that this method is best suited to instruments with electrostatic or electromagnetic feedback, such as the spring gravimeters used in the IDA network.

The initial experiment to determine instrumental phase lag was by Richter and Wenzel (1991) in which they outlined the method and gave results for several spring gravimeters and one SG, the TT60 at Wettzell. Results for the latter showed an average time lag of 38.73 ± 0.14 s, and a phase determination of 0.002° for diurnal tidal waves, at the target accuracy level noted above. Wenzel (1995) later determined even better results for an LCR meter with a group delay accuracy of ± 0.004 s, far superior to the nominal value determined from the electrical components themselves.

Van Camp *et al.* (2000) have discussed in the utmost detail the phase response measurement for a

compact SG, in this case the C012 at Membach. The electronic step was applied to various combinations of filter type and time intervals (1–4 min), and the output was Fourier-analyzed to determine the amplitude and phase response. The time lag results showed an accuracy of ± 0.003 s for the GGP1 filter and ± 0.075 s for the raw gravity signal output. The sine wave method gave very similar results, confirming the integrity of the method. The amplitude gain of the electronics system was determined to be flat from 500 to 2000 s, the longest period determined by either method. Further details are given on the GGP website.

3.04.2.5 Other Corrections to Residual Gravity

3.04.2.5.1 Polar motion

One important signal contained in an SG record is the 14 month (435 day) oscillation of the rotation pole, or Chandler wobble. As noted previously, Richter's (1983) first observation of this signal, with only 5 μGal amplitude, was a turning point in the refinement of gravity residuals. Since then, every SG station has recorded data that when suitably processed show the polar motion (e.g., Harnisch and Harnisch, 2006a). Naturally, some records are very clear and others not so clear, depending on the epoch (amplitude of the motion) and the quality of the instrument and site.

With most data sets, it is not difficult to see the polar motion once tides and atmospheric pressure are subtracted. Indeed, for the most part, the highly accurate space geodetic series for the polar orientation that is given on the IERS website can be used directly at any of the gravity stations. A simple conversion is usually made between the (x, y) amplitudes of polar motion (m_1, m_2) in radians and the gravity effect δg in μGal (e.g., Wahr, 1985):

$$\delta g = 3.90 \times 10^{-9} \sin 2\theta \left[\cos(m_1 \lambda) - \sin(m_2 \lambda)\right] \quad [6]$$

where (θ,λ) are station latitude and longitude. The numerical factor includes the nominal value of 1.16 for the gravimetric delta factor, whereas fitted solutions are usually closer to $\delta = 1.18$ (e.g., Loyer *et al.*, 1999; Harnisch and Harnisch, 2006b). In many studies, the polar motion is considered as a quantity very accurately determined from space geodetic data, but it is interesting to observe its signature in either an individual or collective gravity series.

3.04.2.5.2 Instrument drift

From a historical viewpoint, particularly for spatial gravity surveys, the term 'drift' has been applied to almost any unwanted time-varying gravity signal. This usage persists in the SG literature and sometimes causes confusion. Here we use drift as an instrument characteristic, because all other gravity variations have specific causes.

From an instrumental point of view (e.g., Goodkind, 1999), drift is likely to be either a linear or exponential function of time, but its size is not easy to predict. The exponential behavior can be reset after a loss of levitation or other magnetic changes within the sensor. Under normal operation, the user can generally assume that drift will level off after installation and gradually become more linear as time progresses. Representative values of instrument drift are frequently less than 4 μGal yr^{-1} where these have been checked carefully with AGs (see above).

From a processing point of view, other functions such as polynomials have been used as a model for instrument drift but there is no physical reason to prefer such a choice. We recommend that an exponential drift be assumed from some initialization event for the instrument and later this may be replaced with a simple linear function. Drift is not to be confused with a secular change of gravity, even though the two cannot be separated except using combined SG–AG observations.

3.04.2.5.3 Hydrology

Hydrology is perhaps the most complex of the intermediate scale (hour–year) variations in gravity (e.g., Harnisch and Harnisch, 2006a). This is due to two factors. The first is its variability, due largely to the local water storage balance at the station that involves many components (rain and snowfall, soil moisture, evapotranspiration, and runoff). Rainfall is relatively easy to assess, as is the groundwater level, which is usually measured in a nearby well. The direct measurement of soil moisture is not easy and has not been done at most SG stations.

The second problem is one of length scales. The connectedness (permeability) of the soils and groundwater system is inhomogeneous at the local length scales (meter to kilometers), and so an assessment of the amount of moisture surrounding an SG involves extensive measurements. This quantity predominantly affects the attraction term rather than the loading term.

As a result, even though groundwater variations are extremely useful, they are not entirely reliable for

the purpose of determining an admittance factor for 'correcting' gravity residuals. The simplest case is a horizontal layer (Bouguer slab) of moisture of thickness h and fractional porosity ϕ, yielding a gravity perturbation (e.g., Crossley *et al.*, 1998),

$$\delta g = 2\pi G\rho\phi h = 0.42\phi\,\mu\text{Gal}\,\text{cm}^{-1} \qquad [7]$$

This is similar in application to the single admittance factor for atmospheric pressure, but the porosity (and permeability) can usually be estimated only very approximately, thus limiting the accuracy of the correction. Adding to the complications are SG stations located underground where a soil moisture layer may be present both above and below the instrument. In this case, the hydrology correction becomes quite problematic and is currently pursued as a research problem rather than as a correction that is part of normal processing.

3.04.2.5.4 Residual gravity

Having completed the above processing steps and corrections, one finally arrives at a residual gravity series that represents the unknowns including effects such as ocean currents, secular changes in elevation due to tectonics, gravity changes due to slow and silent earthquakes, or eigenmodes of the Earth (perhaps from the Earth's core). In addition, of course, all the subtle effects of mismodeling will be applied, which may include wrong assumptions regarding disturbances, offsets, drift, loading, and hydrology.

On one conclusion there can be little doubt – the ability of SGs to reliably measure effects at the 0.1 μGal level has opened up many interesting scientific possibilities, as well as posed many challenging issues that will be discussed in the following sections of this chapter.

3.04.3 Scientific Achievements Using SGs

3.04.3.1 The Global Geodynamics Project

GGP is an international research effort that was launched as a SEDI (Study of the Earth's Interior) initiative at the Vienna IUGG General Assembly in 1991. In 2003, it changed to become an Inter-Commission Project of International Association of Geodesy (IAG) and reports to Commission 2 (The Gravity Field) and Commission 3 (Earth Rotation and Geodynamics). It consists of a worldwide network of SGs, currently about 20 instruments, run by independent national groups. The groups agreed to provide vertical gravity acceleration data in a standard form, basically untouched raw data decimated to 1 min samples, and sent at the end of every month to a database. As indicated in **Figure 14**, GGP stations are sparsely distributed worldwide, with only two regional clusters of instruments, one in Europe and a smaller one in Japan. The coverage in the Southern Hemisphere is still weak, despite the effort of installing stations in Australia, Indonesia, and

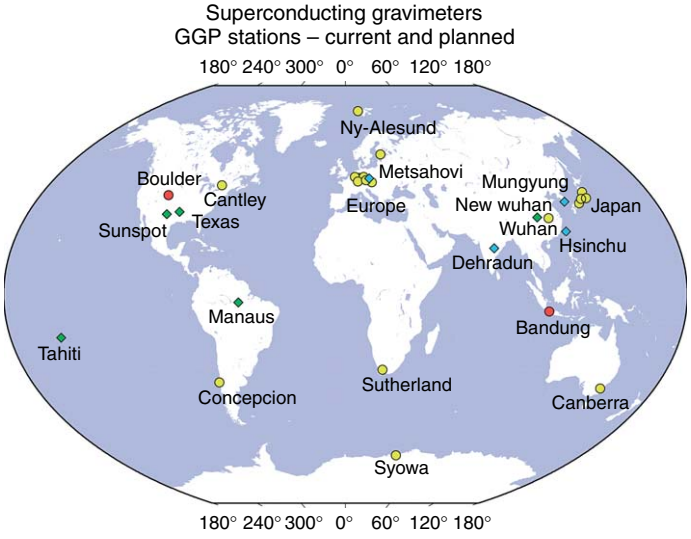

Figure 14 Geographical location of the stations of the GGP (Global Geodynamics Project). Yellow stations are active, red are currently not operating, and green are recently installed.

Antarctica by Japanese colleagues, in South Africa by GFZ Potsdam (Germany), and very recently in South America by BKG (Germany) – the TIGO project. Phase I of GGP was the period 1997–2003 and we are currently in phase II (2003–07).

The scientific objectives of the GGP cover geophysical phenomena throughout the wide period range of the instruments (from 1 s to several years), covering topics such as normal modes, mantle rheology, tides, solid Earth–oceans–atmosphere interactions, hydrology, and Earth rotation. **Figure 15** represents schematically the gravity spectrum that is observable by SGs ranging from seconds (ocean noise) to several years (secular changes). We refer the reader to the EOS article by Crossley *et al.* (1999), where a full description is provided. Other review papers on SGs have also appeared (e.g., Goodkind, 1999; Hinderer and Crossley, 2000; Meurers, 2001a; Hinderer and Crossley, 2004). We will show below some of the most interesting results which owe their existence to the collection of the worldwide GGP data of high quality.

The wide spectrum of geophysical phenomena that are observable with SGs is evident in **Figure 15**. Basically the range of observable periods (or characteristic time constants) covers 8 orders of magnitude from 1 s to several years. The highest frequency detectable by SGs is ~1 s, because of the feedback system limitation, and on the left the figure shows background noise mainly caused by ocean noise with two dominant peaks at 5–6 s and 10–15 s. At slightly longer periods we have the seismology region including the normal modes generated by earthquakes – periods up to 54 min which is the gravest period of the Earth elastic normal modes. Between 150 and 500 s (2–7 mHz), these modes form the incessant oscillations ('hum') unrelated to earthquakes but rather of atmospheric and/or oceanic origin. At periods longer than about 6 h (depending on the core stability profile), another class of eigenmodes are the gravity-inertial modes (also called core modes) predominantly confined to the liquid core. A particularly interesting and isolated long-period oscillation is the Slichter mode (actually a triplet due to rotation and ellipticity) arising from translation of the solid inner core. Its period, between 4 and 8 h, depends primarily on the density jump of the inner-core boundary (ICB).

From 4 h up to 18.6 years, there are many spectral lines due to lunisolar tides, the most important of which are semi-diurnal and diurnal. The study of diurnal gravity tides includes a resonance effect due

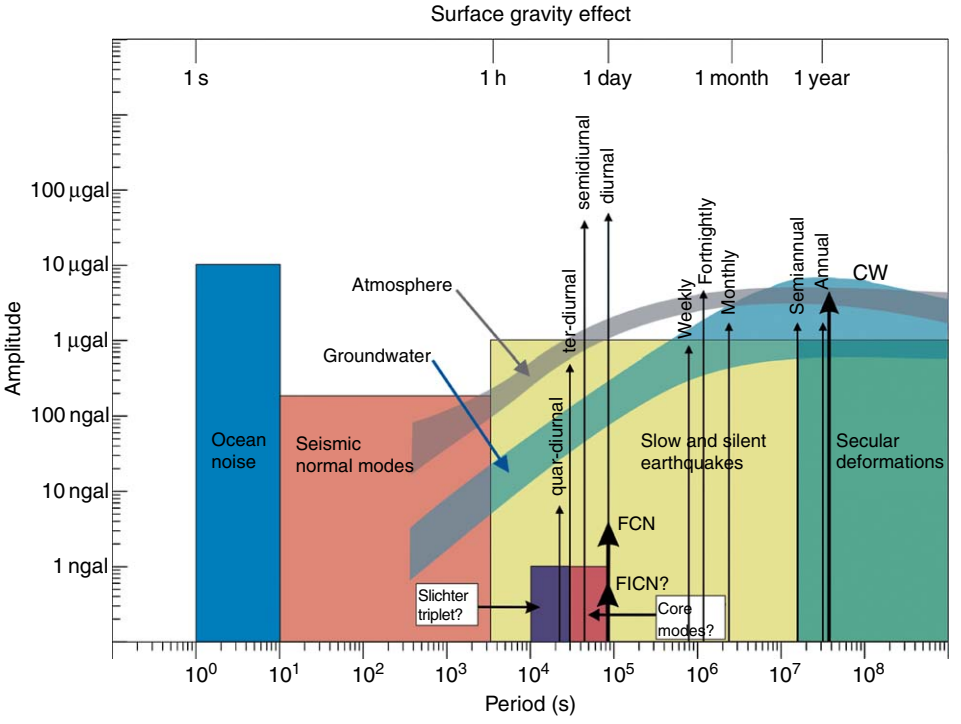

Figure 15 Characteristics of geophysical phenomena observable by SGs.

to the existence of wobble modes for an Earth model with a fluid outer core (FCN) and a solid inner core (free inner core nutation). Toward longer periods, there are many signals (atmospheric pressure, snow, soil water content, ocean circulation, Earth's rotation) that are related to the seasonal solar cycle which lead to contribute to a strong annual term in gravity. CW stands for Chandler wobble, which is another rotational mode of the Earth with a 435-day period; its observation provides valuable information on mantle rheology at long periods.

On the right of the figure we have long-period secular deformations; for instance, gravity changes caused by post-glacial rebound (PGR) or tectonics. Also indicated in shaded bands are the effects due to atmospheric pressure and hydrology (groundwater). In contrast to periodic phenomena that have sharp spectral lines, these effects are broadband and cover a large part of the spectrum, atmospheric effects being roughly 1 order of magnitude larger than hydrologic effects. **Figure 15** is a normalized amplitude spectrum where a sinusoidal wave with unit amplitude will always appear with unit amplitude regardless of the period of observation. On this type of spectrum, noise would decrease as a function of record length. We have chosen to represent the typical variability of hydrology and atmospheric pressure induced effects in gravity (equivalent time standard deviation) as time independent. The two bands are derived from the analysis of water table level and air pressure records of several years length available at some of the GGP stations.

An example of the different contributions to the time-variable gravity signal is shown in **Figure 16** in Strasbourg, France. The largest contribution is of course the solid Earth tides with several hundreds of nanometers per square second and multiple periods (semi-diurnal, diurnal, fortnightly, monthly, semi-annual, annual). Ocean loading is by far smaller of the order of $1\,\mathrm{nm\,s^{-2}}$ (this term can be larger for a station near the oceans). Nontidal ocean loading is slightly larger and exhibits a strong seasonal feature. Atmospheric loading is broadband and can easily cause gravity changes of several tens of nanometers per square second. Hydrology (soil moisture + snow) is predominantly seasonal and can also lead to gravity perturbations of similar amplitude. Finally, the Earth's rotation changes (polar motion and length of day)

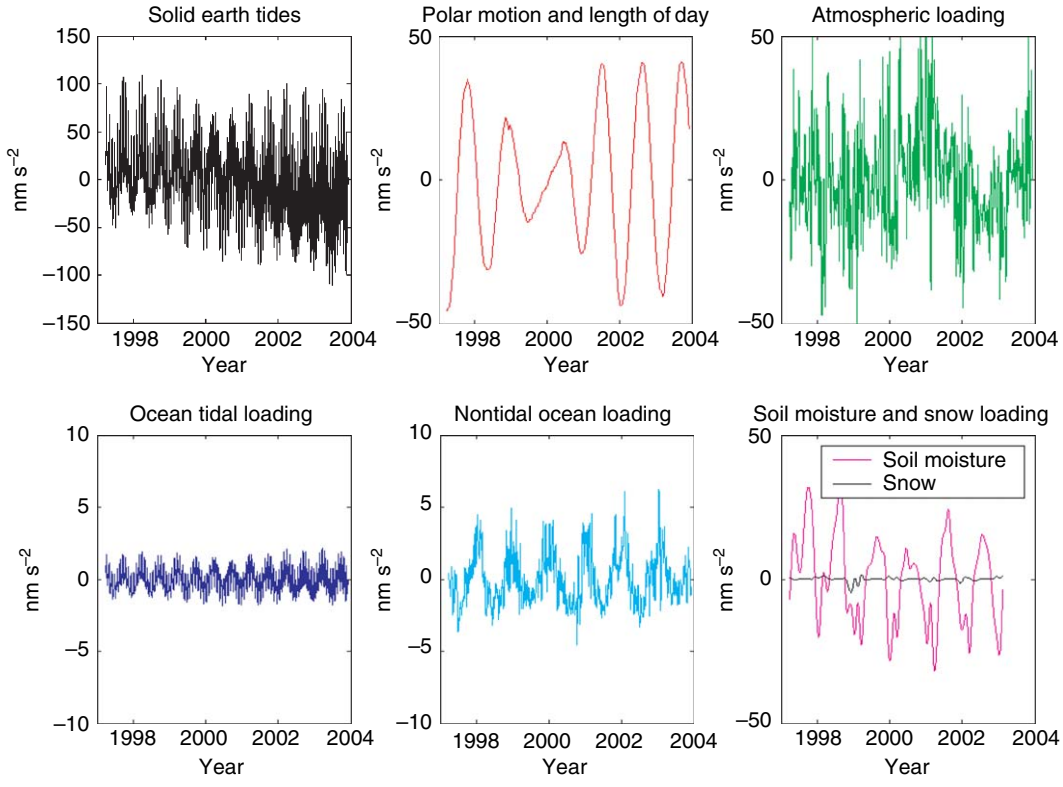

Figure 16 An example of different contributions to the time-varying gravity in Strasbourg. Courtesy: J.-P. Boy.

induce a gravity signal of several tens of nanometers per square second with a dominant beating between an annual term and the 435 day Chandler wobble.

We now review some scientific studies in the various period ranges, as discussed in **Figure 15**. Section 3.04.3.2 deals with the short-period seismic phenomena and other normal modes up to a 1 day period. In Section 3.04.3.3, atmospheric effects on gravity are described while tidal contributions (fluid core resonance effect, linear and nonlinear ocean loading) are discussed in Section 3.04.3.4. Section 3.04.3.5 deals with nontidal ocean loading, hydrology contributions are covered in Section 3.04.3.6, and Section 3.04.3.7 covers Earth rotation and polar motion effects. Section 3.04.3.8 deals with tectonics, and Section 3.04.3.9 considers the problem of the calibration/validation of gravity satellite data with SG ground observations. Finally, Section 3.04.3.10 suggests new projects, especially using SGs in regional arrays.

3.04.3.2 Seismic and Subseismic Signals

Investigation with SGs of the seismic normal modes excited by large earthquakes has led to some new and impressive results, due primarily to the low noise levels of SGs at periods longer than 500 s, as indicated in **Figure 17** (Rosat *et al.*, 2003a). At periods longer than 1000 s, the best SGs have lower noise than the worldwide seismometer limit NLNM (new low noise model, Peterson, 1993); noisier SG stations cross the NLNM at longer periods (4.2 h for the station Be, for instance). This extensive compilation of all the GGP stations extends earlier results from just a few SG stations but which already were convincing in terms of low noise (Banka and Crossley, 1999; Van Camp, 1999). In addition, metrological comparisons between SGs and broadband seismometers (Freybourger *et al.*, 1997; Hinderer *et al.*, 2002b), as well as between AGs and SGs over a large spectral range (Crossley *et al.*, 2001; Francis *et al.*, 2004), have demonstrated the excellent characteristics of SGs.

Of recent large earthquakes, the 2001 Peru event of magnitude M = 8.4 strongly excited the long-period seismic modes, and significant observations were made by the GGP network. In particular, the fully split ${}_0S_2$ multiplet (with five individual singlets), which has been rarely visible on a single instrument, could be fully analyzed from the Strasbourg C026 instrument (Rosat *et al.*, 2003a) but was also present at other SG stations.

The most important new result was the detection of the overtone ${}_2S_1$ (see **Figure 18**), which is an elastic mode, unlike the Slichter triplet ${}_1S_1$ whose

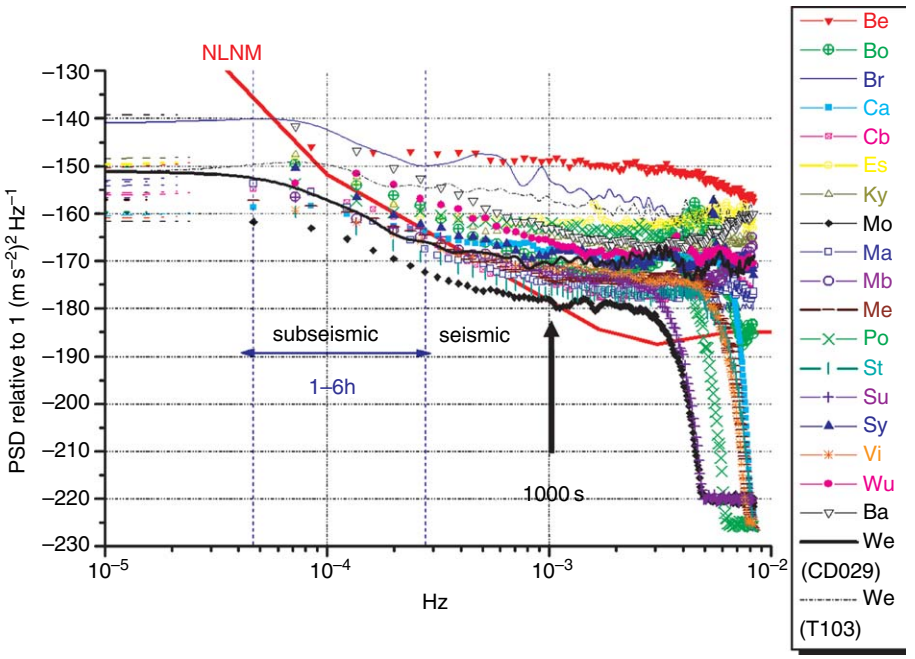

Figure 17 Noise levels of the SGs from the GGP network. Reproduced from Rosat S, Hinderer J, Crossley D, and Rivera L (2003a) The search for the Slichter Mode: Comparison of noise levels of superconducting gravimeters and investigation of a stacking method. *Physics of the Earth and Planetary Interiors* 140: 183–202, with permission from Elsevier.

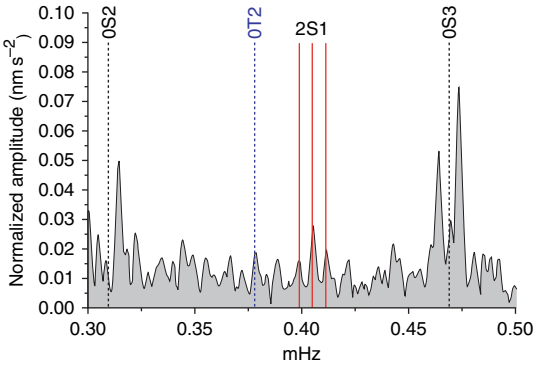

Figure 18 Normalized amplitude spectrum (in nm s^{-2}) in the frequency band 0.3–0.5 mHz after the $M_w = 8.4$ Peru event exhibiting the triplet of the $_2S_1$ mode. Reproduced from Rosat S, Rogister Y, Crossley D, and Hinderer J (2006) A search for the Slichter triplet with superconducting gravimeters: Impact on the density jump at the inner core boundary. *Journal of Geodynamics* 41: 296–306, with permission from Elsevier.

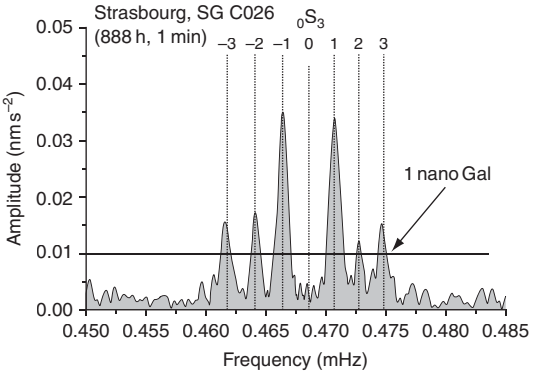

Figure 19 Observation of the well-resolved singlets of $_0S_3$ at Strasbourg using 888 h of data after the 2004 Sumatra earthquake of magnitude $M = 9.3$. The singlet $m = 0$ was not excited at Strasbourg. Reproduced from Rosat S, Sato T, Imanishi Y, *et al*. (2005) High-resolution analysis of the gravest seismic normal modes after the 2004 $M_w = 9$ Sumatra earthquake using superconducting gravimeter data. *Geophysical Research Letters* 32: L13304 (doi:10.1029/2005GL023128), with permission from Elsevier.

period is determined primarily by a gravitational restoring force. The eigenfunctions of the two modes share some similarities (Rosat *et al*., 2003b). The detection of this mode strongly benefited from the stacking method proposed by Courtier *et al*. (2000), also used by Guo *et al*. (2006), that is applicable to all degree 1 modes with their associated surface gravity changes.

The $M_w = 9.3$ Sumatra huge earthquake on 26 December 2004 even more strongly excited the low-frequency seismic modes and provided a unique opportunity to improve the determination of the period and Q of the gravest seismic modes. An example of the strong signal-to-noise ratio is shown in **Figure 19**, where all singlets of the spheroidal mode $_0S_3$ are visible on the Strasbourg SG (Rosat *et al*., 2005).

We also show the background normal modes of the Earth (frequently referred to as the 'hum') that were first discovered in the Syowa, Antarctica, SG record (Nawa *et al*., 1998), and later seen on other SG records (Nawa *et al*., 2000; Rosat *et al*., 2003b; Widmer-Schnidrig, 2003). **Figure 20** shows the power spectral density in the frequency band 1.5–5.5 mHz of the gravity data observed in Strasbourg during the period 1997–2001 with SG C026. The spectral peaks of the fundamental spheroidal modes are clearly visible. Rather than selecting periods without earthquakes above a specific magnitude, we used a statistical approach by computing the quartiles of all available gravity data in period of study.

The discovery of the hum has generated numerous studies in observational seismology and also led to theoretical arguments suggesting that the preferred excitation mechanism is not earthquakes, but rather the atmosphere (Lognonné *et al*., 1998; Kobayashi and Nishida, 1998; Nishida and Kobayashi, 1999; Nishida *et al*., 2000, 2002; Suda *et al*., 1998; Tanimoto *et al*., 1998; Tanimoto and Um, 1999; Roult and Crawford, 2000). Two recent array-based studies in seismology, however, suggest an alternative explanation in terms of interactions between the atmosphere, the oceans, and the seafloor in case of stormy weather (Rhie and Romanowitz, 2004; Tanimoto, 2005).

One major goal of GGP was to detect the translational motion of the solid inner core (the Slichter triplet $_1S_1$), because knowing its period(s) would bring a new constraint on the density contrast at the ICB (Rosat *et al*., 2006) and possibly also on viscosity just above the ICB (Smylie *et al*., 2001). We do not review here previous studies and controversies on the theoretical issues in modeling this eigenmode, nor different claims for detection and counter studies; instead, we refer the reader to the review in Hinderer *et al*. (1995).

It is, however, worth showing the current status of the search. For example, in **Figure 21** (Rosat *et al*., 2004), we see that there is obviously no clear observational evidence in this stacking of SG data of any of the theoretically predicted triplets. Evidently, many spectral peaks may emerge slightly above the background level of 0.01 nm s^{-2}, but as pointed out by

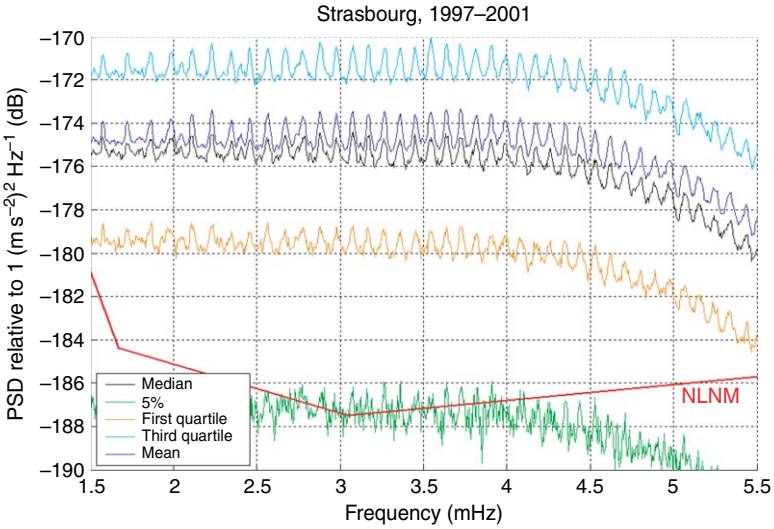

Figure 20 Power spectral density of the gravity data observed in Strasbourg during the period 1997–2001 clearly exhibiting the presence of the 'hum'. Courtesy: S. Rosat.

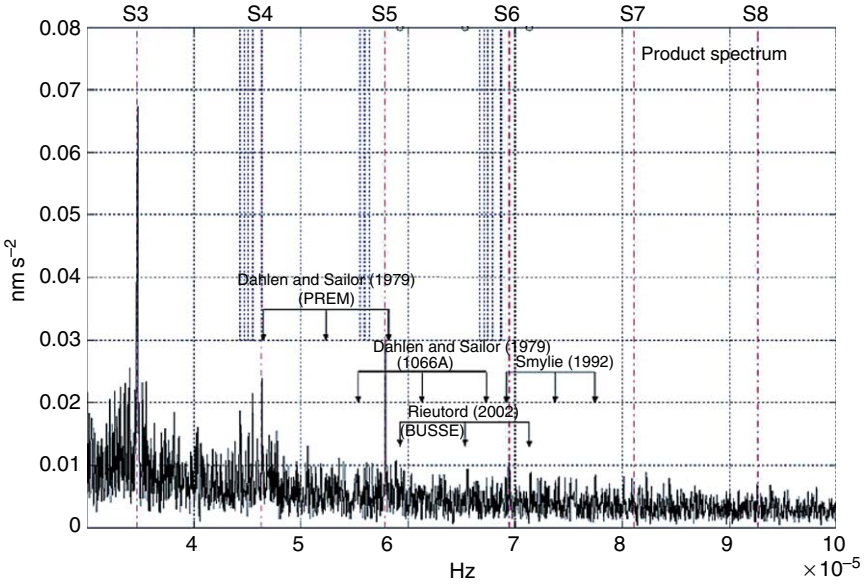

Figure 21 Product spectrum resulting from the multistation analysis method applied to five SGs. The three frequencies computed according to the splitting formula of Dahlen and Sailor (1979) for the Earth models 1066A and PREM, predicted by Rieutord (2002) based on the Earth's model by Busse (1974), and the peaks that Smylie (1992) identified in SG observations to be the inner-core translation, are indicated by vertical arrows. The modulations of the diurnal harmonic S_1 of the atmosphere from S_3 to S_8 (vertical dashed and dotted lines) and nonlinear tides (vertical dotted lines) around 4 and 6 h are also shown. Reproduced from Rosat S, Hinderer J, Crossley D, and Boy J-P (2004) Performance of superconducting gravimeters from long-period seismology to tides. *Journal of Geodynamics* 38: 461–476, with permission from Elsevier.

Florsch *et al.* (1995a), these are no more significant than statistical fluctuations. Some claims have been made (e.g., Guo *et al.*, 2006), but they are (as yet) generally unsupported by other observations and by the SG community.

Although not yet observed, the identification of $_1S_1$ remains a unique topic for the GGP network and interest remains high. This has led to the development of techniques for stacking the SG records, all based on the original idea of Cummins *et al.* (1991) as

developed in Courtier *et al.* (2000). Despite low noise levels in the band from 3 to 6 h, and despite the methodological attempts to enhance any global signature of degree 1 triplet (see Rosat *et al.* 2003a), the problem probably remains one of excitation, as discussed by Crossley (1993). Even for the largest modern earthquake (Chile 1960, magnitude 9.5), the seismic moment yields a gravity signal of no more than 1 nGal, and to be observed this amplitude needs to be maintained for some time beyond the earthquake. An alternative possibility, first used by Smylie (1992), is that the excitation could be intermittent or randomly caused perhaps by fluid motions in the outer core.

3.04.3.3 Atmospheric Loading

As discussed earlier, several methods of correcting for the atmosphere have been proposed. We now show a specific example of the 2-D atmospheric pressure corrections done by Boy *et al.* (1998, 2001, 2002), and other groups in Japan (Mukai *et al.*, 1995), using 2-D pressure data originating from the weather prediction centers such as NCEP (National Center for Environmental Predictions) or ECMWF (European Centre for Medium-Range Weather Forecasts). **Figure 22** shows the computations for the stations Canberra in Australia and Strasbourg in France, where the residual gravity level (in $\mathrm{nm\,s^{-2}}$) is plotted as a function of the solid angle in degrees around the station.

Except for small angles (close to the station), the 2-D correction performs better than the local barometric admittance close to $3\,\mathrm{nm\,s^{-2}}\,\mathrm{hPa^{-1}}$ (straight horizontal line – note this is the same as $-0.3\,\mu\mathrm{Gal\,mb^{-1}}$ quoted earlier). Because of the known correlation between length and timescales in the atmospheric processes (Green, 1999), long-period pressure effects (exceeding a few days) require large-scale loading computations to be adequately represented. The results from a coastal station from the GGP network (CB station in **Figure 22**) clearly discriminated against the use of the NIB (noninverted barometer) ocean reaction to air pressure changes.

As we previously discussed, in order to have the most accurate atmospheric corrections for the new gravity satellite missions, *CHAMP* and *GRACE*, 2-D pressure loading computations have been extended to 3-D modeling where pressure, temperature, and humidity data varying with height are also taken into account in addition to the surface data (see Svenson and Wahr, 2002; Boy and Chao, 2005; Neumeyer *et al.*, 2004a). It was recently shown for the station Medicina, with the help of balloon radio sounding, that there is a seasonal vertical air mass change in the atmosphere without ground pressure changes which is caused by warming and cooling (Simon, 2002) and that leads by attraction to a non-negligible gravity effect of the order of 1 μGal.

In an attempt to model the atmosphere not just as a source of noise, but to investigate actual meteorological effects in gravity, Meurers (1999, 2000, 2001b) analyzed SG measurements from the Vienna station and found an interesting new phenomenon. It appears that during some weather disturbances, rainfall occurs without generating a large ground pressure change but causing a significant gravity drop. Meurers (1999) model suggests that vertical

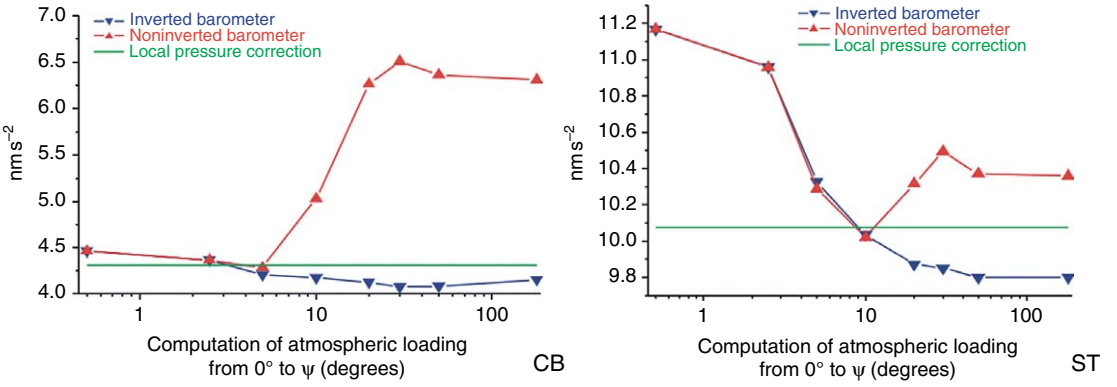

Figure 22 Variance reduction of gravity residuals (in $\mathrm{nm\,s^{-2}}$) due to different pressure loading corrections (2-D load with inverted or noninverted barometer response, local admittance); left is for Canberra (CB) station in Australia and right for Strasbourg (ST) station in France. Reproduced from Boy J-P, Gegout P, and Hinderer J (2001) Gravity variations and global pressure loading. *Journal of Geodetic Society of Japan* 47(1): 267–272, with permission from Geodetic Society of Japan.

convective air motion (air mass exchange or water transport) does not alter the ground pressure (total air column mass unchanged) but does modify gravity through Newtonian attraction. This is an example where gravity could be of indirect use to meteorologists to indicate air movements without detectable ground pressure signature.

3.04.3.4 Tides and Nearly Diurnal Earth Wobbles

As discussed previously, Earth and ocean tides are by far the largest components of surface gravity changes. The SGs have brought two areas of improvement to tidal studies. First, the high sensitivity of these meters which enables them to detect small-amplitude tidal signals previously hidden in noise (e.g., nonlinear ocean tides) and to retrieve with better precision larger tidal signals (see Ducarme *et al.*, 2002). With this high precision, Xu *et al.* (2004a) revisited the question of the possible latitude dependence of tidal gravimetric factors. Using 19 GGP stations they found that the discrepancy of the four principal waves (O_1 and K_1 in the diurnal band, M_2 and S_2 in the semi-diurnal band) between observations and theoretical models (Dehant *et al.*, 1999; Mathews, 2001) is less than 0.2%. This means that there is no significant latitude dependence. Second, the much lower instrumental drift of SGs versus mechanical spring meters permits more precise studies of long period tides (M_f, M_m, S_{Sa}, and S_a) (Sato *et al.*, 1997a; Hinderer *et al.*, 1998; Mukai *et al.*, 2001; Ducarme *et al.*, 2004; Boy *et al.*, 2006).

3.04.3.4.1 Resonance effects in diurnal tides

Of the tides themselves, the largest components occur in both semi-diurnal and diurnal frequency bands. Within the diurnal band, some waves are affected by a resonance that occurs due to the nearly diurnal free wobble (NDFW), also called FCN, which is a differential rotation of the fluid outer core with respect to the mantle. In a co-rotating reference frame, the FCN period is of course nearly diurnal; in an absolute frame, it is approximately 430 days. The observation of this resonance requires precise amplitude and phase measurements of the diurnal tidal waves that are close in frequency to the eigenfrequency. In particular, the small-amplitude waves ψ_1 and φ_1 are critical in the retrieval of the FCN parameters, that is, the period and damping of this resonance mode. A very clear example of this can be found in Hinderer *et al.* (2000), where there is a noticeable improvement in the FCN adjustment when using data from the compact SG (C026) compared to earlier data from the TT70 in Strasbourg (see their figures 4 and 6).

We do not discuss here the numerous papers using GGP data to derive the FCN parameters and refer the reader to previous reviews on this subject (Hinderer and Crossley, 2000, 2004). A study combining the analysis of six SGs by Sun *et al.* (2002) leads to an FCN period of 429.0 (424.3–433.7) sidereal days and a Q factor of 9500 (6400, 18 700). A more global analysis by Xu *et al.* (2004), who used simultaneously tidal gravity observations at 19 GGP stations, leads to an FCN period of 429.9 (427.2–432.7) sidereal days and a Q value about 20 000 (12 000–72 000). The FCN period is in good agreement with space geodetic studies (Herring *et al.*, 1986; Neuberg *et al.*, 1987; Merriam, 1994; Defraigne *et al.*, 1994). However, most of the time, the gravity-derived Q factor is much smaller than that obtained using VLBI (Herring *et al.*, 1986). An artifact of the analysis is sometimes even a negative Q (see table 1 in Florsch and Hinderer (2000); Sun *et al.*, 2002, 2004). The Q discrepancy between gravimeters and VLBI measurements is not due to imprecision in the gravity observations, but is rather of a methodological nature. The classical least-squares method usually applied to the determination of the resonance parameters (obviously, a linearized form applied to a nonlinear problem) is inadequate because it implies Gaussian statistics (Sato *et al.*, 2002; Sun *et al.*, 2004) that are not correct for this problem. Florsch and Hinderer (2000) have demonstrated that an appropriate Bayesian method is required to solve for the FCN parameters due to the nonstandard form of the probability distribution for Q.

Figure 23 shows the Bayesian approach applied to Canberra (CB) SG data by plotting the joint probability distribution for the eigenperiod T and quality factor Q. Taking a vertical slice through the distribution shows that the shape is somewhat Gaussian for the period T, leading to values found in previous studies based on the least-squares method. This is no longer the case for a horizontal slice in which the distribution of Q shows a preferred range of high values exceeding 10^4 (including infinity which means no damping at all) in agreement with estimates from lunisolar nutation observations by VLBI.

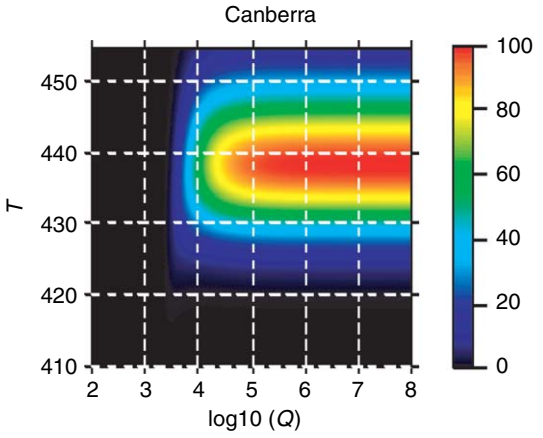

Figure 23 Joint probability density function for eigenperiod *T* and quality factor *Q* using SG data from Canberra (CB) station. Courtesy: N. Florsch.

3.04.3.4.2 Ocean loading

3.04.3.4.2.(i) Semi-diurnal and diurnal tides We have previously discussed the ocean loading correction to gravity and referred to the articles of Baker and Bos (2003), Boy *et al.* (2003), and Bos and Baker (2005). Clearly, observations from the GGP network can be compared to computations from different global ocean tide models, some of them being partly hydrodynamic, including the often-quoted classical Schwiderski (1980) model, or assimilating data derived directly from satellite altimetry.

The present situation, from the comprehensive treatment by Bos and Baker (2005) is that the class of recent ocean tide models, specifically GOT00 (Ray, 1999), NAO99b (Matsumoto *et al.*, 2000), and FES99 (Lefévre *et al.*, 2002), is in better agreement with SG observations than earlier models such as Schwiderski (1980). When differences are carefully examined, most models are in agreement and there is no 'best' model valid in all areas of the world. One must mention that the spread along the real (in-phase) axis of the tidal residuals is in general larger than along the imaginary axis (out-of-phase) related to possible amplitude calibration problems. By contrast, the out-of-phase component seems to be more reliable because of a better determination of the instrumental phase lag (Van Camp *et al.*, 2000) and is hence a strong validation tool for ocean tides.

A corollary to this investigation is the limits we can place on Earth's inelasticity from the gravimetric amplitude factors and phase delays after correction for ocean tidal loading. This was pointed out by Baker and Bos (2003), where they compared for some waves the gravimetric amplitude factor and phase delay to some reference elastic or slightly inelastic values (Dehant *et al.*, 1999). In particular, they used the small value ($\leq$0.2 μGal) of ocean loading for wave O1 in Europe for testing inelasticity in the Earth's tidal response with European SG stations. These observations could help in rejecting inelasticity models exhibiting an increase in amplitude larger than 0.3%. The small phase lag of a few hundredths of a degree is consistent with the Mathews (2001) inelastic body tide model for 0_1.

3.04.3.4.2.(ii) Long-period tides We have pointed out that the SGs have a very small instrumental drift compared to classical spring meters and this is why the investigation of long-period tides is particularly suited to SG data. In a recent paper, Boy *et al.* (2006) analyzed long series from 18 GGP stations to estimate the ocean loading for the monthly (M_m) and fortnightly (M_f) tides. The available models were an equilibrium tide (Agnew and Farrell, 1978), Schwiderski (1980), and three recent hydrodynamical models with satellite altimeter data assimilation – NAO99b (Matsumoto *et al.*, 2000), FES99 (Lefévre *et al.*, 2002), and TPXO.6 (Egbert and Erofeeva, 2002). They concluded that the uncertainty for M_m is still too large to discriminate between the newer models. On the other hand, the hydrodynamical models for M_f are clearly closer to the SG observations than the equilibrium tidal model or the older model proposed by Schwiderski (1980) (see **Figure 24**).

3.04.3.4.2.(iii) Nonlinear tides Almost all tidal theory and associated ocean tide loading follow the response method (reviewed earlier and classically used in oceanography). Merriam (1995; 2000) shows that nonlinear tides can be seen in SG records. At CA (Cantley) in Canada, it is possible to see clearly these small abnormal waves originating from nonlinearities in the ocean tidal response at the Bay of Fundy. The sensitivity inferred from the SG measurements is equivalent to 1 mm of open ocean tide, which means that these observations are a unique tool for validating these small ocean tidal waves that exist only near the coastlines (e.g., Sinha and Pingree, 1997).

Some years ago, Florsch *et al.* (1995b) identified small signals of a few nGal in the SG residuals with periods around 6 h from Strasbourg and Cantley stations. A more systematic study by Boy *et al.* (2004) on various GGP stations demonstrated that these signals are indeed due to nonlinear tides in the quar-diurnal frequency band.

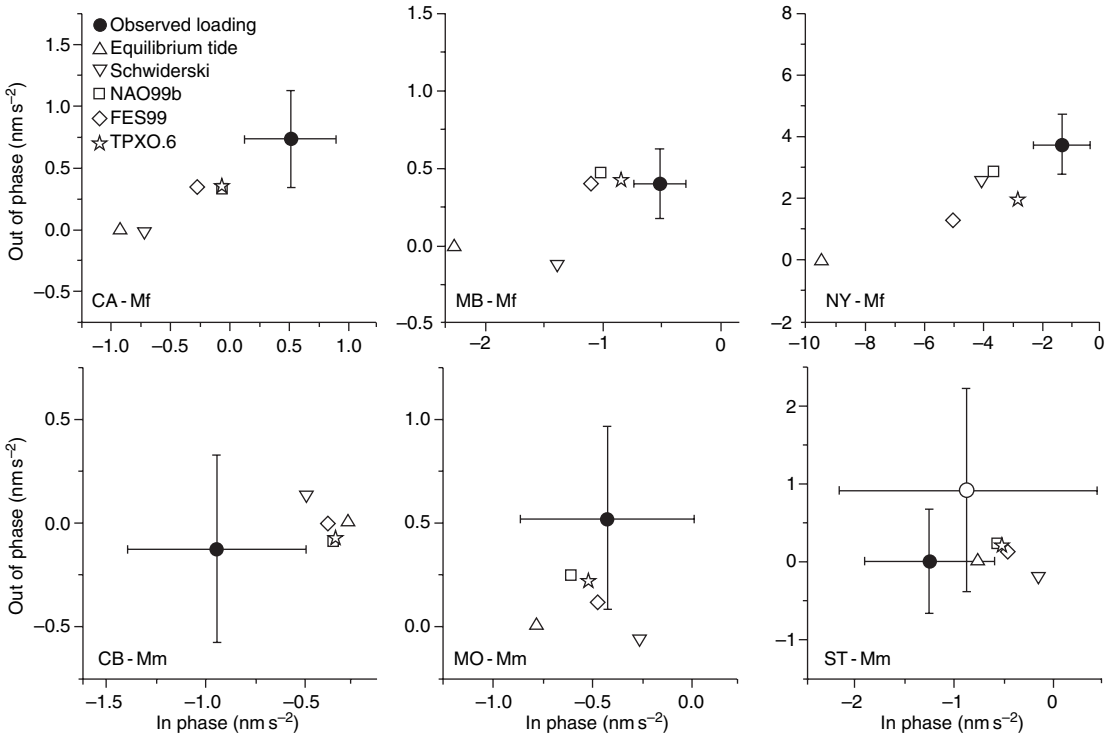

Figure 24 Observed tidal loading for M_f (top) and M_m (bottom) waves and estimated tidal loading for six SGs and five ocean models. Reproduced from Boy J-P, Llubes M, Ray R, Hinderer J, and Florsch N (2006) Validation of long-period oceanic tidal models with superconducting gravimeters. *Journal of Geodynamics* 41: 112–118, with permission from Elsevier.

Figure 25 shows the fair agreement for the M_4 nonlinear tide both in amplitude and phase between SG observations and the predicted contributions from recent ocean tidal models (Flather (1976), Mog2D, and Pingree and Griffiths (1980, 1981)). Mog2D (2-D gravity wave model) is a barotropic, nonlinear model from Lynch and Gray (1979), that was later developed for tidal- and atmospheric-driven applications both at coastal and global scales.

Due to the integrative properties of the gravity-loading Green's functions, inland SG observations act as a complementary large-scale validation tool to point-like tide gauge observations of nonlinear ocean tides. The latter are generated only in shallow water near the coasts and hence mostly escape detection by satellite altimeters like TOPEX/POSEIDON or JASON.

3.04.3.5 Nontidal Ocean Circulation

In addition to tidal oceanic contributions, nontidal effects related to the general oceanic circulation are also detectable in SG measurements. Virtanen and Mäkinen (2003) investigated the loading effect of the Baltic Sea on the Metsahovi (Finland) instrument (T020), which is located only 15 km away from the open sea. They found a good correlation between SG residuals and sea-level changes from the nearby Helsinki tide gauge. Short-period variations are mostly driven by wind stress moving water only locally, whereas long-term variations are caused by water exchange through the Danish Straits. It is therefore useful to combine gravity observations with tide gauge measurements (and with precise positioning measurements) to better test the loading from Baltic Sea.

Sato *et al.* (2001) made another important contribution to nontidal effects using SG records from Esashi, Canberra, and Syowa to investigate the nontidal annual contribution from sea-level changes (see also Fukuda and Sato, 1997). They demonstrated the importance of the steric correction to sea-surface height (SSH) change – this is the coefficient used to compensate the thermal expansion of the oceans due to sea-surface temperature (SST) change. The steric part does not involve any additional mass change and hence does not alter gravity by loading; thus, inland SG measurements are a unique tool to distinguish between steric and nonsteric SSH components.

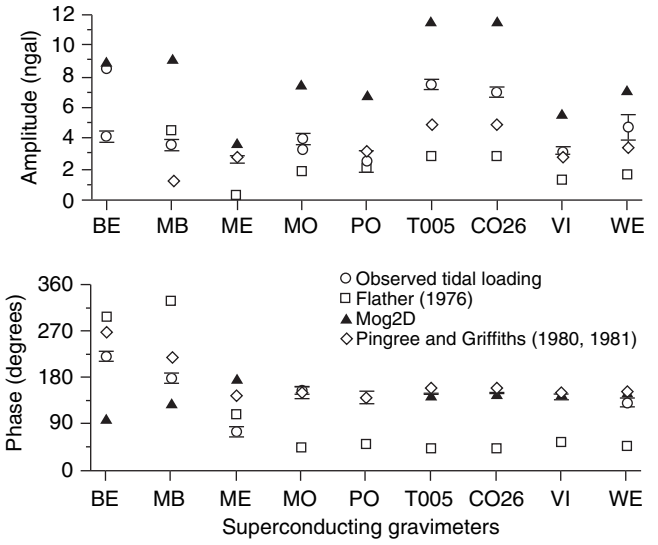

Figure 25 Amplitude (nGal) and phase (in degree with respect to Greenwich) of M_4 observed tidal loading and loading predictions according to recent tidal ocean models. Reproduced from Boy J-P, Llubes M, Ray R, *et al*. (2004) Non-linear oceanic tides observed by superconducting gravimeters in Europe. *Journal of Geodynamics* 38: 391–405, with permission from Elsevier.

3.04.3.6 Hydrology

Early studies in gravity focused mainly on tides, oceanic and atmospheric effects – starting with the references already made to Warburton and colleagues in the 1970s. In the last decade, however, more and more attention has been paid to the hydrology signature in gravity, especially in SG data where the drift is not a large issue. Most of the studies are restricted to modeling local effects by trying to find correlations between gravity residuals and a relevant hydrological parameter such as water table level, rainfall, or soil moisture (see, e.g., Crossley and Xu, 1998; Virtanen, 2001; Kroner, 2001; Kroner *et al*., 2004; Takemoto *et al*., 2002; Ijpelaar *et al*., 2002; Harnisch and Harnisch, 2002). A typical data set over a 2 week period is shown in **Figure 26**.

Most authors use an admittance (in μGal per millimeter of water) that depends on local porosity and permeability (neither of which is well characterized by spot measurements). The difficulty is in separating local effects from a regional or even continental hydrology signal (see van Dam *et al*., 2001a, 2001b) knowing that both will share a similar seasonal variation because the meteorological forcing is similar. For this reason, active experiments, where known amounts of water were added to specific areas in the gravimeter vicinity, were conducted at Moxa Observatory and helped significantly in the validation and parametrization of hydrology models (Kroner and Jahr, 2006).

More recently, a study was devoted to the seasonal changes in SGs (Boy and Hinderer, 2006). These changes can be linked to global hydrology models such as LadWorld (Milly and Shmakin, 2002) or GLDAS (Rodell *et al*., 2004), as shown in **Figure 27**. For Cantley there is a strong snow contribution in winter, adding to the soil humidity, while in Wettzell it is much smaller. For both stations, there is a good agreement between the gravity residuals and the estimated continental water storage loading effects. In fact, for more than half of the 20 analyzed SGs, there is such a good correlation, as shown in **Figure 28**. For the other stations, the discrepancies may be associated with local hydrology effects, especially when a station is partly underground like Moxa or Strasbourg.

Finally, a series of papers (Zerbini *et al*., 2001, 2002; Romagnoli *et al*., 2003; Richter *et al*., 2004) carefully examined both height and gravity changes from continuous GPS and SG (C023) observations at the station Medicina (Italy). These studies, from which we show an example in **Figure 29**, provide a convincing interpretation of the seasonal signal from the combined loading contributions of air pressure, ocean circulation, and hydrology (surficial water table), illustrating once more the need to have simultaneous height and gravity measurements in addition to the monitoring of various environmental parameters in the close vicinity of the station.

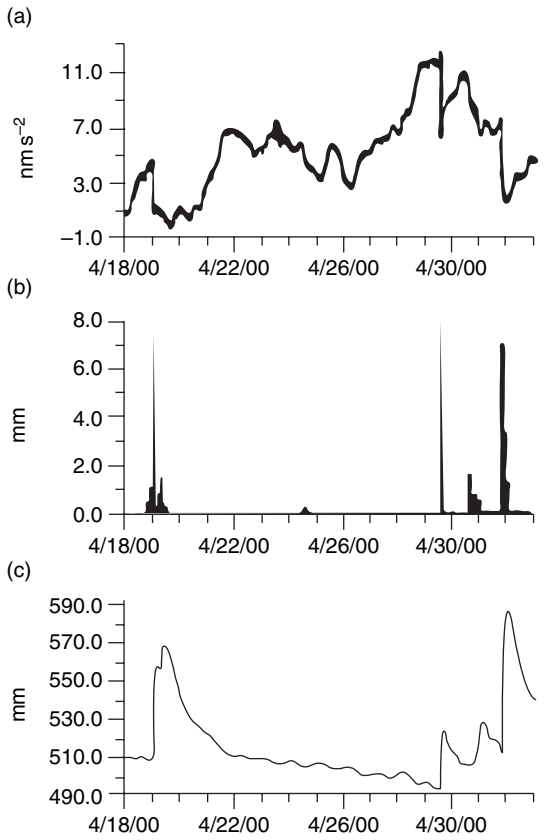

Figure 26 Gravity residual observations (a), accumulated precipitation (per hour) (b), and groundwater table level (c) at Moxa, Germany, from 18 Apr. to 2 May 2000. Reproduced from Kroner C, Jahr T, and Jentzsch G (2004) Results from 44 months of observations with a superconducting gravimeter at Moxa/Germany. *Journal of Geodynamics* 38(3–5): 263–280, with permission from Elsevier.

3.04.3.7 Earth Rotation

At the long period end of the observable spectrum of gravity (**Figure 15**), there are two isolated theoretical periods of the Earth's normal-mode spectrum. One is the inner-core wobble (ICW), whose period is of the order of years. For model PREM, wobble programs yield a value of about 700 days, but the theory is hardly suitable for such a long-period motion. Mathews *et al.* (2002) quote a value of 6.6 yr that is derived from their theory and with VLBI observations and models, but at either period the predicted small amplitude makes this a difficult target (e.g., Guo *et al.*, 2006).

The other mode is much more accessible, and is of course the CW, with a period of about 435 days in the mantle reference frame. This is one of the two components of polar motion normally seen in gravity studies, the other being the smaller amplitude forced annual wobble that is seen in combination with the annual tide and other seasonal effects. Note that at much longer periods there is an 18.6 lunisolar year tide that will be extremely difficult to identify in gravity. Discussion of Richter's (1983) observation of the CW has been mentioned earlier and almost every SG in the GGP network has reported a clear signal of the CW – see, for example, Richter *et al.* (1995b) and Sato *et al.* (1997b) for the Japanese Antarctic station. Here, we review only a few results.

Loyer *et al.* (1999) showed the importance of using a long data set when trying to infer the transfer function of the polar motion; clearly more than

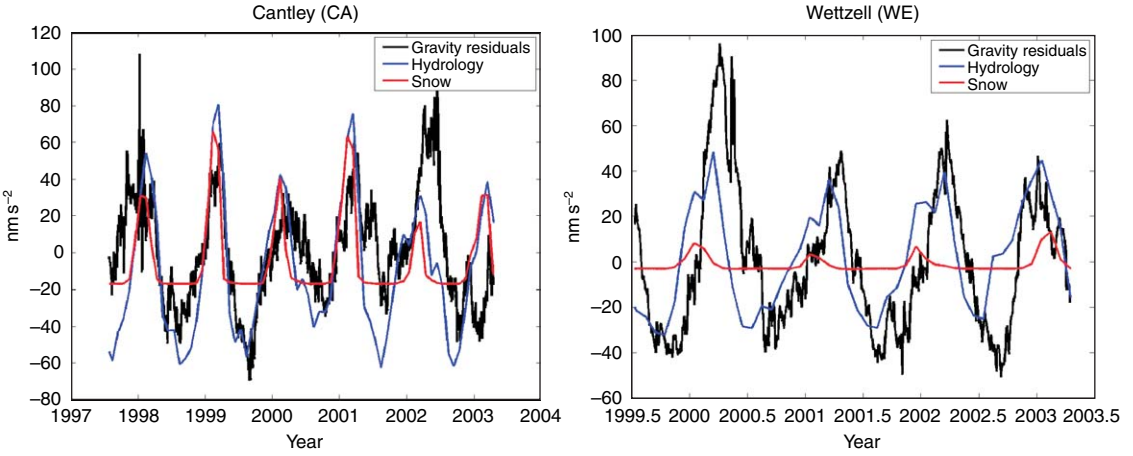

Figure 27 Gravity residuals, hydrology (soil moisture + snow), and snow-modeled contributions at stations Cantley (Canada) and Wettzell (Germany). Reproduced from Boy J-P and Hinderer J (2006) Study of the seasonal gravity signal in superconducting gravimeter data. *Journal of Geodynamics* 41: 227–233, with permission from Elsevier.

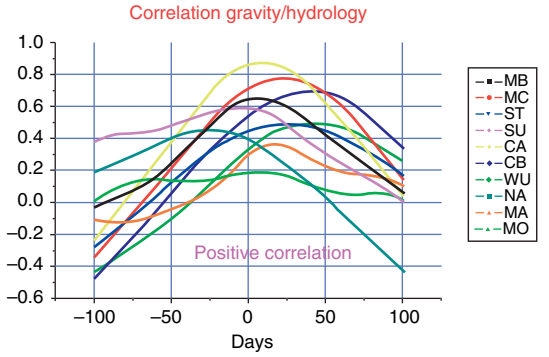

Figure 28 Correlation between gravity and hydrology (continental soil moisture + snow) for some GGP stations; there is a clear positive value with a time lag depending on the station location.

6.5 years of continuous data are required to separate the annual component (whatever its origin) from the 435 day term. They found a gravimetric amplitude factor $\delta = 1.18 \pm 0.10$ and a phase delay of a few degrees using only the Strasbourg station. Harnisch and Harnisch (2006b) generalized this study by using data from 12 GGP stations with lengths varying between 4 and 18 years to investigate the polar motion contribution to gravity. They found that in general the gravimetric amplitude factors for the Chandler wobble are close to the nominal value of 1.16 and phase lags of a few degrees. Xu *et al.* (2004b) also made a similar study on five SGs from the GGP network, and we show in **Figure 30** the typically good agreement between gravity residuals and polar motion for the stations Membach and Potsdam. Combining the results leads to a δ factor of 1.16 ± 0.07 and to a phase delay of $-1.30° \pm 1.33°$. Finally, a data set of nine SGs was analyzed for the polar motion response by Ducarme *et al.* (2006), who found a mean δ factor of 1.179 ± 0.004, similar to Loyer *et al.* (1999).

A value slightly larger than the nominal value of 1.16 is to be expected when including mantle inelasticity and/or ocean pole tide contribution. The variability on the phase delays between different stations is however still large and unexplainable in terms of Earth's rheological properties.

3.04.3.8 Tectonic Effects

The final class of long-term gravity changes is not periodic, but secular (i.e., aperiodic) and primarily due to active tectonics or PGR. Until recently, most studies have been done using AGs (e.g., Niebauer *et al.*, 1995), rather than SGs. One reason for this is that an SG needs a much longer residence time at a station to get a good result, due to instrumental considerations. Thus, there is rarely an SG located close enough to the zone of interest for a particular study.

A second reason is that the SGs have a small instrument drift that must be accounted for as part of any estimate of the secular gravity trend. The potential of

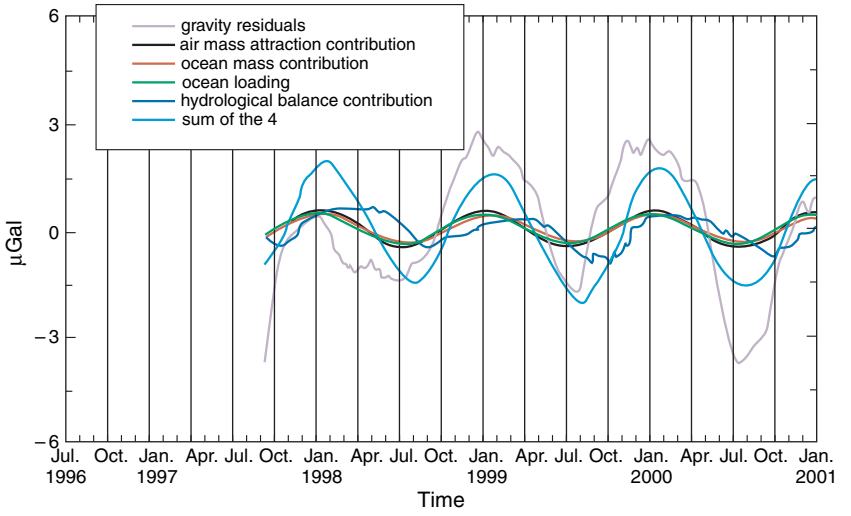

Figure 29 Observed and modeled seasonal gravity changes at Medicina, Italy. Reproduced from Zerbini S, Negusini M, Romagnoli C, Domenichini F, Richter B, and Simon D (2002) Multi-parameter continuous observations to detect ground deformation and to study environmental variability impacts. *Global and Planetary Changes* 34: 37–58, with permission from Elsevier.

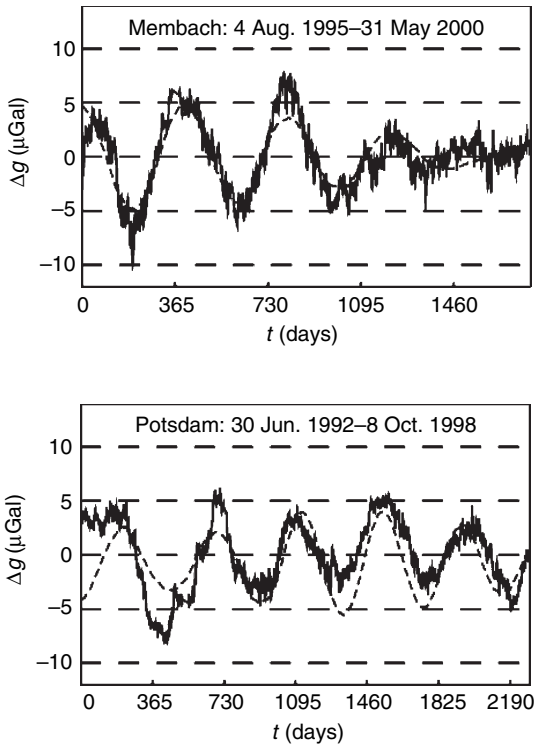

Figure 30 Comparison between gravity residuals (solid line) and polar motion gravity prediction (dashed line) at stations Membach (Belgium) and Potsdam (Germany). Reproduced from Xu J-Q, Sun H-P, and Yang X-F (2004b) A study of gravity variations caused by polar motion using superconducting gravimeter data from the GGP network. *Journal of Geodesy* 78: 201–209 (doi: 10.1007/s00190-004-0386-1), with permission from Springer.

long-term gravity measurements to solve tectonic problems is however significant, as clearly demonstrated by a recent study (Lambert *et al.*, 2006) devoted to PGR in North America. In particular, they could show that the admittance of gravity to height changes (in μGal per millimeter) deduced from combined GPS and AG measurements is indeed close to the theoretically predicted value by Wahr *et al.* (1995) and by James and Ivins (1998) for a viscoelastic model.

In fact, combining gravity and height changes measurements is very efficient in discriminating PGR effects from present-day ice melting contributions as shown by a recent investigation of the long-term gravity changes in Svalbard (Sato *et al.*, 2006a, 2006b). Another study based on 7 years of collocated gravity measurements of SG and AG at Membach (Belgium) by Francis *et al.* (2004) indicates that there is a small decrease in gravity connected to uplift seen by GPS at the same location. A longer data set is required to determine if this gravity decrease is due to PGR or active tectonics in the Ardenne mountains (see also Van Camp *et al.*, 2002).

Such comparisons of AG and GPS measurements are much easier to do when there are continuous SG measurements at the same location. In fact, the continuity of the SG record is often important to check the integrity of the AG measurements (discussed earlier in connection with the SG calibration) and to model effects such as hydrology that increase the AG scatter. Amalvict *et al.* (2004, 2006) analyzed the long-term gravity changes of the Strasbourg SG with regular AG measurements and collocated GPS and interpreted the results in terms of hydrology and tectonics of the Rhine graben. **Figure 31** shows the gravity trend which seems to be present in an 8 year data set (1997–2004) and how hydrological contributions partly explain some of the gravity features.

3.04.3.9 Ground/Satellite Gravity Field Comparison

There is a major international effort in the present decade to measure variations in the Earth's global gravity field using low-orbit satellites. The first satellite *CHAMP* was launched in 2000 and was followed 2 years later by *GRACE*. In the near future, there will be a third mission called *GOCE* that will orbit even closer to the ground and hence be even more sensitive to smaller-scale gravity changes. The primary goal of these missions is to use the temporal changes of the Earth's gravity field to infer changes in regional and continental water storage, and ocean circulation (see Wahr *et al.*, 1998; Rodell and Famiglietti, 1999).

A major concern with satellite measurements of time-varying gravity is how to calibrate and validate such observations. In addition to comparisons with models (the primary technique used to date), there are several possibilities using actual measurements at the ground (GPS, gravity) or at the ocean bottom (water pressure). This problem is important because if successful, it would produce an independent method of validation that does not rely solely on modeling. We will show hereafter that surface measurements from the GGP network provide a useful additional constraint on space gravity data. The validation signal is related to seasonal gravity changes that are coherent on length scales appropriate to satellite altitudes (typically a few hundreds of kilometers).

A first study directly comparing *CHAMP* data to six SG ground observations was done by Neumeyer *et al.* (2004b) and has led to satisfactory results for all the stations in the 1 year analysis period (from

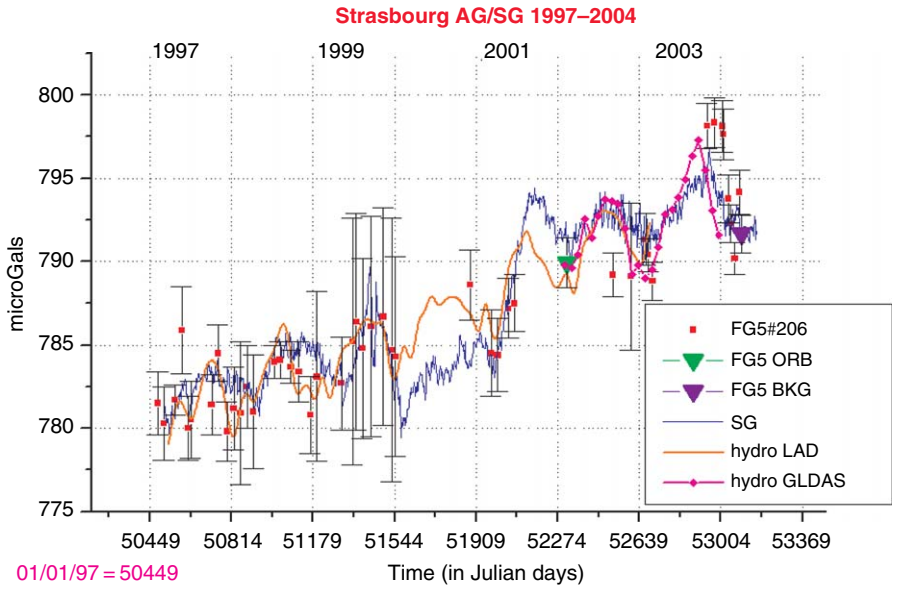

Figure 31 An example of SG/AG superposition at Strasbourg (France) from 1997 to 2004. The gravity observations are corrected for tides (solid + ocean load), air pressure, and polar motion; the instrumental drift of the SG has been removed and hydrological contributions added. Reproduced from Amalvict M, Hinderer J, and Rozsa S (2006) Crustal vertical motion along a profile crossing the Rhine graben from the Vosges to the Black Forest Mountains: Results from absolute gravity, GPS and levelling observations. *Journal of Geodynamics* 41: 358–368, with permission from Elsevier.

December 2000 to December 2001). The superposition of the monthly gravity mean values from the SG residuals (after correction for solid tides, ocean and atmospheric loadings, and polar motion) with the *CHAMP*-reconstructed values at the SG sites is rather good. Neumeyer *et al.* (2006) recently extended this study to *GRACE* data, pointing out again the partial agreement between surface and satellite-derived gravity at specific locations. Before a detailed comparison can be made, however, one has to remember that ground gravity measurements include necessarily a contribution from the vertical motion of the instrument through the ambient gravity field. This signal does not affect the orbiting satellite, and hence there is a difference in the gravity changes as seen at (moving) ground level and by the satellite (Hinderer *et al.*, 2006).

We note in these studies that the comparison of single station results with the large-scale satellite solutions is problematic due to the completely different error budgets involved. *GRACE* data, for example, are good to 1 μGal only over length scales longer than 500–1000 km, whereas SGs are good to the same accuracy (or better) at a single point. In order to average SG measurements and reduce local effects, there have been attempts to assemble a network solution from nearby SG stations rather than doing the above single-station comparison. Within the existing rather sparse GGP network, Europe is obviously the best place to try such an approach.

The approach was first initiated using 1 year of SG data by Crossley and Hinderer (2002) and Crossley *et al.* (2003) and extended to longer data sets by Crossley *et al.* (2003, 2004, 2005). This approach was further extended to a 21 month time interval to intercompare surface data (GGP European subnetwork), satellite data from *GRACE*, and theoretical predictions for two hydrology models (LAD and GLDAS) (Andersen *et al.*, 2005a; Hinderer *et al.*, 2006). The results show the existence of an annual signal that is coherent over Europe with an amplitude of a few μGal, mostly due to the seasonal loading from continental hydrology (soil moisture + snow) according to recent models such as LadWorld (Milly and Shmakin, 2002) or GLDAS (Rodell *et al.*, 2004). There is even a possibility to detect in *GRACE* data interannual signals (Andersen and Hinderer, 2005) and, in particular, there is a clear evidence that *GRACE* has been affected by the heat wave that occurred in summer 2003 in Europe (Andersen *et al.*, 2005b). The Wettzell (Germany) and the Medicina (Italy) SG data seem to confirm this point as shown by **Figure 32**.

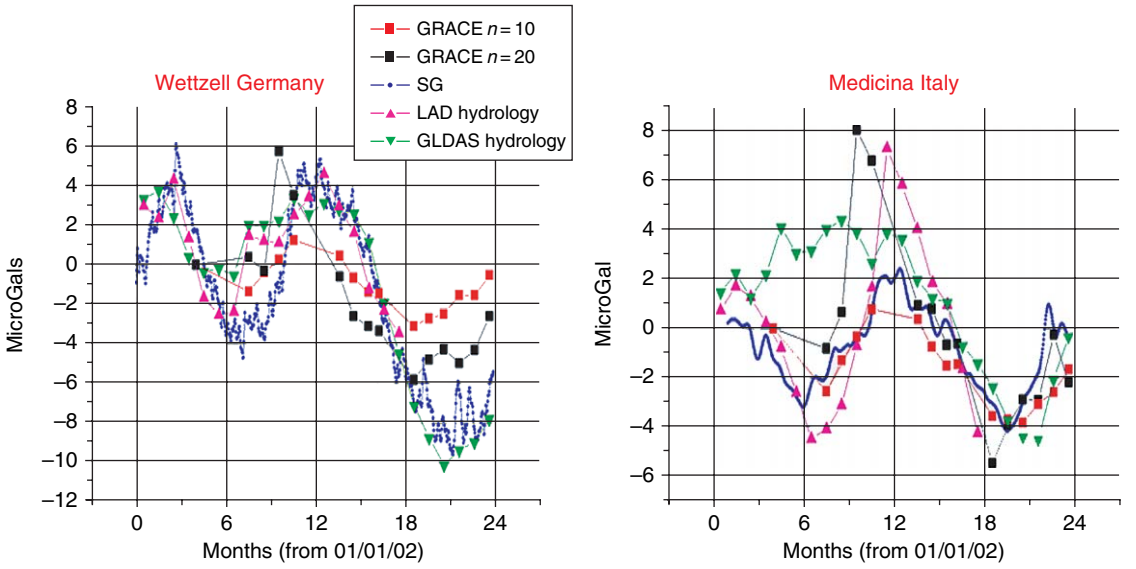

Figure 32 An example of the superposition of gravity changes seen by *GRACE* (in red for $n = 10$ and in black for $n = 20$) and the superconducting gravimeter in Wettzell (Germany) and Medicina (Italy) (in blue) and contributions from continental hydrology models like GLDAS (in green) and LADWorld (in purple).

3.04.3.10 Future Possibilities

Several recent SG results point the way to future studies involving gravity. One of these is the study by Imanishi *et al.* (2004) of coseismic displacements that accompanied a large $M_w = 8.0$ earthquake in Japan. Using three SGs in a linear array (**Figure 33**), they showed that gravity offsets occurred that matched the theoretical prediction of static displacements that accompany a fault rupture process. The offsets were 0.58, 0.10, and 0.07 μGal at stations ES, MA, and KY respectively, in line with the epicenter at Tokachi-oki (near Hokkaido). Such small offsets (especially close to 0.1 μGal) would hardly be identified in an individual record, but this is the first time a gravity array has performed at this level of precision.

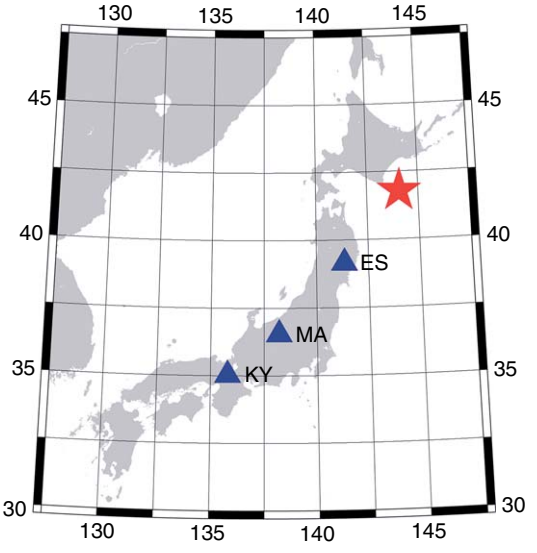

Figure 33 Japan SG array (blue stations) that observed gravity offsets due to a local large earthquake (red).

The significance of this result can be transferred to another context, that of subduction-induced silent earthquakes that have been identified off the coast of Japan and in the Cascadia subduction zone off Vancouver Island. In the latter region, episodic tremor that accompanies the silent slip events can last for several days, but there is no identifiable earthquake. Such events are identified primarily as horizontal displacements on GPS arrays, but Lambert *et al.* (2006) have shown (**Figure 34**) that AG measurements also reveal coincident offsets in gravity of several μGal, in between which there is a secular drift (in this case a negative trend). Imagine how precisely this signal would be measured by an inline SG array of the same type that exists in Japan!

It needs hardly be said that hydrology will continue to increase in importance as one of the important targets for future geodetic and geophysical measurements. At the present time, an SG is part of a project to monitor the state of underground water

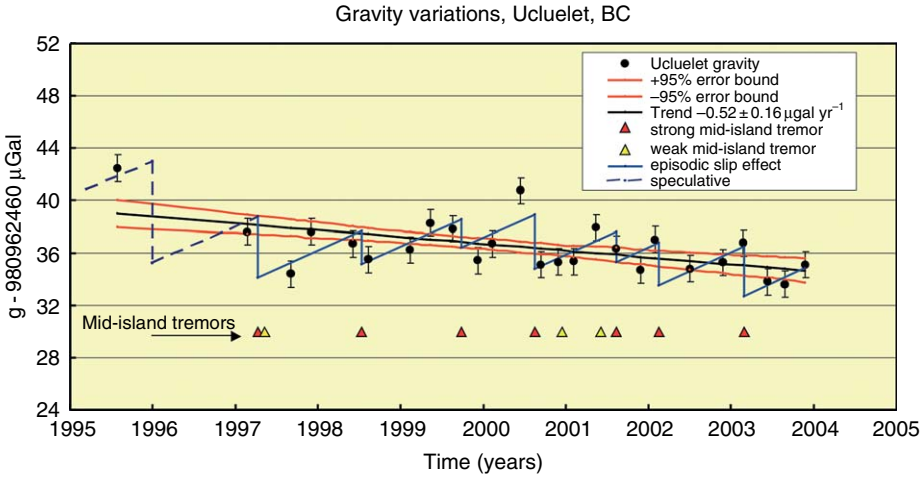

Figure 34 Variations in AG at Ucluelet (western coast of Vancouver Island) showing some concordance with the episodic slip and seismic tremor activity above the Cascadia subduction zone. Courtesy: T. Lambert.

storage at the Texas Hydrological Observatory, that is, surface watersheds and underlying aquifers (C. Wilson, U. Texas), and there have been some proposals to use gravity to monitor active subsurface tectonics in the US (Harry, 1997).

The question of monitoring tectonic processes from *GRACE* data has been raised (Mikhailov *et al.*, 2004), but of course a combination with SG measurements would give a much stronger data set. Also of recent interest is the proposal to use AG measurements in conjunction with *GRACE* data to monitor Fennoscandian post-glacial uplift, and such a project would benefit considerably from one or two stations that have an SG for continuous monitoring. Along the same lines, a proposal is underway to combine an SG with AG and portable Scintrex-type gravimeters to calibrate/validate *GRACE* satellite measurements in West Africa (Hinderer *et al.*, 2005). One profile covers the extremely dry regions from the central Sahara desert down to the coast of Benin, and another is a triplet of stations in the monsoon region of very high rainfall in the Cameroon region.

Our final suggestion for the future deployment of SGs is for the monitoring of volcanoes – both their slow deformation and their explosive activity. Carbone *et al.* (2003) reported several years of gravity along an NS profile on the flank of Mt. Etna that showed variations of more than 50 mGal using Scintrex portable instruments and a continuously operating LCR base station. Had the base station been equipped with an SG, the results would have been even more impressive.

As has been shown by Rymer and Locke (1995), the combination of gravity measurements with surface elevation changes is capable of distinguishing between several different modes of volcanic behavior: surface lowering can accompany either loss of magma or magma injection, and surface elevation (inflation) again associated with either loss or gain of magma. Both gravity and GPS measurements were done in the study of Furuya *et al.* (2003) – shown in **Figure 35** – and this allows a more detailed interpretation of the subsurface mass changes than using either method alone. The gravity signals are very large (~100 µGal) compared to those discussed elsewhere in this chapter, and there would be no question of their detection by an SG, even without detailed AG backup measurements.

3.04.4 Conclusions

We now summarize the main points of the use of SGs in geodetic measurements:

1. Over the 40 years since it was first developed, the SG has proved to be an extremely reliable instrument for determining gravity variations from 1 s to periods of several years, and several instruments have been operated for more than a decade without interruption.
2. Calibration changes in SGs are virtually nonexistent, and drift rates are at the level of a few µGal per year, making them ideal for long-term monitoring of the gravity field (tectonics, seasonal changes, and polar motion).
3. The precision of 0.1 nGal in frequency domain and an accuracy of better than 0.1 µGal in the time

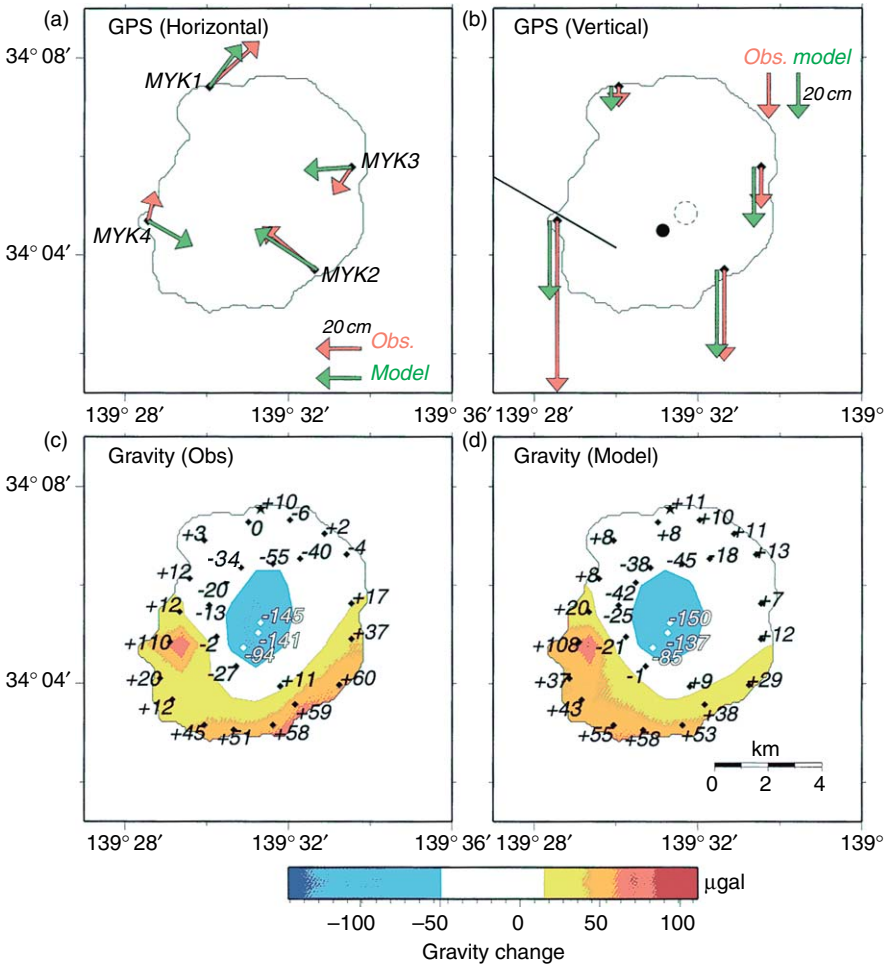

Figure 35 Observed and modeled combinations of GPS and gravity variations, prior to the caldera collapse at Miyakejima Volcano, Japan, in 2000. Reproduced from Furuya M, Okubo S, Sun W, Tanake Y, Oikawa J, and Watanabe H (2003) Spatio-temporal gravity changes at Miyakejima Volcano, Japan: Caldera collapse, explosive eruptions, and magma movement. *Journal of Geophysical Research* 108(B4): 2219, with permission from American Geophysical Union.

domain have contributed to major improvements in tidal analysis, ocean loading computations, and atmospheric effects that were not possible with other types of gravimeter.

4. With SGs, it is now possible to seriously model the gravity effects in hydrology due to rainfall and to quantify these effects in soil moisture, groundwater variations, and atmospheric mass changes.

5. The SG has proven to be very useful, in the same way that spring gravimeters were, in the study of the Earth's free oscillations, particularly at periods longer than 500 s.

6. The combination of SGs and satellite measurements of the gravity field is proving to be consistent and complementary indicators of regional hydrology.

7. New possibilities exist for the use of SGs in hydrology, tectonics, and the monitoring of volcanoes.

8. Future studies in gravity would be much enhanced if SGs can be deployed in array form and combined, where appropriate, with AGs, portable gravimeters, and GPS receivers.

Acknowledgments

Much of the development of the SG has been carried out at GWR by contracts initiated by Bernd Richter and funded by the Institut für Angewandte Geodäsie (IFAG, Frankfurt, Germany) and later by the Bundesamt für Kartographie und Geodäsie (BKG, Frankfurt). Without this involvement, the commercial

venture would have been difficult to maintain. We also acknowledge the support of the US Department of Energy under Grant No. DE-FG03-95ER81979 and the US National Science Foundation under Grants No. 9529827 and EAR Award No. 0409381.

References

Achilli V, Baldi P, Casula G, *et al.* (1995) A calibration system for superconducting gravimeters. *Bulletin Geodesique* 69: 73–80.

Agnew DC (1997) NLOADF: A program for computing ocean-tide loading. *Journal of Geophysics* 102: 5109–5110.

Agnew DC and Farrell WE (1978) Self-consistent equilibrium ocean tides. *Geophysical Journal of the Royal Astronomical Society* 55: 171–181.

Amalvict M, Hinderer J, Boy J-P, and Gegout P (2001a) A three year comparison between a superconducting gravimeter (GWR C026) and an absolute gravimeter (FG5#206) in Strasbourg (France). *Journal of Geodetic Society of Japan* 47: 410–416.

Amalvict M, McQueen H, and Govind R (2001b) Absolute gravity measurements and calibration of SG-CT031 at Canberra, 1999–2000. *Journal of Geodetic Society of Japan* 47: 334–340.

Amalvict M, Hinderer J, Gegout P, Rosat S, and Crossley D (2002) On the use of AG data to calibrate SG instruments in the GGP network. *Bulletin d'Informations des Marées Terrestres* 135: 10621–10626.

Amalvict M, Hinderer J, Makinen J, Rosat S, and Rogister Y (2004) Long-term and seasonal gravity changes and their relation to crustal deformation and hydrology. *Journal of Geodynamics* 38: 343–353.

Amalvict M, Hinderer J, and Rozsa S (2006) Crustal vertical motion along a profile crossing the Rhine graben from the Vosges to the Black Forest Mountains: Results from absolute gravity, GPS and levelling observations. *Journal of Geodynamics* 41: 358–368.

Andersen O and Hinderer J (2005) Global inter-annual gravity changes from GRACE: Early results. *Geophysical Research Letters* 32: L01402 (doi:10.1029/2004GL020948).

Andersen O, Hinderer J, and Lemoine FG (2005a) Seasonal gravity field variations from GRACE and hydrological models. In: Jekeli C, Bastos L, and Fernandes J (eds.) *Gravity, Geoid and Space Missions. IAG Symposia*, vol. 129, pp. 316–321. Berlin: Springer Verlag.

Andersen O, Seneviratne S, Hinderer J, and Viterbo P (2005b) GRACE-derived terrestrial water storage depletion associated with the 2003 European heat wave. *Geophysical Research Letters* 32: L18405 (doi:10.1029/2005GL023574).

Baker T and Bos M (2003) Validating Earth and ocean tide models using tidal gravity measurements. *Geophysical Journal International* 152: 468–485.

Banka D and Crossley D (1999) Noise levels of superconducting gravimeters at seismic frequencies. *Geophysical Journal International* 139: 87–97.

Berger J, Davis P, and Ekström G (2004) Ambient Earth noise: A survey of the Global Seismographic Network. *Journal of Geophysical Research* 109: B11307 (doi:10.1029/204JB003408).

Bos MS and Baker TF (2005) An estimate of the errors in gravity ocean tide loading computations. *Journal of Geodesy* 79: 50–63.

Bos M, Baker TF, Lyard FH, Zürn W, and Rydelek PA (2000) Long-period lunar tides at the geographic South Pole and recent models of ocean tides. *Geophysical Journal International* 143: 490–494.

Bower DR, Liard J, Crossley D, and Bastien R (1991) Preliminary calibration and drift assessment of the superconducting gravimeter GWR12 through comparison with the absolute gravimeter JILA 2, Proceedings of the Workshop: Non Tidal Gravity Changes Intercomparison Between Absolute and Superconducting Gravimeters, Conseil de l'Europe, *Cahiers du Centre Europeen de Geodynamique et de Seismologie* 3, Luxembourg, pp. 129–142.

Boy J-P and Chao BF (2005) Precise evaluation of atmospheric loading effects on Earth's time-variable gravity field. *Journal of Geophysical Research* 110: B08412 (doi:10.1029/2002JB002333).

Boy J-P and Hinderer J (2006) Study of the seasonal gravity signal in superconducting gravimeter data. *Journal of Geodynamics* 41: 227–233.

Boy J-P, Hinderer J, and Gegout P (1998) Global atmospheric loading and gravity. *Physics of the Earth and Planetary Interiors* 109: 161–177.

Boy J-P, Hinderer J, Amalvict M, and Calais E (2000) On the use of long records of superconducting and absolute gravity observations with special application to the Strasbourg station, France, Proceedings of the Workshop: High-Precision Gravity Measurements with Application to Geodynamics and Second GGP Workshop. *Cahiers du Centre Européen de Géodynamique et de Séismologie*, 17, Luxembourg, pp. 67–83.

Boy J-P, Gegout P, and Hinderer J (2001) Gravity variations and global pressure loading. *Journal of Geodetic Society of Japan* 47: 1, 267–272.

Boy J-P, Gegout P, and Hinderer J (2002) Reduction of surface gravity data from global atmospheric pressure loading. *Geophysical Journal International* 149: 534–545.

Boy J-P, Llubes M, Hinderer J, and Florsch N (2003) A comparison of tidal ocean loading models using superconducting gravimeter data. *Journal of Geophysical Research* 108(B4): 2193 (doi:10.1029/2002JB002050).

Boy J-P, Llubes M, Ray R, *et al.* (2004) Non-linear oceanic tides observed by superconducting gravimeters in Europe. *Journal of Geodynamics* 38: 391–405.

Boy J-P, Llubes M, Ray R, Hinderer J, and Florsch N (2006) Validation of long-period oceanic tidal models with superconducting gravimeters. *Journal of Geodynamics* 41: 112–118.

Busse FH (1974) On the free oscillation of the Earth's inner core. *Journal of Geophysical Research* 79: 753–757.

Carbone D, Greco F, and Budetta G (2003) Combined discrete and continuous gravity observations at Mount Etna. *Journal of the Volcanology and Geothermal Research* 123(1–2): 123–135.

Cartwright DE and Taylor RJ (1971) New computations of the tide generating potential. *Geophysical Journal of the Royal Astronomical Society* 23(1): 45–74.

Cartwright DE and Edden CA (1973) Corrected tables of spherical harmonics. *Geophysical Journal of the Royal Astronomical Society* 33(3): 253–264.

Courtier N, Ducarme B, Goodkind J, *et al.* (2000) Global superconducting gravimeter observations and the search for the translational modes of the inner core. *Physics of the Earth and Planetary Interiors* 117: 3–20.

Crossley D (1993) Core modes and Slichter modes – fact and fancy. *Bulletin d'Informations des Marées Terrestres* 117: 8628–8638.

Crossley D (2004) Preface to the global geodynamics project. *Journal of Geodynamics* 38: 225–236.

Crossley D and Xu X (1998) Analysis of superconducting gravimeter data, from Table Mountain, Colorado. *Geophysical Journal International* 135: 835–844.

Crossley D and Hinderer J (2002) GGP Ground truth for satellite gravity missions. *Bulletin d'Informations des Marées Terrestres* 136: 10735–10742.

Crossley D and Hinderer J (2005) Using SG arrays for hydrology in comparison with GRACE satellite data, with extension to seismic and volcanic hazards. *Korean Journal of Remote Sensing* 21(1): 31–49.

Crossley D, Jensen O, Xu H, and Hinderer J (1993) A slew rate detection criterion applied to SG data processing. *Bulletin d'Informations des Marées Terrestres* 117: 8675–8704.

Crossley D, Jensen O, and Hinderer J (1995) Effective barometric admittance and gravity residuals. *Physics of the Earth and Planetary Interiors* 90: 221–241.

Crossley D, Xu H, and Van Dam T (1998) Comprehensive analysis of 2 years of data from Table Mountain, Colorado. In: Ducarme B and Paquet P (eds.) *Proceedings of the 13th International Symposium on Earth Tides*, pp. 659–668. Brussels: Observatoire Royal de Belgique.

Crossley D, Hinderer J, Casula G, *et al.* (1999) Network of superconducting gravimeters benefits a number of disciplines. *EOS, Transactions, American Geophysical Union* 80: 121–126.

Crossley D, Hinderer J, and Amalvict M (2001) A spectral comparison of absolute and superconducting gravimeter data. *Journal of Geodetic Society of Japan* 47: 373–379.

Crossley D, Hinderer J, Llubes M, and Florsch N (2003) The potential of ground gravity measurements to validate GRACE data. *Advances in Geosciences* 1: 1–7.

Crossley D, Hinderer J, and Boy J-P (2004) Regional gravity variations in Europe from superconducting gravimeters. *Journal of Geodynamics* 38: 325–342.

Crossley D, Hinderer J, and Boy J-P (2005) Time variation of the European gravity field from superconducting gravimeters. *Geophysical Journal International* 161: 257–264.

Cummins P, Wahr J, Agnew D, and Tamura Y (1991) Constraining core undertones using stacked IDA gravity records. *Geophysical Journal International* 106: 189198.

Dahlen FA and Sailor RV (1979) Rotational and elliptical splitting of the free oscillations of the Earth. *Geophysical Journal of the Royal Astronomical Society* 58: 609–623.

Defraigne P, Dehant V, and Hinderer J (1994) Stacking gravity tide measurements and nutation observations in order to determine the complex eigenfrequency of the nearly diurnal free wobble. *Journal of Geophysical Research* 99(B5): 9203–9213.

Dehant V, Defraigne P, and Wahr J (1999) Tides for a convective Earth. *Journal of Geophysical Research* 104: 1035–1058.

De Meyer F and Ducarme B (1989) Non-tidal gravity changes observed with a superconducting gravimeter. In: Helsinki E (ed.) *Proceedings of 11th International Symposium on Earth Tides*, pp. 167–184. Stuttgart: Schweizerbart'sche Verlagsbuchhandlung.

Dickman SR (2005) Rotationally consistent Love numbers. *Geophysical Journal International* 161: 31–40.

Dierks O and Neumeyer J (2002) Comparison of Earth Tides Analysis Programs. *Bulletin d'Informations des Marées Terrestres* 135: 10669–10688.

Doodson AT (1921) The harmonic development of the tide generating potential. *Proceedings of the Royal Society of London* A 100: 306–328.

Dragert H, Wang K, and James T (2001) A silent slip event on the deeper Cascadia subduction interface. *Science* 292: 1525–1528.

Ducarme B (1983) Tidal gravity parameters at Brussels reconfirmed by a superconducting gravimeter. *Physics of Earth and Planetary Interiors* 32: 1–3.

Ducarme B, Sun H-P, and Xu J-Q (2002) New investigation of tidal gravity results from the GGP network. *Bulletin d'Informations des Marées Terrestres* 136: 10761–10776.

Ducarme B, Venedikov A, Arnoso J, and Vieira R (2004) Determination of the long period tidal waves in the GGP superconducting gravity data. *Journal of Geodynamics* 38: 307–324.

Ducarme B, Venedikov A, Arnoso J, Chen X-D, Sun H-P, and Vieira R (2006) Global analysis of the GGP superconducting gravimeters network for the estimation of the pole tide gravimetric amplitude factor. *Journal of Geodynamics* 41: 334–344.

Dziewonski AM and Anderson DL (1981) Preliminary reference Earth model. *Physics of Earth and Planetary Interiors* 25: 297–356.

Egbert GD and S Erofeeva E (2002) Efficient inverse modeling of barotropic ocean tides. *Journal of Atmospheric and Oceanic Technology* 19: 183–204.

Elstner C and Schwahn W (1997) Precise mean parameters for daily and subdaily persistent air pressure waves at Potsdam for the period 1893–1992. In: Ducarme B and Paquet P (eds.) *Proceedings of the 13th International Symposium on Earth Tides*, pp. 469–476. Brussels: Observatoire Royal de Belgique.

Falk R, Harnisch M, Harnisch G, Nowak I, Richter B, and Wolf P (2001) Calibration of superconducting gravimeters SG103, C023, CD029, and CD030. *Journal of Geodetic Society of Japan* 47(1): 22–27.

Farrell WE (1972) Deformation of the Earth by surface loads. *Review of Geophysics. Space Physics* 10(3): 751–797.

Flather RA (1976) A tidal model of the North-West European continental shelf. *Mémoires de la Société Royale des Sciences de Liège* 9: 141–164.

Florsch N and Hinderer J (2000) Bayesian estimation of the Free Core Nutation parameters from the analysis of precise tidal gravity data. *Physics of Earth and Planetary Interiors* 117: 21–35.

Florsch N, Hinderer J, and Legros H (1995b) Identification of quarter diurnal waves in superconducting gravimeter data. *Bulletin d'Informations des Marées Terrestres* 122: 9189–9198.

Florsch N, Legros H, and Hinderer J (1995a) The search for weak harmonic signals in a spectrum with application to gravity data. *Physics of Earth and Planetary Interiors* 90: 197–210.

Francis O (1997) Calibration of the C021 superconducting gravimeter in Membach (Belgium) using 47 days of absolute gravity measurements, in Gravity, Geoid and Marine Geodesy, Tokyo, Japan, IAG Symposium 117, Springer, pp. 212–219.

Francis O and Hendrickx M (2001) Calibration of the LaCoste-Romberg 906 by comparison with the spring gravimeter C021 in Membach (Belgium). *Journal of Geodetic Society of Japan* 47(1): 16–21.

Francis O, Niebauer T, Sasagawa G, Klopping F, and Gschwind J (1998) Calibration of a superconducting gravimeter by comparison with an absolute gravimeter FG5 in Boulder. *Geophysical Research Letters* 25(7): 1075–1078.

Francis O, Van Camp M, van Dam T, Warnant R, and Hendrickx M (2004) Indication of the uplift of the Ardenne in long-term gravity variations in Membach (Belgium). *Geophysical Journal International* 158: 346–352.

Freybourger M, Hinderer J, and Trampert J (1997) Comparative study of superconducting gravimeters and broadband seismometers STS-1/Z in subseismic frequency bands. *Physics of the Earth and Planetary Interiors* 101: 203–217.

Fukuda Y and Sato T (1997) Gravity effects of sea level variation at the Superconducting Gravimeter sites, estimated from ERS-1 and Topex-Poseidon altimeter data. In: Segawa, *et al.* (eds.) *IAG Symposia vol. 117, Gravity, Geoid, and Marine Geodesy*, pp. 107–114. Berlin: Springer-Verlag.

Furuya M, Okubo S, Sun W, Tanake Y, Oikawa J, and Watanabe H (2003) Spatio-temporal gravity changes at Miyakejima Volcano, Japan: caldera collapse, explosive eruptions, and magma movement. *Journal of Geophysical Research* 108(B4): 2219.

Goodkind JM (1983) Q of the nearly diurnal free wobble. In: Kuo JT (ed.) *Proceedings of The 9th International Symposium on Earth Tides*, pp. 569–575.. New York: E. Schweizerbartsche Verlagsbuchhandlung.

Goodkind JM (1991) The superconducting gravimeter: principles of operation, current performance and future prospects, Proc. Workshop: Non Tidal Gravity Changes Intercomparison Between Absolute and Superconducting Gravimeters, Conseil de l'Europe, Cahiers du Centre Europeen de Geodynamique et de Seismologie, 3, Luxembourg, pp. 81–90.

Goodkind JM (1996) Test of theoretical solid earth and ocean gravity tides. *Geophysical Journal International* 125: 106–114.

Goodkind JM (1999) The superconducting gravimeter. *Review of Scientific Instruments* 70(11): 4131–4152.

Goodkind JM, Czipott PV, Mills AP, *et al.* (1993) Test of the gravitational square law at 0.4 to 1.4 m mass separation. *Physical Review D* 47(4): 1290–1297.

Green J (1999) *Atmospheric Dynamics*. New York: Academic Press.

Guo J-Y, Dierks O, Neumeyer J, and Shum CK (2006) Weighting algorithms to stack superconducting gravimeter data for the potential detection of the Slichter modes. *Journal of Geodynamics* 41: 326–333.

Harnisch M and Harnisch G (1995) Processing of the data from two superconducting gravimeters, recorded in 1990–1991 at Richmond (Miami, Florida). Some problems and results. *Bulletin d'Informations des Marées Terrestres* 122: 9141–9147.

Harnisch M and Harnisch G (1997) Long time behaviour of superconducting gravimeters derived from observed time series. *Bulletin d'Informations des Marées Terrestres* 127: 9796–9805.

Harnisch M and Harnisch G (2002) Seasonal variations of hydrological influences on gravity measurements at Wettzell. *Bulletin d'Informations des Marées Terrestres* 137: 10.

Harnisch G and Harnisch M (2006a) Hydrological influences in long gravimetric data series. *Journal of Geodynamics* 41: 1–3, 276–287.

Harnisch M and Harnisch G (2006b) Study of long-term gravity variations, based on data of the GGP co-operation. *Journal of Geodynamics* 41(1–3): 318–325.

Harnisch M, Harnisch G, Richter B, and Schwahn W (1998) Estimation of polar motion effects from time series recorded by superconducting gravimeters. In: Ducarme B and Paquet P (eds.) *Proceedings of the 13th International Symposium. Earth Tides, Brussels 1997*, pp. 511–518. Brussels: Observatoire Royal de Belgique.

Harnisch M, Harnisch G, Nowak I, Richter B, and Wolf P (2000) The dual sphere superconducting gravimeter C029 at Frankfurt a.M. and Wettzell. First results and calibration. Proc. of the Workshop: High-Precision Gravity Measurements with Application to Geodynamics and Second GGP Workshop, Cahiers du Centre Européen de Géodynamique et de Séismologie, 17, Luxembourg, pp. 39–56.

Harnisch M, Harnisch G, and Falk R (2002) Improved scale factors of the BKG superconducting gravimeters, derived from comparisons with absolute gravity measurements. *Bulletin d'Informations des Marées Terrestres* 135: 10627–10642.

Harry DL (1997) The use of GPS and microgal absolute gravimetry to constrain active tectonics in the subsurface: Preliminary report, AGU Chapman Conference on Microgal Gravimetry, St. Augustine, Fl.

Hartmann T and Wenzel H-G (1995a) The HW95 tidal potential catalogue. *Geophysical Research Letters* 22, 24: 3553–3556.

Hartmann T and Wenzel H-G (1995b) Catalog HW95 of the tide generating potential. *Bulletin d'Informations des Marées Terrestres* 123: 9278–9301.

Herring TA, Gwinn CR, and Shapiro II (1986) Geodesy by radioInterferometry: Studies of the forced nutations of the Earth: I. Data analysis. *Journal of Geophysical Research* 91(B5): 4745–4754.

Hinderer J and Legros H (1989) Gravity perturbations of annual period. In: Helsinki E (ed.) *Proceedings of the 11th International Symposium. Earth Tides*, pp. 425–429. Stuttgart: Schweizerbart'sche Verlagsbuchhandlung.

Hinderer J and Crossley D (2000) Time variations in gravity and inferences on the Earth's structure and dynamics. *Surveys in Geophysics* 21: 1–45.

Hinderer J and Crossley D (2004) Scientific achievements from the first phase (1997–2003) of the Global Geodynamics Project using a worldwide network of superconducting gravimeters. *Journal of Geodynamics* 38: 237–262.

Hinderer J, Florsch N, Mäkinen J, Legros H, and Faller JE (1991) On the calibration of a superconducting gravimeter using absolute gravity measurements. *Geophysical Journal International* 106: 491–497.

Hinderer J, Crossley D, and Xu H (1994) A two year comparison between the French and Canadian superconducting gravimeter data. *Geophysical Journal International* 116: 252–266.

Hinderer J, Crossley D, and Jensen O (1995) A search for the Slichter triplet in superconducting gravimeter data. *Physics of Earth and Planetary Interiors* 90: 183–195.

Hinderer J, Boy JP, and Legros H (1998) A 3000 day registration of the superconducting gravimeter GWR T005 in Strasbourg, France. In: Ducarme B and Paquet P (eds.) *Proceedings of the 13th International Symposium on Earth Tides*, pp. 617–624. Brussels: Observatoire Royal de Belgique.

Hinderer J, Boy JP, Gegout P, Defraigne P, Roosbeek F, and Dehant V (2000) Are the free core nutation parameters variable in time? *Physics of Earth and Planetary Interiors* 117: 37–49.

Hinderer J, Rosat S, Crossley D, Amalvict M, Boy J-P, and Gegout P (2002a) Influence of different processing methods on the retrieval of gravity signals from GGP data. *Bulletin d'Informations des Marées Terrestres* 123: 9278–9301.

Hinderer J, Amalvict M, Crossley D, Rivera L, Leveque J-J, and Luck B (2002b) Tides, earthquakes and ground noise as seen by an absolute gravimeter and its superspring; a comparison with a broadband seismometer and a superconducting gravimeter. *Metrologia* 39: 495–501.

Hinderer J, de Linage C, and Boy J-P (2005) Issues in the ground validation of satellite-derived gravity measurements: A proposal to validate GRACE in Africa from the Sahara to the equatorial monsoon. *EOS Transactions*, *American Geophysical Union* 85(52): *Fall Meeting Supplement* Abstract G33A-0028.

Hinderer J, Andersen O, Lemoine F, Crossley D, and Boy J-P (2006) Seasonal changes in the european gravity field from GRACE: A comparison with superconducting gravimeters and hydrology model predictions. *Journal of Geodynamics* 41: 59–68.

Hsu H-T, Tao GQ, Song XL, Baker TF, Edge RJ, and Jeffries G (1989) Gravity tidal datum at Wuchang of China. In: Helsinki E (ed.) *Proceedings of the 11th International Symposium on Earth Tides*, pp. 187–195. Stuttgart: Schweizerbart'sche Verlagsbuchhandlung.

Ijpelaar R, Troch P, Warderdam P, Stricker H, and Ducarme B (2002) Detecting hydrological signals in time series of *in-situ* gravity measurements. *Bulletin d'Informations des Marées Terrestres* 135: 10837–10838.

Imanishi Y (2005) On the possible cause of long period instrumental noise (parasitic mode) of a superconducting gravimeter. *Journal of Geodesy* 78(11–12): 683–690.

Imanishi Y, Higashi T, and Fukuda Y (2002) Calibration of the superconducting gravimeter T011 by parallel observation with the absolute gravimeter FG5 210 – a Bayesian approach. *Geophysical Journal International* 151: 867–878.

Imanishi Y, Sato T, Higashi T, Sun W, and Okubo S (2004) A network of superconducting gravimeters detects submicrogal coseismic gravity changes. *Science* 306: 476–478.

Iwano S and Fukuda Y (2004) Superconducting gravimeter observations without a tilt compensation system. *Physics of the Earth and Planetary Interiors* 147(4): 343–351.

Iwano S, Kimura I, and Fukuda Y (2003) Calibration of the superconducting gravimeter TT70 #016 at Syowa station by parallel observation with the absolute gravimeter FG5 #203. *Polar Geoscience* 16: 22–28.

James TS and Ivins ER (1998) Predictions of Antarctic crustal motions driven by present-day ice sheet evolution and by isostatic memory of the Last Glacial Maximum. *Journal of Geophysical Research* 103: 4993–5017.

Jentzsch G, Kroner C, Flach D, and Gommlich G (1995) Long and aperiodic effects in the recording of the superconducting gravimeter in the Asse salt mine in Northern Germany, Proc. 2nd Workshop: Non Tidal Gravity Changes Intercomparison Between Absolute and Superconducting Gravimeters, Conseil de l'Europe, Cahiers du Centre Européen de Géodynamique et de Séismologie, 11, Luxembourg, pp. 187–189.

Klopping FJ, Peter G, Berstis KA, Carter WE, Goodkind JM, and Richter BD (1995) Analysis of two 525 day long data sets obtained with two side-by-side, simultaneously recording superconducting gravimeters at Richmond, Florida, U.S.A., Proc. 2nd Workshop: Non Tidal Gravity Changes Intercomparison Between Absolute and Superconducting Gravimeters, Conseil de l'Europe, Cahiers du Centre Europeen de Geodynamique et de Seismologie, 11, Luxembourg, pp. 57–69.

Kobayashi N and Nishida K (1998) Continuous excitation of planetary free oscillations by atmospheric disturbances. *Nature* 395: 357–360.

Kroner C (2001) Hydrological effects on gravity at the Geodynamic Observatory Moxa. *Journal of the Geodetic Society of Japan* 47(1): 353–358.

Kroner C and Jentzsch G (1999) Comparison of different pressure reductions for gravity data and resulting consequences. *Physics of the Earth and Planetary Interiors* 115: 205–218.

Kroner C and Jahr T (2006) Hydrological experiments around the superconducting gravimeter at Moxa Observatory. *Journal of Geodynamics* 41: 268–275.

Kroner C, Jahr T, and Jentzsch G (2004) Results from 44 months of observations with a superconducting gravimeter at Moxa/Germany. *Journal of Geodynamics* 38(3-5): 263–280.

Kroner C, Dierks O, Neumeyer J, and Wilmes H (2005) Analysis of observations with dual sensor superconducting gravimeters. *Physics of the Earth and Planetary Interiors* 153: 210–219.

Lambert A (1974) Earth tide analysis and prediction by the response method. *Journal of Geophysical Research* 79(32): 4952–4960.

Lambert A, Pagiatakis SD, Billyard AP, and Dragert H (2003) Improved ocean tidal loading corrections for gravity and displacement: Canada and northern United States. *Journal of Geophysical Research* 103(B12): 30231–30244.

Lambert A, Courtier N, and James TS (2006) Long-term monitoring by absolute gravimetry:Tides to postglacial rebound. *Journal of Geodynamics* 41: 307–317.

Larson JV and Harrison JC (1986) An improved analysis of the electrostatic feedback of LaCoste and Romberg gravity meters. In: *Proceedings of the 10th International Symposium on Earth Tides, Madrid 1985*, pp. 1–8. Madrid: Consejo Superior de Investigaciones Cientificas.

Lefèvre F, Lyard F, Le Provost C, and Schrama EJO (2002) FES99: A global tide finite element solution assimilating tide gauge and altimetric information. *Journal of the Atmospheric and Oceanic Technology* 19: 1345–1356.

Lognonné P, Clevede E, and Kanamori H (1998) Computation of seismograms and atmospheric oscillations by normal-mode summation for a spherical earth model with realistic atmosphere. *Geophysical Journal International* 135: 388–406.

Loyer S, Hinderer J, and Boy JP (1999) Determination of the gravimetric factor at the Chandler period from Earth's orientation data and superconducting gravimetry observations. *Geophysical Journal International* 136: 1–7.

Lynch DR and Gray WG (1979) A wave equation model for finite element tidal computations. *Computers and Fluids* 7: 207–228.

Matsumoto K, Takanezawa T, and Ooe M (2000) Ocean tide models developed by assimilating TOPEX/Poseidon altimeter data into hydro-dynamical model: A global model and a regional model around Japan. *Journal of Oceanography* 56: 567–581.

Matsumoto K, Sato T, Takanezawa T, and Ooe M (2001) GOTIC2: A program for the computation of ocean tidal loading effect. *Journal of Geodetic Society of Japan* 47: 243–248.

Mathews PM (2001) Love numbers and gravimetric factor for diurnal tides. *Journal of Geodetic Society of Japan* 47: 231–236.

Mathews PM, Herring TA, and Buffett B (2002) Modeling of nutation and precession: new nutation series for nonrigid Earth and insights into the Earth's interior. *Journal of Geophysical Research* 107(B4): 10.1029/2001JB000390.

Melchior P and Georis B (1968) Earth tides, precession-nutations and the secular retardation of Earth's rotation. *Physics of Earth and Planetary Interiors* 1(4): 267–287.

Melchior P and Ducarme B (1986) Detection of inertial gravity oscillations in the Earth's core with a superconducting gravimeter at Brussels. *Physics of Earth and Planetary Interiors* 42: 129–134.

Merriam J (1992a) An ephemeris for gravity tide predictions at the 1 ngal level. *Geophysical Journal International* 108: 415–422.

Merriam J (1992b) Atmospheric pressure and gravity. *Geophysical Journal International* 109: 488–500.

Merriam J (1993a) A comparison of recent tide catalogues. *Bulletin d'Informations des Marées Terrestres* 115: 8515–8535.

Merriam J (1993b) Calibration, phase stability, and a search for non-linear effects in data from the superconducting gravimeter at Cantley, Quebec. In: Hsu H-T (ed.) *Proceedings of the 12th International Symposium on Earth Tides, Beijing, China*, pp. 12. Beijing: Science Press.

Merriam J (1994) The nearly diurnal free wobble resonance in gravity measured at Cantley, Quebec. *Geophysical Journal International* 119: 369–380.

Merriam J (1995) Non-linear tides observed with the superconducting gravimeter at Cantley, Quebec. *Geophysical Journal International* 123: 529–540.

Merriam J (2000) The response method applied to the analysis of superconducting gravimeter data. *Physics of the Earth and Planetary Interiors* 121(3–4): 289–299.

Merriam J, Pagiatakis S, and Liard J (2001) Reference level stability of the Canadian superconducting gravimeter installation. *Journal of Geodetic Society of Japan* 47(1): 417–423.

Meurers B (1999) Air pressure signatures in the SG data of Vienna. *Bulletin d'Informations des Marées Terrestres* 131: 10195–10200.

Meurers B (2000) Gravitational effects of atmospheric processes in SG gravity data. In: Ducarme B and Barthelemy J (eds.) *Proceedings of the Workshop: 'High Precision Gravity Measurements with Application to Geodynamics and Second GGP Workshop'*, vol. 17, pp. 57–65. Luxembourg: 1999, ECGS Cahiers.

Meurers B (2001a) Superconducting gravimetry in Geophysical research today. *Journal of Geodetic Society of Japan* 47(1): 300–307.

Meurers B (2001b) Tidal and non-tidal gravity variations in Vienna – A Five Years' SG Record. J. *Journal of Geodetic Society of Japan* 47(1): 392–1397.
Meurers B (2002) Aspects of gravimeter calibration by time domain comparison of gravity records. *Bulletin d'Informations des Marées Terrestres* 135: 10643–10650.
Meurers B (2004) Investigation of temporal gravity variations in SG-records. *Journal of Geodynamics* 38: 423–435.
Mikhailov V, Tikhotsky S, Diament M, Panet I, and Ballu V (2004) Can tectonic processes be recovered from new gravity satellite data? *Earth and Planetary Science Letters* 228(3-4): 281–297.
Milly C and Shmakin A (2002) Global modeling of land water and energy balances. Part I: The land dynamics (LaD) model. *Journal of Hydrometeorology* 3: 283–299.
Mukai A, Higashi T, Takemoto S, Nakagawa I, and Naito I (1995) Accurate estimation of atmospheric effects on gravity observations made with a superconducting gravimeter at Kyoto. *Physics of the Earth and Planetary Interiors* 91: 149–159.
Mukai A, Takemoto S, Higashi T, and Fukuda Y (2001) Oceanic tidal loadings estimated from gravity observations in Kyoto and Bandung. *Journal of Geodetic Society of Japan* 47(1): 261–266.
Müller T and Zürn W (1983) Observation of gravity changes during the passage of cold fronts. *Journal of Geophysics* 53: 155–162.
Nawa K, Suda N, Fukao Y, Sato T, Aoyama Y, and Shibuya K (1998) Incessant excitation of the Earth's free oscillations. *Earth Planets Space* 50: 3–8.
Nawa K, Suda N, Fukao Y, *et al.* (2000) Incessant excitation of the Earth's free oscillations: Global comparison of superconducting gravimeter records. *Physics of the Earth and Planetary Interiors* 120: 289–297.
Neuberg J, Hinderer J, and Zürn W (1987) Stacking gravity tide observations in Central Europe for the retrieval of the complex eigen-frequency of the nearly diurnal free wobble. *Geophysical Journal of the Royal Astronomical Society* 91: 853–868.
Neumeyer J (1995) Frequency-dependent atmospheric pressure correction on gravity variations by means of cross-spectral analysis. *Bulletin d'Informations des Marées Terrestres* 122: 9212–9220.
Neumeyer J and Stobie B (2000) The new Superconducting Gravimeter Site at the South African Geodynamic Observatory Sutherland (SAGOS), Proceedings of the Workshop: High-Precision Gravity Measurements with Application to Geodynamics and Second GGP Workshop, Cahiers du Centre Européen de Géodynamique et de Séismologie, 17, Luxembourg, 85-96.
Neumeyer J, Hagedoorn J, Leitloff, and Schmidt R (2004a) Gravity reduction with three-dimensional atmospheric pressure data for precise ground gravity measurements. *Journal of Geodynamics* 38: 437–450.
Neumeyer J, Schwintzer P, Barthelmes F, *et al.* (2004b) Comparison of superconducting gravimeter and CHAMP satellite derived temporal gravity variations. In: Reigber Ch, Lühr H, Schwintzer P, and Wickert J (eds.) *Earth Observations with CHAMP Results from Three Years in Orbit,* pp. 31–36.
Neumeyer J, Barthelmes F, Dierks O, *et al.* (2006) Combination of temporal gravity variations resulting from Superconducting Gravimeter (SG) recordings, GRACE satellite observations and global hydrology models. *Journal of Geodesy* (DOI:10.1007/s00190-005-0014-8).
Niebauer T, Sasagawa G, Faller J, Hilt R, and Klopping F (1995) A new generation of absolute gravimeters. *Metrologia* 32: 159–180.
Nishida K and Kobayashi N (1999) Statistical features of Earth's continuous free oscillations. *Journal of Geophysical Research* 104: 28741–28750.
Nishida K, Kobayashi N, and Fukao Y (2000) Resonant oscillations between the solid Earth and the atmosphere. *Science* 287: 2244–2246.
Nishida K, Kobayashi N, and Fukao Y (2002) Origin of Earth's ground noise from 2 to 20 mHz. *Geophysical Research Letters* 29: 52-1–52-4.
Okubo S, Yoshida S, Sato T, Tamura Y, and Imanishi Y (1997) Verifying the precision of an absolute gravimeter FG5: Comparison with superconducting gravimeters and detection of oceanic tidal loading. *Geophysical Research Letters* 24: 489–492.
Pagiatakis SD (2000) Superconducting gravimeter data treatment and analysis. *Cahiers du Centre Européen de Géodynamique et Séismologie* 17: 103–113.
Peterson J (1993) Observations and modelling of seismic background noise, Open-File Report 93-332, U.S. Department of Interior, Geological Survey, New Mexico: Albuquerque.
Pingree RD and Griffiths KD (1980) Currents driven by a steady uniform windstress on the shelf seas around the British Isles. *Oceanologica Acta* 3: 227–235.
Pingree RD and Griffiths KD (1981) S2 tidal simulations on the North-West European Shelf. *Journal of the Marine Biological Association of the United Kingdom* UK 61: 609–616.
Prothero WA (1967) A cryogenic gravimeter, PhD Thesis, University of California at San Diego, La Jolla.
Prothero WA and Goodkind JM (1968) A superconducting gravimeter. *Review of Scientific Instruments* 39: 1257–1262.
Prothero WA and Goodkind JM (1972) Earth tide measurements with the superconducting gravimeter. *Journal of Geophysical Research* 77: 926–932.
Rabbell W and Zschau J (1985) Static deformations and gravity changes at the earth's surface due to atmospheric loading. *Journal of Geophysics* 56: 81–99.
Ray RD (1999) A global ocean tide model from TOPEX/Poseidon altimeter: GOT99.2, NASA Tech. Memo., TM-209478, 58 pp.
Rhie J and Romanowitz B (2004) Excitation of Earth's continuous free oscillations by atmosphere–ocean–seafloor coupling. *Nature* 431: (doi:10.1038/nature02942).
Richter B (1983) The long-period tides in the Earth tide spectrum. In: Proceedings of XVIII Gen. Ass. IAG, Hamburg, 1, pp. 204–216. Columbus, Ohio: Ohio State University Press, 1984: Ohio State University Press.
Richter B (1985) Three years of registration with the superconducting gravimeter. *Bulletin d'Informations des Marées Terrestres* 94: 6344–6352.
Richter B (1987) Das supraleitende Gravimeter, Deutsche Geodät. Komm., Reihe C, 329, Frankfurt am Main, 124pp.
Richter B (1990) In: McCarthy D and Carter W (eds.) *IUGG Geophysical Monograph No. 59 (9): The Long Period Elastic Behavior of the Earth,* pp. 21–25.
Richter B (1991) Calibration of superconducting gravimeters, Proceedings of the Workshop: Non Tidal Gravity Changes Intercomparison Between Absolute and Superconducting Gravimeters, Conseil de l'Europe, *Cahiers du Centre Europeen de Geodynamique et de Seismologie* 3, Luxembourg, pp. 99–107.
Richter B and Wenzel H-G (1991) Precise instrumental phase lag determination by the step response method. *Bulletin d'Informations des Marées Terrestres* 111: 8032–8052.
Richter B and Warburton RJ (1998) A new generation of superconducting gravimeters. In: *Proceedings of the 13th International Symposium on Earth Tides, Brussels 1997*, pp. 545–555. Brussels: Observatoire Royal de Belgique.
Richter B, Wilmes H, and Nowak I (1995a) The Frankfurt calivration system for relative gravimeters. *Metrologia* 32: 217–223.
Richter B, Wenzel H-G, Zürn W, and Klopping F (1995b) From Chandler wobble to free oscillations: Comparison of

cryogenic gravimeters and other instruments over a wide period range. *Physics of the Earth and Planetary Interiors* 91: 131–148.

Richter B, Zerbini S, Matonti F, and Simon D (2004) Long-term crustal deformation monitored by gravity and space techniques at Medicina, Italy and Wettzell, Germany. *Journal of Geodynamics* 38: 281–292.

Rieutord M (2002) Slichter modes of the Earth revisited. *Physics of the Earth and Planetary Interiors* 131: 269–278.

Rodell M and Famiglietti J (1999) Detectability of variations in continental water storage from satellite observations of the time dependent gravity field. *Water Resources Research* 35(9): 2705–2723.

Rodell M, Houser PR, Jambor U, *et al.* (2004) The global land data assimilation system. *Bulletin of the American Meteorological Society* 85(3): 381–394.

Romagnoli C, Zerbini S, Lago L, *et al.* (2003) Influence of soil consolidation and thermal expansion effects on height and gravity variations. *Journal of Geodynamics* 521–539.

Roosbeek F (1996) RATGP95: A harmonic development of the tide-generating potential using an analytic method. *Geophysical Journal International* 126: 197–204.

Rosat S, Hinderer J, Crossley D, and Rivera L (2003a) The search for the Slichter Mode: Comparison of noise levels of superconducting gravimeters and investigation of a stacking method. *Physics of the Earth and Planetary Interiors* 140: 183–202.

Rosat S, Hinderer J, and Rivera L (2003b) First observation of ${}_2S_1$ and study of the splitting of the football mode ${}_0S_2$ after the June 2001 Peru event of magnitude 8.4. *Geophysical Research Letters* 30: 21 2111 (doi:10.1029/2003GL018304).

Rosat S, Hinderer J, Crossley D, and Boy J-P (2004) Performance of superconducting gravimeters from long-period seismology to tides. *Journal of Geodynamics* 38: 461–476.

Rosat S, Sato T, Imanishi Y, *et al.* (2005) High-resolution analysis of the gravest seismic normal modes after the 2004 $M_w = 9$ Sumatra earthquake using superconducting gravimeter data. *Geophysical Research Letters* 32: L13304 (doi:10.1029/2005GL023128).

Rosat S, Rogister Y, Crossley D, and Hinderer J (2006) A search for the Slichter triplet with superconducting gravimeters: Impact on the density jump at the inner core boundary. *Journal of Geodynamics* 41: 296–306.

Roult G and Crawford W (2000) Analysis of 'background' free oscillations and how to improve resolution by subtracting the atmospheric pressure signal. *Physics of the Earth and Planetary Interiors* 121: 325–338.

Rymer H and Locke C (1995) Microgravity and ground deformation precursors to eruption: A review, In: Proceedings of the Workshop: New Challenges for Geodesy in Volcano Monitoring. Cah. Cent. Europ. Géodyn. et Séism., Luxembourg 8, pp. 21–39.

Sato T, Shibuya K, Ooe M, *et al*. (1991) Long term stability of the superconducting gravimeter installed at Syowa station, Antarctica, Proceedings of the 2nd Workshop: Non Tidal Gravity Changes Intercomparison Between Absolute and Superconducting Gravimeters, Conseil de l'Europe, Cahiers du Centre Européen de Géodynamique et de Séismologie, Luxembourg, 11, pp. 71–75.

Sato T, Ooe M, Nawa K, Shibuya K, Tamura Y, and Kaminuma K (1997a) Long-period tides observed with a superconducting gravimeter at Syowa station, Antarctica, and their implication to global ocean tide modeling. *Physics of the Earth and Planetary Interiors* 103: 39–53.

Sato T, Nawa K, Shibuya K, *et al.* (1997b) Polar motion effect on gravity observed with a superconducting gravimeter at Syowa station, Antarctica. In: IAG Symposia. Segawa *et al.* (eds.) *Gravity, Geoid, and Marine Geodesy,* vol. 117, pp. 99–106. Berlin: Springer-Verlag.

Sato T, Fukuda Y, Aoyama Y, *et al.* (2001) On the observed annual gravity variation and the effect of sea surface height variations. *Physics of the Earth and Planetary Interiors* 123: 45–63.

Sato T, Tamura Y, Matsumoto K, Imanishi Y, and McQueen H (2002) Parameters of the fluid core resonance estimated from superconducting gravimeter data. *Bulletin d'Informations Marées Terrestres* 136: 10751–10760.

Sato T, Boy J-P, Tamura Y, *et al.* (2006a) Gravity tide and seasonal gravity variation at Ny-Ålesund, Svalbard in Arctic. *Journal of Geodynamics* 41: 234–241.

Sato T, Okuno J, Hinderer J, *et al.* (2006b) A geophysical interpretation of the secular displacement and gravity rates observed at Ny-Alesund, Svalbard in the Arctic – Effects of the post-glacial rebound and present-day ice melting. *Geophysical Journal International* 165: 729–743, doi: 10.1111/1365-246X.2006.02992.x.

Scherneck H-G (1991) A parameterized Earth tide observation model and ocean tide loading effects for precise geodetic measurements. *Geophysical Journal International* 106: 677–695.

Schwahn W, Baker T, Falk R, *et al*. (2000) Long-Term Increase of Gravity at the Medicina Station (Northern Italy) Confirmed by Absolute and Superconducting Gravimetric Time Series, Proceedings of the Workshop: High-Precision Gravity Measurements with Application to Geodynamics and Second GGP Workshop, Cahiers du Centre Européen de Géodynamique et de Séismologie, 17, Luxembourg, pp. 145–168.

Schwiderski EW (1980) On charting global ocean tides. *Rev. Geophys.* 18: 243–268.

Seama N, Fukuda Y, and Segawa J (1993) Superconducting gravimeter observations at Kakioka, Japan. *Journal of Geomagnetism and Geoelectricity* 45: 1383–1394.

Simon D (2002) Modeling of the field of gravity variations induced by the seasonal air mass warming during 1998–2000. *Bulletin d'Informations Marées Terrestres* 136: 10821–10836.

Sinha B and Pingree RD (1997) The principal lunar semidiurnal tide and its harmonics: Baseline solutions for M2 and M4 constituents on the North-West European continental shelf. *Continental Shelf Research* 17: 1321–1365.

Smylie DE (1992) The inner core translational triplet and the density near Earth's center. *Science* 255: 1678–1682.

Smylie D, Francis O, and Merriam J (2001) Beyond tides-Determination of core properties from superconducting gravimeter observations. *Journal of the Geodetic Society of Japan* 47(1): 364–372.

Spratt RS (1982) Modelling the effects of the atmospheric pressure variations on gravity. *Geophysical Journal of the Royal Astronomical Society* 71: 173–186.

Suda N, Nawa K, and Fukao Y (1998) Earth's background free oscillations. *Science* 279: 2089–2091.

Sun H-P (1995) Static deformation and gravity changes at the Earth's surface due to atmospheric pressure, PhD thesis, Obs. Roy. de Belgique, Bruxelles.

Sun H-P, Hsu H-T, Jentzsch G, and Xu J-Q (2002) Tidal gravity observations obtained with a superconducting gravimeter at Wuhan/China and its application to geodynamics. *Journal of Geodynamics* 33: 187–198.

Sun H-P, Jentzsch G, Xu J-Q, Hsu H-Z, Chen X-D, and Zhou J-C (2004) Earth's free core nutation determined using C032 superconducting gravimeter at station Wuhan/China. *Journal of Geodynamics* 38: 451–460.

Svenson S and Wahr J (2002) Estimated effects of the vertical structure of atmospheric mass on the time-variable geoid. *Journal of Geophysical Research* 107(B9): 2194 (doi:10.1029/2000JB000024).

Takemoto S, Fukuda Y, Higashi T, *et al.* (2002) Effect of groundwater changes on SG observations in Kyoto and Bandung. *Bulletin d'Informations Marées Terrestres* 135: 10839–10844.

Tamura Y (1987) A harmonic development of the tide generating potential. *Bulletin d'Informations des Marées Terrestres* 99: 6813–6855.

Tamura Y (1993) *Additional terms to the tidal harmonic tables, Proceedings of 12th International Symposium. Earth Tides, Beijing 1993*, pp. 345–350, Beijing/New York: Science Press.

Tamura Y, Sato T, Ooe M, and Ishiguro M (1991) A procedure for tidal analysis with a Bayesian information criterion. *Geophysical Journal International* 104: 507–516.

Tanimoto T (2005) The oceanic excitation hypothesis for the continuous oscillations of the Earth. *Geophysical Journal International* 160: 276–288.

Tanimoto T, Um J, Nishida K, and Kobayashi N (1998) Earth's continuous oscillations observed on seismically quiet days. *Geophysical Research Letters* 25: 1553–1556.

Tanimoto T and Um J (1999) Cause of continuous oscillations of the Earth. *Journal of Geophysical Research* 104: 28723–28739.

Tsubokawa T (1991) Absolute and superconducting gravimetry in Japan, Proceedings of 2nd Workshop: Non Tidal Gravity Changes Intercomparison Between Absolute and Superconducting Gravimeters, Conseil de l'Europe, *Cahiers du Centre Europeen de Geodynamique et de Seismologie* 11, Luxembourg, pp. 47–71.

Van Camp M (1995) Noise induced by the refrigerating device of a superconducting gravimeter in the seismological station of Membach (Belgium). *Bulletin d'Informations des Marées Terrestres* 123: 9302–9314.

Van Camp M (1999) Measuring seismic normal modes with the GWR C021 superconducting gravimeter. *Physics of the Earth and Planetary Interiors* 116: 81–92.

Van Camp M and Vauterin P (2005) Tsoft: graphical and interactive software for the analysis of time series and Earth tides. *Computers in Geosciences* 31(5): 631–640.

Van Camp M, Wenzel H-G, Schott P, Vauterin P, and Francis O (2000) Accurate transfer function determination for superconducting gravimeters. *Geophysical Research Letters* 27: 1, 37–40.

Van Camp M, Camelbeeck T, and Francis O (2002) Crustal motions across the Ardenne and the Roer Graben (north western Europe) using absoluite gravity measurements. *Metrologia* 39: 503–508.

Van Camp M, Williams DP, and Francis O (2005) Uncertainty of absolute gravity measurements. *Journal of Geophysical Research* 110: B05406 (doi:10.1029/2004JB003497).

Van Dam TM and Wahr JM (1987) Displacements of the Earth's surface due to atmospheric loading: Effects on gravity and baseline measurements. *Journal of Geophysical Research* 92(82): 1281–1286.

Van Dam T, Wahr J, Milly P, *et al.* (2001a) Crustal displacements due to continental water storage. *Geophysical Research Letters 28,* 4: 651–654.

Van Dam T, Wahr J, Milly P, and Francis O (2001b) Gravity changes due to continental water storage. *Journal of Geodetic Society of Japan* 47(1): 249–1254.

Van Ruymbeke M (1989) A calibration system for gravimeters using a sinusoidal acceleration resulting from a periodic movement. *Bulletin Géodesique* 63: 223–235.

Venedikov A and Viera R (2004) Guidebook for the practical use of the computer program VAV – Version 2003. *Bulletin d'Informations des Marées Terrestres* 121: 11037–11103.

Virtanen H (2001) Hydrological studies at the gravity station Metsahovi, Finland. *Journal of Geodetic Society of Japan* 47(1): 328–333.

Virtanen H and Mäkinen J (2003) The effect of the Baltic Sea level on gravity at the Metsähovi station. *Journal of Geodynamics, 35,* 4–5: 553–565.

Warburton RJ and Goodkind JM (1977) The influence of barometric-pressure variations on gravity. *Geophysical Journal of the Royal Astronomical Society* 48: 281–292.

Warburton RJ and Goodkind JM (1978) Detailed gravity-tide spectrum between one and four cycles per day. *Geophysical Journal of the Royal Astronomical Society* 52: 117–136.

Warburton RJ and Brinton EW (1995) Recent developments in GWR Instruments' superconducting gravimeters, Proc. 2nd Workshop: Non-tidal gravity changes Intercomparison between absolute and superconducting gravimeters, Cahiers du Centre Européen de Géodynamique et de Séismologie, Luxembourg, 11, pp. 3–56.

Warburton RJ, Beaumont C, and Goodkind JM (1975) The effect of ocean tide loading on tides of the solid earth observed with the superconducting gravimeter. *Geophysical Journal of the Royal Astronomical Society* 43: 707–720.

Warburton RJ, Brinton EW, Reineman R, and Richter B (2000) Remote operation of superconducting gravimeters, Proceeding of the Workshop: High-Precision Gravity Measurements with Application to Geodynamics and Second GGP Workshop, Cahiers du Centre Européen de Géodynamique et de Séismologie, 17, Luxembourg, pp. 125–136.

Wahr JM (1985) Deformation induced by polar motion. *Journal of Geophysical Research* 90(B11): 9363–9368.

Wahr J, Han D, and Trupin A (1995) Predictions of vertical uplift caused by changing polar ice volumes on a viscoelastic Earth. *Geophysical Research Letters* 22: 977–980.

Wahr J, Molenaar M, and Bryan F (1998) Time variability of the Earth's gravity field: hydrological and oceanic effects and their possible detection using GRACE. *Journal of Geophysical Research* 103(B12): 30205–30229.

Wang R (1997) In: Helmut W, Zürn W, and Wenzel H-G (eds.) Tidal response of the Earth, in Tidal Phenomena, Lecture Notes in Earth Sciences, pp. 27–57. Berlin: Springer.

Wenzel H-G (1994) Accurate instrumental phase lag determination for feedback gravimeters. *Bulletin d'Informations des Marées Terrestres* 118: 8735–8751.

Wenzel H-G (1995) Accurate Instrumental Phase Lag Determination for Feedback Gravimeters. In: Hsu HT (ed.) *Proceedings of the 12th International Symposium. Earth Tides*, pp. 191–198. Beijing, New York: Science Press.

Wenzel H-G (1996a) Accuracy assessment for tidal potential catalogues. *Bulletin d'Informations des Marées Terrestres* 124: 9394–9416.

Wenzel H-G (1996b) The nanogal software: Earth tide processing package ETERNA 3.30. *Bulletin d'Informations des Marées Terrestres* 124: 9425–9439.

Widmer-Schnidrig R (2003) What can superconducting gravimeters contribute to normal mode seismology. *Bulletin of the Seismological Society of America* 93(3): 1370–1380.

Wilmes H, Boer A, Richter B, *et al.* (2006) A new data series observed with the remote superconducting gravimeter GWR R038 at the geodetic fundamental station TIGO in Concepción (Chile). *Journal of Geodynamics* 41: 5–13.

Xi Q-W (1987) A new complete development of the tide generating potential for the epoch J200.0. *Bulletin d'Informations des Marées Terrestres* 99: 6766–6681.

Xi Q-W (1989) The precision of the development of the tidal generating potential and some explanatory notes. *Bulletin d'Informations des Marées Terrestres* 105: 7396–7404.

Xu J-Q, Sun H-P, and Ducarme B (2004a) A global experimental model for gravity tides of the Earth. *Journal of Geodynamics* 38: 293–306.

Xu J-Q, Sun H-P, and Yang X-F (2004b) A study of gravity variations caused by polar motion using superconducting gravimeter data from the GGP network. *Journal of Geodesy* 78: 201–209 (doi:10.1007/s00190-004-0386-1).

Zerbini S, Richter B, Negusini M, *et al.* (2001) Height and gravity various by continuous GPS, gravity and environmental parameter observations in the southern Po Plain, near Bologna, Italy. *Earth and Planetary Science Letters* 192: 267–279.

Zerbini S, Negusini M, Romagnoli C, Domenichini F, Richter B, and Simon D (2002) Multi-parameter continuous observations to detect ground deformation and to study environmental variability impacts. *Global and Planetary Changes* 37–58.

Relevant Websites

http://www.eas.slu.edu – GGP Home Page, Department of Earth & Atmospheric Sciences, Saint Louis University.

http://ggp.gfz-potsdam.de – Global Geodynamic Project Information System and Data Center.